Neural Network Based

Optimal Control of HVAC&R Systems

Min Ning

A Thesis
in
The Department
of
Building, Civil and Environmental Engineering

Presented in Partial Fulfillment of the Requirements
for the Degree of Doctoral of Philosophy at
Concordia University
Montreal, Quebec, Canada

March 2008

Your file Votre référence
ISBN: 978-0-494-37738-3
Our file Notre référence
ISBN: 978-0-494-37738-3

ABSTRACT

Neural Network Based Optimal Control of HVAC&R Systems

Min Ning, Ph.D
Concordia University, 2008

Heating, Ventilation, Air-Conditioning and Refrigeration (HVAC&R) systems have wide applications in providing a desired indoor environment for different types of buildings. It is well acknowledged that 30% - 40% of the total energy generated is consumed by buildings and HVAC&R systems alone account for more than 50% of the building energy consumption. Low operational efficiency especially under partial load conditions and poor control are part of reasons for such high energy consumption. To improve energy efficiency, HVAC&R systems should be properly operated to maintain a comfortable and healthy indoor environment under dynamic ambient and indoor conditions with the least energy consumption.

This research focuses on the optimal operation of HVAC&R systems. The optimization problem is formulated and solved to find the optimal set points for the chilled water supply temperature, discharge air temperature and AHU (air handling unit) fan static pressure such that the indoor environment is maintained with the least chiller and fan energy consumption. To achieve this objective, a dynamic system model is developed first to simulate the system behavior under different control schemes and operating conditions. The system model is modular in structure, which includes a water-

cooled vapor compression chiller model and a two-zone VAV system model. A fuzzy-set based extended transformation approach is then applied to investigate the uncertainties of this model caused by uncertain parameters and the sensitivities of the control inputs with respect to the interested model outputs. A multi-layer feed forward neural network is constructed and trained in unsupervised mode to minimize the cost function which is comprised of overall energy cost and penalty cost when one or more constraints are violated. After training, the network is implemented as a supervisory controller to compute the optimal settings for the system. In order to implement the optimal set points predicted by the supervisory controller, a set of five adaptive PI (proportional-integral) controllers are designed for each of the five local control loops of the HVAC&R system. The five controllers are used to track optimal set points and zone air temperature set points. Parameters of these PI controllers are tuned online to reduce tracking errors .The updating rules are derived from Lyapunov stability analysis.

Simulation results show that compared to the conventional night reset operation scheme, the optimal operation scheme saves around 10% energy under full load condition and 19% energy under partial load conditions.

Acknowledgements

I would like to express my sincere gratitude to my supervisor, Dr. M. Zaheer-uddin, for his excellent and continuous guidance, suggestions, motivation and supports throughout this research work. Without any of these, this work would never be able to be accomplished.

I also thank my colleagues, for their helpful discussions and constructive suggestions to my study. My special appreciations also go to Ms. Jiabing Wang and Mr. Tao Liang for their encouragement and moral support.

Finally, I would like to dedicate this thesis to my families, my father, Cheng Ning, my mother Suyu Jiang and my sisters, Qin Ning and Chang Ning. Without their continuous encouragement and unconditional supports, I would never be able to finish this study.

Table of Contents

List of Figures ..... **ix**

List of Tables ..... **xi**

Symbols ..... **xii**

Chapter 1 Introduction **1**

1.1 Background 1

1.1.1 Variable Air Volume Systems 2

1.1.2 Building Energy Management Systems 2

1.1.3 Control of HVAC&R Systems 4

1.2 Research Objectives and Thesis Outline 6

Chapter 2 Literature Review and Objectives **8**

2.1 Modeling of HVAC and Refrigeration Systems and Components 8

2.1.1 Modeling of Refrigeration Systems/Components 9

2.1.2 Modeling of HVAC Systems 13

2.1.3 Black Box Models 17

2.1.4 Software Packages 19

2.2 Uncertainty analysis 20

2.3 Optimal Control/Operation of HVAC&R Systems 22

2.4 HVAC&R System Controller Design 28

2.5 Summary and Conclusions 32

Chapter 3 Dynamic Model of a VAV-HVAC System with Water-Cooled Vapor Compression Chiller **36**

3.1 Description of a Two-Zone VAV-HVAC and Refrigeration System 37

3.2 Dynamic Model of a Two-Zone VAV System 39

3.2.1 Airflow Subsystem Model 40

3.2.2 Thermal Subsystem Model 42

3.2.3 Water Flow Subsystem Model 44

3.2.4 VAV System Model 45

3.3 Dynamic Model of a Water Cooled Vapor Compression Chiller 45

3.3.1 Evaporator Model 46
3.3.2 Condenser Model 54
3.3.3 Thermal Expansion Valve (TEV) Model 61
3.3.4 Variable Speed Compressor Model 62
3.3.5 Water Cooled Vapor Compression Chiller Model 64
3.4 Combined System Model and Open-Loop Simulation Results 65
3.4.1 Simulation - CASE 1 66
3.4.2 Simulation - CASE 2 76
Chapter 4 Fuzzy-Set Based HVAC&R Model Uncertainty and Sensitivity Analysis 84
4.1 Background of Fuzzy-Set Theory 85
4.2 The Transformation Method 86
Case 1 - Transformation Matrix in General Form 87
4.3 The Extended Transformation Method 91
4.4 Fuzzy-Set Based HVAC&R System Model Uncertainty Analysis 94
4.4.1 Uncertain Parameter Analysis 94
4.4.2 Numerical Results 97
4.5 Fuzzy-Set Based Control Variable Sensitivity Analysis 108
Chapter 5 Neural Network Based Optimal Control of HVAC&R Systems 118
5.1 Background of Neural Networks 120
5.2 Formulation of Optimization Problem for HVAC&R System Operation 123
5.3 NN Based Optimization Algorithm 127
5.3.1 Network Construction 131
5.3.2 Adjusting the Network Weights 132
5.3.3 Derivative Calculation 134
5.4 Simulation Results 136
Chapter 6 Adaptive Control Design for HVAC&R Systems 148
6.1 NN-Based auto-tuning PI Control 150
6.1.1 The Structure of NN Model Prediction Based Adaptive Control 150
6.1.2 Adaptive Neural Network Model 151
6.1.3 Adaptation Rules 151

6.1.4 Simulation Results 156
6.2 Implementation of the Optimal Set Points – Local Control Design 158
6.2.1 Construction of Local Neural Network Models 158
6.2.2 Simulation Results 162
Chapter 7 Conclusions and Suggested Future Work 166
7.1 Summary and Conclusions 166
7.2 Contributions of This Study 172
7.3 Recommendations for Future Work 174
References 176

List of Figures

Figure 3-1 Schematic Diagram of a Typical Two-Zone VAV-HVAC&R System 38

Figure 3-2 Air Flow Loops in a Two-Zone VAV-HVAC System 40

Figure 3-3 Refrigerant Phase Change and Heat Flow Direction within Evaporator 47

Figure 3-4 Refrigerant Phase Change and Heat Flow Directions within Condenser 55

Figure 3-5 Open-Loop Simulation Results of Chiller..... 67

Figure 3-6 Open-Loop Simulation Results of VAV System 71

Figure 3-7 Open-Loop Simulation Results of Integrated System – Chiller..... 73

Figure 3-8 Open-Loop Simulation Results of Integrated System – VAV System 74

Figure 3-9 Open-Loop Simulation Results Due to a Step Change in Load & Ucom..... 79

Figure 3-10 Open-Loop Simulation Results Due to a Step Change in Load & Uval..... 80

Figure 3-11 Open-Loop Simulation Results Due to a Step Change in Load, Uz1, Uz2 & Ufan..... 81

Figure 4-1 α-cut Decomposition of a Fuzzy Parameter with Triangular Membership Functions..... 86

Figure 4-2 Insertion of Additional Point(s) in General Transformation Method (m=4) . 88

Figure 4-3 Results of Classification of Uncertain Parameters -- $\tau_1 - \tau_6$ V.S. Model Predictions..... 98

Figure 4-4 System Dynamic Responses and Approximate Distributions under Uncertain Model Parameters 101

Figure 4-5 Derive Approximate Distributions from Distribution Figure 102

Figure 4-6 Model Dynamic Predictions and Approximate Distributions under Variations of Control inputs 111

Figure 5-1 Architecture of a Three-Layer Feed forward Neural Network 120

Figure 5-2 Transfer Functions 120

Figure 5-3 Neural Network Based Optimization Process 127
Figure 5-4 NN based Optimization Algorithm Flow Chart 129
Figure 5-5 Outdoor Air Temperature and Zone Cooling Load Profiles – Full Load 135
Figure 5-6 Outdoor Air Temperature and Zone Cooling Load Profiles – Partial Load . 135
Figure 5-7 Simulation Results from Optimal Operation – Full Load Case 139
Figure 5-8 Simulation Results from Optimal Operation – Partial Load Case 140
Figure 5-9 Simulation Results from Night Reset Operation Scheme – Full Load 142
Figure 5-10 Simulation Results from Night Reset Operation Scheme – Partial Load .. 144
Figure 6-1 Block Diagram of Neural Network Based Adaptive Control 149
Figure 6-2 Flow Chart of Neural Network Based Adaptive Control 154
Figure 6-3 Response of Discharge Air Temperature with Adaptive PI Control 156
Figure 6-4 Response of Discharge Air Temperature with PI Control 156
Figure 6-5 Response of Integrated Two-Zone VAV-HVAC&R System with Adaptive PI Control (Full Load) 162

List of Tables

Table 3–1 Effects of Step Variations of Control Inputs and Loads on System Responses 78

Table 4–1 Model Steady State Prediction Variations with Uncertain Parameters 103

Table 4–2 Normalized Effects of Uncertain Parameters on Model Predictions 105

Table 4–3 Normalized Effects of Variation of Control Inputs on Model Predictions... 112

Table 5–1 System Operation Conditions 136

Table 5–2 Night Reset Operation Scheme 141

Table 5–3 Energy consumption Comparison of Two Operation Schemes 144

Table 6–1 Comparisons of adaptive PI and PI controllers 156

Table 6–2 Structural Details of Neural Network Models 160

Symbols

$a_1, a_2...$	data fitting coefficients, dimensionless
A	heat transfer area per unit length, m
A_c	cross-sectional area, m^2
B	frictional factor, kg-m^2/s
$c_{a,v}$ / $c_{a,p}$	specific heat of air at constant volume / pressure, kJ/kg- °C
$c_{fin} / c_t / c_w$	specific heat of fin / tube / water, kJ/kg- °C
$c_{p,r}$	specific heat of refrigerant at constant pressure, kJ/kg- °C
C	thermal capacity, J/ °C
$CAPACITY$	refrigeration capacity, W
C_h	fan pressure head coefficient, dimensionless
C_v	orifice coefficient of the thermal expansion valve, dimensionless
CL	compressor clearance volume rate, dimensionless
COP	coefficient of performance, dimensionless
d / D	diameter, m
ΔD	damper pressure loss, Pa
e	armature voltage, V
E	energy consumption, W
g	gravitational acceleration, m/s^2
G	mass velocity, kg/s-m^2

h	heat transfer coefficient, W/ °C-m^2
$h_{m,cc}$	cooling and dehumidifying coil mass transfer coefficient, kg/s-m^2
H	approximate Hessian matrix of the performance function
i	enthalpy, J/kg
i_{fg}	latent heat of vaporization, J/kg
I	motor current, A
k	thermal conductivity, W/m-°C
k_b	back emf constant, V/rad-sec
k_i	PI/PID controller integral gain, dimensionless
k_i	motor torque constant, N-m/A
k_p	PI/PID controller proportional gain, dimensionless
K	isentropic exponent, dimensionless
J	moment of inertia, kg-m^2
L	length, m
L_a	motor armature inductance, H
l_r	neural network learning rate, dimensionless
m	mass, kg
m	refinement number, dimensionless
mc	neural network training momentum coefficient, dimensionless
$\dot{m}$	mass flow rate, kg/s
N	motor rotational speed, rpm

P	pressure, Pa
Pr	Prandtl number, dimensionless
ΔP_{fan}	fan pressure gain, Pa
ΔP_{loss}	duct pressure loss, Pa
Q	heat transfer rate, W
q_l	latent load, W
q_s	sensible load, W
R_a	motor armature resistance, Ω
R_e	Reynolds number, dimensionless
RN	drive ratio, dimensionless
s	sensitivity coefficient of fuzzy variable, dimensionless
S	overall effects of fuzzy variable, dimensionless
S	weight of the penalty term, dimensionless
SH	refrigerant degree of superheat at evaporator outlet, °C
SH_{ss}	static superheat degree required to overcome TEV spring force, °C
SN	normalized effect of fuzzy variable, dimensionless
t	time, second
T	temperature, °C
$\overline{T}$	mean temperature, °C
U	normalized control input, dimensionless
V	volume, m^3

$V_{clearance}$	clearance volume of the compressor, m^3
V_{com}	compressor cylinder volume, m^3
W	neural network weights, dimensionless
W_a	humidity ratio of air, kg/kg
W_{com}	compressor work, W
$\overline{W}_{a,cc}$	mean humidity ratio of the air in the cooling coil, kg/kg
$\overline{W}_{t,sat}$	humidity ratio of saturated air at coil wall temperature, kg/kg
x	refrigerant quality, dimensionless

Greek letters

γ	refrigerant void fraction, dimensionless
$\bar{\gamma}$	refrigerant mean void fraction, dimensionless
η	efficiency, dimensionless
η_{com}	compressor adiabatic efficiency, dimensionless
$\eta_{v,com}$	compressor volumetric efficiency, dimensionless
$\eta_{m,ov}$	coil surface effectiveness in mass transfer, dimensionless
η_s	cooling coil fin efficiency, dimensionless
$\eta_{s,ov}$	coil surface effectiveness in sensible heat transfer, dimensionless
μ	dynamic viscosity, kg/m-s
μ_F	membership of fuzzy variable, dimensionless
ρ	density, kg/m^3

τ	effectiveness of fuzzy variable on model output, dimensionless

Subscripts

a	air / cooling coil air side
c / con	(inside) condenser
cc	cooling and dehumidifying coil
com / COM	compressor
dis	discharge condition
*e / e*va	(inside) evaporator
eq	equivalent value
ex	exhausted air
f / fan	fan
fin	fin or fin material
in	inlet condition
l	liquid
m	motor
max	maximal value
oa	outdoor fresh air
out	outlet condition
Pc	condenser pressure condition
Pe	evaporator pressure condition

r	refrigerant or refrigerant side
re	recirculated air / return condition
rt	heat flow from refrigerant to tube
sat	saturated condition
satv	saturated vapor
satl	saturated liquid
sc	sub-cooled section
sh	superheated section
suc	suction condition
sup	supply condition
t	tube / tube wall
TEV	thermal expansion valve
tp	two-phase section
tr	heat flow from tube to refrigerant
tw	heat flow from tube to water
v	vapor
val	chilled water valve
w	water or water side
wt	heat flow from water to tube
z	air-conditioned zone
zi	the i^{th} zone (i = 1,2)

∞	infinite

Chapter 1 Introduction

1.1 Background

Heating, ventilation, air-conditioning and refrigeration (HVAC&R) systems have been used to provide desired indoor environment in buildings for decades. It is well acknowledged that 30% - 40% of the total energy generated is consumed by buildings and that HVAC&R systems alone account for more than 50% of the building energy consumption. These percentages are still growing. The inefficient operation of HVAC&R systems especially under partial load conditions, poor tuning and malfunction of controllers all increase the energy consumption of the system.

The escalating energy costs have led to more and more research efforts to reduce the energy use of the HVAC&R systems from the design stage to the operation stage, such as the design of better building envelopes, the selection of energy efficient equipment, improved control sequence and introducing efficient energy saving operation schemes. However, once a building is constructed and a HVAC&R system is installed, energy consumption of the HVAC&R system is mainly dependent on the operation, maintenance and the use of the building. Knowing the functional use of the building, the energy efficiency of the HVAC&R system can be improved by employing improved control strategies and proper maintenance. There is more than one operation scheme that can maintain the same indoor conditions, but energy consumption may be different. Among these, the optimal operation scheme is the one that consumes the least energy.

1.1.1 Variable Air Volume Systems

Variable air volume (VAV) systems maintain desired space temperature by adjusting the VAV box damper opening such that the amount of conditioned air entering the space is modulated to match the load requirement. Compared to its counterpart, the constant air volume (CAV) system where the space temperature is controlled by regulating the discharge air temperature (temperature of the air leaving the coil), the advantages of the VAV systems include the flexibility to adapt to individual space load requirement and huge energy saving potential, especially when the systems have variable speed fans run by variable speed motors. The energy savings of VAV systems come from the reduction of air mass flow rate under partial load conditions, which not only reduces fan energy consumption but also reduces the cooling load requirements for refrigeration systems.

Although the VAV system has great energy saving potential, it may perform very poorly without good commissioning and robust control. Poor operation of a VAV system often results in uncomfortable indoor environment, low energy efficiency and poor indoor air quality (IAQ) (Klaczek et al., 2005).

1.1.2 Building Energy Management Systems

More and more buildings these days are equipped with building energy management systems (BEMS) to audit the energy performance and control the system operation to improve the building energy performance. There are two levels of control in BEMS, a higher level supervisory control and a lower level local control. Historical climate and operational information are recorded at supervisory level. With this information, the operation schemes are determined based on the pre-programmed

operation sequences. Local controllers implement the control strategies either according to the downloaded set points from supervisory control or pre-programmed logic. General control strategies in BEMS include optimal on-off control, night reset control, demand reset control, outdoor air enthalpy control etc.

The proper selection/determination of the operation scheme is not an easy task because of the high coupling characteristics of the HVAC&R system and time-variant operating conditions. So far, most EMSs determine operation schemes at the local loop level independently without considering the rest of the system. Unfortunately, most of the time, the performance of the system is not as good as expected because of the influence of other interacting loops. In other words, the system doesn't work at its best. Studies of Hartman (1988), Braun et al. (1989A, 1990) and Zheng (1997) showed that HVAC&R system was a highly coupled system, the control loops had great impacts on each other. There are trade-offs between individual local control and overall system energy consumption. Therefore, the optimal operation of single loop won't result in optimal operation of the overall system. For example, for outdoor air enthalpy control, the basic idea is to take advantage of the cool outdoor air to reduce the cooling from the chiller. The cooler the outdoor air is, the more outdoor air is introduced into the building to reduce the chiller's energy use to the maximum extent. However, fan energy consumption may increase at the same time because more air needs to be circulated by the fan. Therefore, from the view point of energy consumption of the entire system, using more cold outdoor air does not necessarily reducing the total energy consumption. Same is the case in the discharge air temperature control. Increasing the discharge air temperature decreases chiller and chilled water pump energy consumption on one hand

because less chilled water required, but on the other hand, increases fan energy consumption due to a higher air flow rate. Therefore, the efficient operation of HVAC&R systems should consider the interactions of local loops and the evaluation of the system energy performance should be based on the system level rather than from the view point of saving energy of a single component or a single loop. With proper control, it is possible to reduce energy consumption of the entire system without sacrificing thermal comfort in the building.

1.1.3 Control of HVAC&R Systems

SISO (single-input-single-output) PID (proportional-integral-derivative) and PI (proportional and integral) controllers have extensive applications in industry because of their simplicity, cost effectiveness, robustness and reliability. In practice, PID/PI controllers work either with default control parameters/gains from the manufacturer or with fixed parameters determined at commissioning stage. However, a HVAC&R system is a highly non-linear, time-variant system and needs to respond to varied set points for different operating conditions. Using controllers with fixed parameters to control such a complicated system may cause control problems when working conditions are away from the commissioning one. To address this, variable control gains or adaptive controls are introduced to maintain consistent good performance. The practical methods include gain scheduling and auto-tuning. Gain scheduling has wide applications for systems (processes) whose dynamics can be characterized by measurable variables, named as regulator parameters. Controller gains are calibrated under different operating conditions through open loop tests and are stored in a lookup table. When applied on-line, control parameters are selected according to the real operating conditions and regulator

parameters (Astrom and Wittenmark, 1989). Auto-tuning adjusts controller parameters automatically according to certain regulation rules to respond to the variations in system dynamics and operating conditions. These adaptive techniques could not only solve most control problems encountered in HVAC&R applications, especially those caused by the time-varying dynamics and changes in operating conditions, but also have other advantages such as easy commissioning and energy saving potential compared to conventional control schemes. But the high coupling nature of the local loops in HVAC&R system deteriorates the control performance of SISO controllers because tuning one controller may deteriorate the performance of other controllers. To solve this problem, MIMO (multi-input-multi-output) control, which uses multiple feedback signals to generate multiple control inputs, is used. However, due to the complexity of the controller structure, there are not many applications of MIMO control in HVAC&R industry.

The design of optimal operation strategies for HVAC&R systems is a challenging task. The design methodologies must compensate for the following complex dynamic interactions of HVAC&R systems:

- The operation is a multi-objective problem. The operation of the system not only needs to satisfy indoor environment requirements, but also needs to consider the efficiency of the operation. Multi control variables have to be coordinated to achieve satisfactory system responses.
- A HVAC&R system is a highly nonlinear system with different scale of time constants. Longer time lags have to be compensated to improve the regulation properties of controllers.

- System dynamics change with operating conditions. The control system has to respond to these changes.
- The mathematical system model is subjected to uncertainties. This is because some dynamics are unknown and some are hard to be described mathematically. Also accurate values of some model parameters are hard to determine. Consequently, the prediction results from the uncertain model exhibit uncertainties. The determination of operation schemes, the design and tuning of controllers are based on the predictions of an uncertain model.

1.2 Research Objectives and Thesis Outline

The main objective of this research is to develop and realize global optimal operation strategies for a VAV-HVAC&R system aiming to maintain a desired indoor environment under time variant ambient and indoor conditions with the least energy consumption. This includes the determination of an optimal operation strategy at the supervisory level and its subsequent implementation at the local level. The dynamic interactions among the building, the HVAC&R system and the control system will be taken into account in the analysis to improve energy efficiency and achieve better performance.

This thesis is organized as follows. After a brief introduction of VAV systems, and the operation and control of HVAC&R systems, the objectives of present research are stated in Chapter 1. In Chapter 2, a review of previous research in modeling, operation of HVAC&R systems, and controller design and tuning methods is given followed by a summary of the limitations of previous research work. Finally, the major steps leading to

the optimal operation of HVAC&R systems are presented at the end of Chapter 2. A dynamic model of a two-zone VAV-HVAC and refrigeration system is developed and open loop simulation results are presented and discussed in Chapter 3. Model uncertainty analysis and control sensitivity analysis are conducted in Chapter 4. Important uncertain model parameters and the significance of the uncertain parameters and control inputs on model outputs are identified. In Chapter 5, a neural network based supervisory optimal operation strategy is proposed and compared with the conventional night reset operation strategies. In Chapter 6, multi adaptive PI controllers are designed and implemented to realize the closed-loop optimal operation of the system. Chapter 7 summarizes conclusions and presents recommendations for future work.

Chapter 2 Literature Review and Objectives

The increasing concern of improving building energy efficiency has motivated extensive research on the efficient operation of HVAC&R systems, including (1) modeling of HVAC&R components and systems; (2) optimal control and efficient operation of HVAC&R systems and components; (3) controller design for HVAC&R system including PI control, PID control, neural control, adaptive control, fuzzy control, and multiple-input multiple-output (MIMO) control; (4) fault detection and diagnosis; (5) energy consumption analysis and (6) efficient building and system design. This chapter will cover the review on the first three topics, most relevant to the research work conducted in this thesis.

2.1 Modeling of HVAC and Refrigeration Systems and Components

A good understanding of the performance of mechanical and control systems forms the basis for developing successful operation and control strategies for HVAC&R systems. Compared to the monitoring of a real plant, model based simulation provides an easier, faster and cheaper substitute to gather operating information, evaluate control strategies and the performance of HVAC&R systems and components. Intensive HVAC&R components and systems models, including steady state models and dynamic models, have been developed in the past decades.

Most system models are modular based. Models of main components are developed and then connected to each other according to the input and output information to construct the system model. In most studies, the HVAC system and the refrigeration

system are treated and modeled as separate systems. The main components in a HVAC system include cooling/heating coil, supply/return fan, air-conditioned space and air duct. The main components in a refrigeration system are compressor, evaporator, condenser and throttling device.

2.1.1 Modeling of Refrigeration Systems/Components

Compressor and Expansion Valve Models

Compressor and expansion valve models are usually used to predict the flow rate and state of refrigerant at the outlet of the compressor and the expansion valve. The most popular compressor and expansion valve models are based on a steady state analysis because the respective time constants of the compressor and expansion valve are much smaller than the time constants of other components in the refrigeration systems and thus their dynamics won't significantly affect the dynamics of the whole refrigeration system.

The methodologies employed to model compressor and expansion valve are very similar in literature (Jian, 1996; He and Liu, 1998; Kim and Bullard 2001, Koury et al., 2001; Jiang and Radermacher, 2003). The quasi steady state expansion valve models are derived from the orifice flow under the assumption of isenthalpic flow. The compressor models are derived from thermodynamic rules with the assumption of isentropic compression process and neglecting (1) the pressure losses along the refrigerant path, (2) the refrigerant mass variations in the compressor, (3) the oil effects on the refrigerant, (4) the variations in refrigerant kinetic energy and potential energy, and (5) the heat transfer between shells and ambient. For reciprocating type compressor, the mass flow rate of refrigerant is computed using compressor volumetric efficiency which accounts for the free expansion of vapor refrigerant trapped in the clearance volume. Energy consumption

is calculated with compressor isentropic efficiency which is either assumed to be constant (Koury et al., 2001, Fu et al., 2002) or identified with manufacturer's data (Jiang and Radermacher, 2003) or modeled with a simple function, for example, Kim and Bullard (2001) expressed the compressor efficiency as a linear function of the shell temperature with coefficients determined from in-situ data; Browne and Bansal (2002) expressed isentropic efficiency as a bi-quadratic function of refrigerant flow rate and system pressure with experimental data.

Condenser and Evaporator Models

Condenser and evaporator are heat exchange components in refrigeration system. The dynamics of the refrigeration system is dominated by the condenser and evaporator because they have large time constants. The main differences between different refrigeration system models come from the methodologies used to model the evaporator and condenser. The moving boundary approach and the finite difference approach are two prevailing approaches used to model the evaporator and the condenser.

In the moving boundary approach, condenser/evaporator is divided into two to three sections, a super-heated section, a two-phase section and a sub-cooled section, according to the state of refrigerant exhibited in the heat exchanger. The length of each section varies with time since the saturated liquid and vapor boundaries move during transients. The governing equations for each section are derived from the energy, mass conservation principles and the momentum conservation principle if pressure variation along tubes is considered. Thermo-physical properties of the refrigerant and the secondary fluid are assumed to be uniform for each section. Consequently, heat exchanger models derived from moving boundary method are lumped parameter models.

States of the refrigerant and the secondary fluid at the heat exchanger exit and pressure loss in tubes are described by ordinary differential equations (ODEs). Although model equations are simple, the accuracy of this type of model is sufficient for most applications. E.g. He and Liu (1998) design a MIMO controller for a refrigeration system based on a system model with moving boundary heat exchanger model. Refrigeration system model with moving boundary heat exchanger model developed by Willatzen et al. (1998) was used to study the transient responses of system start-up and shut-down. Their model included numerical handling of the formation and disappearance of the liquid, two-phase or vapor zones. Cheng et al. (2005) developed a moving boundary heat exchanger model to calculate the heat transfer rate and the length of two-phase section in the heat exchanger. Rasmussen and Alleyne (2004) developed a 11th-order dynamic heat exchanger model using moving boundary approach. Simulation results showed that the system exhibited multiple time scale behavior and then a reduced 5th-order model was derived using singular perturbation techniques to eliminate the fast dynamic states. Simulation results showed that eliminating the states with fast responses had negligible impact on the transient responses of overall system.

In the finite difference method, heat exchanger is divided into a number of control volumes. Governing equations of mass, momentum and energy conservation for each control volume are expressed as partial differential equations (PDEs) in both space and time domains. These equations are solved with local thermo-physical properties and heat transfer coefficients. Heat exchanger models derived from this method are distributed models. The distributions of velocity, void fraction, temperature and pressure of the refrigerant and the secondary fluid in both space and time domains can be simulated with

this type of model such as the ones developed by Oskarsson et al. (1990), Wang and Touber (1991), Bensafi et al. (1997), Jiang and Radermacher (2003), Bendapudi et al. (2005). Distributed models also have found wide applications due to the detail information they could provide. E.g. Distributed heat pump model developed by MacArthur and Grauld (1987) was used to simulate the transient responses of the system especially the start-up and shut-down transients. Distributed air cooler (evaporator) models developed by Jia et al. (1995, 1999) were used to investigate the effects of different flow models on the estimation of evaporator performance. Distributed refrigeration system model developed by Mithraratne et al. (2000) was used to study the stabilities of TEV controlled water cooling evaporator under typical load fluctuations such as changes in the return chilled water temperature. Distributed refrigeration system model developed by Koury et al. (2001) was used to investigate the possibility of controlling refrigeration system and refrigerant superheat degree at evaporator exit simultaneously by regulating compressor speed and throttling valve opening. Harms et al. (2004) developed two models for a unitary air conditioning system, one was detailed model that considered every circuit in heat exchangers separately, and the other was simplified model based on the assumption of identical performance of every circuit, to investigate the influences of airside heat transfer coefficient, void fraction and friction factors etc model parameters on model predictions. Simulation results indicated that model predictions were sensitive to the airside heat transfer coefficient and void fraction employed, while not sensitive to the friction factors. Both void fraction model and condenser parameters affected the compressor discharge pressure and compressor energy consumption; while the evaporator parameters mainly affected the refrigerant mass flow

rate and the heat transfer coefficients in both heat exchangers.

Void fraction, defined as the sectional area ratio occupied by the refrigerant vapor in the heat exchanger, has significant effect on heat exchanger performance. However, it is difficult to calculate its value directly. Void fraction models were developed and used to compute void fraction values, especially when the effects of refrigerant charge were considered, as the ones developed by Tandon et al. (1985), Dowlati (1996) and Harm (2004). Rice (1987), Casciaro and Thome (2001) presented comprehensive reviews on the available analytical and empirical void fraction models and stated that there was no sufficient data to justify one model was better than others and no independent database was available for the evaluation. Due to the complexity of calculation of void fraction, the concept of mean void fraction was employed to describe the overall effects of vapor refrigerant in the two-phase section in most lumped parameter models such as the ones developed by MacArthur (1984), Browne and Bansal (2002). Beck and Wedekind (1981) stated that mean void fraction was a valid assumption for most quasi-steady transitions.

2.1.2 Modeling of HVAC Systems

Coil Models

Finned-tube cross flow heating/cooling coils have wide applications in HVAC systems. Coil models describe the states of water and air inside the coil and/or at the coil outlet. Modeling of cooling coil is much more complicated than modeling of heating coil because of the complexity of mass transfer (condensation of the water vapor) involved in cooling process. The air-side tubes are wetted or partially wetted once dehumidification occurres. The description of this process is difficult and complex.

Most coil models are based on steady state analysis. Steady states of air and water

leaving the coil are calculated with empirical relations, NTU (number of transfer units) method or heat transfer effectiveness approach, as in the coil models developed by Miller (1982), Braun et al. (1989B), Hill and Jeter (1991), Khan (1994) and Wang et al. (2004).

Besides steady state models, there are dynamic coil models to describe the dynamics of the coil. One type of dynamic model uses first order plus time constant differential equation(s) to describe the coil dynamics with time constant determined through experiments and steady states of the air and water leaving the coil derived from steady state analysis, as in the coil models developed by Gartner (1972), Clark et al. (1985) and Wang (1999). This type of model is suitable for on-line applications due to its simplicity. The more detailed dynamic models are derived from theoretical analysis; differential equations are derived from the energy and mass conservation principles. This type of model can be further divided into lumped parameter models and distributed models. The coil is treated as one node or several connected nodes in lumped parameter modeling. Based on the assumption of uniform air and water thermo-physical properties for each node, ordinary differential equations are developed to describe the dynamics of water temperature, air temperature and humidity at the coil outlet, as in the coil model developed by Zheng (1997). For distributed models, heat and mass transfer analysis is performed tube by tube and the dynamics of water temperature, air temperature and humidity along the tube are described by partial differential equations in both time and space domains as in the coil models developed by Gartner and Harrison (1963, 1965, 1969) and Yao (2004).

Air-Loop Models

Air-loop model describes air flow behavior and fan pressure rise in the system

which usually includes a fan model and an air flow model. Usually, air flows in VAV system are more complex than those in CAV system because (1) the air flow rates in VAV system are determined by both fan behavior and opening of VAV dampers and (2) the modeling of variable speed fan in VAV system is more complicated than the modeling of constant speed fan.

Since time constant of fan is much less than the time constants of other components in the HVAC system, such as the coil and air conditioned space, most fan models are based on steady state analysis and derived from fan laws as in the fan models developed by Hill (1985) and Wang et al. (2000). However, in order to describe the dynamics of the air flow or fan pressure, dynamic fan model is required. Zheng (1997) developed a dynamic model for a variable speed fan with D.C. motor. Governing equations for fan motor were derived from torque balance and Kirchhoff's law. The fan speed and fan pressure gain were varied with applied voltage on the fan motor.

The methods used to model the air flows in the system are similar. First the air duct is divided into several closed circuits or sections and the pressure losses in every section/circuits are computed. Governing equations for each section/circuit are then derived from the mass conservation and pressure balance principles. The main differences in different air flow models come from the way of dividing duct into sections and the way of computing pressure losses along the duct. Zheng (1997) divided duct system into independent closed circuits. Pressure losses along every section were described as functions of the mass flow rate of the air passing that section and friction loss coefficient. Liu (2003) introduced flow resistance factor, defined as the ratio of the pressure loss to the square of the airflow rate, to describe the pressure loss. Resistance

factor was set as constant except for dampers, for which the resistance factor was determined by damper opening. Wang (1999) divided the duct system into a number of sections according to the duct length and air velocity range and assumed pressure loss of each section was constant except for losses caused by air dampers.

Zone Models

Zone model aims at describing the indoor thermal behavior and/or indoor air quality (IAQ) under the effect of HVAC system and heating/cooling load. Existing zone models vary widely in complexity from simple lumped parameter models with the assumption of perfect air mixing in the conditioned space such as the zone model developed by Zheng (1997) to complex CFD (computational fluid dynamics) models which describe detailed airflow and temperature profiles in the zone by partial differential equations in both space and time domains such as the zone models developed by Ratnam et al. (1998), Serbric et al. (2000) and Huang and Haghighat (2005). CFD zone models are more suitable for comfort studies, airflow and temperature distribution predictions, while the lumped parameter models are more practical for control studies and on-line applications. Borresen (1981) developed four simple dynamic zone models based on the assumption of good air mixing in the conditioned zone for zone air temperature control analysis. Kimbara et al. (1995) developed an autoregressive zone model to simulate the humidity ratio and temperature of the air in conditioned space using experimental data from real plant. Wang (1999) developed a zone model to simulate dynamic responses of air-conditioned space. The space was treated as connected nodes, and each node was described by its thermal resistance, thermal capacity and air volume. Assuming perfect air mixing, differential equations were derived from the energy and mass conservation

principles at each node. Kasahara et al. (2000) divided air conditioned space into five zones and described the dynamics of each zone by lumped capacity model based on physical laws. Kasahara et al. further stated that the zone dynamics could be represented by a first-order plus dead time equation. Two typical time constants were found in their study, the zone containing envelopes reached steady state much faster than the interior zones due to the small heat capacity. Borresen (1981) and Kasahara et al. (2001) all concluded that simplified first order time constant models based on good air mixing assumption were accurate enough for most control applications.

2.1.3 Black Box Models

Above mentioned models are derived from thermal and physical principles. Besides this type of theoretical models, there are other types of models derived from mapping the inputs and outputs directly, such as neural network based models, fuzzy-rule based models and polynomial fitting models. This type of black box models requires much less computations than theoretical models during simulation stage; and therefore is usually used for on-line applications. Another advantage of black box models is that when the simulation process is too complicated to be described accurately by analytical methods, black box models provide good simulation results. The disadvantages of black-box models include lacking transparency, the requirement of prior knowledge (input and output information), and the accuracy of the model relies on the quality and range of prior knowledge.

Neural networks (NNs) have been proven to be able to approximate arbitrary nonlinear functions with any predefined accuracy (Veelenturf, 1995). There are two phases to implement NN based modeling. The first phase is the training phase,

experimental or simulation data are collected to train the NN. The second phase is the application phase, the NN is used to simulate process responses with given input information. If the measurements are available later, the discrepancies in the measurements and NN predictions can be used to retrain the NN to improve the accuracy.

NNs have wide applications in system modeling due to the universal approximation and error tolerance properties. Curtiss et al. (1993) modeled a reciprocating chiller and other HVAC equipment using NNs for energy management of HVAC plants. Parlos et al. (1994) developed a recurrent multi-layer NN based dynamic heat exchanger model. The model has a validity range of 5-100% of full capacity and an accuracy of 10% in off-line learning phase. Massie et al. (1998) developed a NN based chiller and ice storage tank model to simulate the chiller performance. Tanyolu (1999) developed a NN based inverse dehumidifying cooling coil identifier. NN inputs were selected through principal component analysis. Bechtler et al. (2001) used three recurrent MISO (multi-input-single-output) NNs to model the COP (coefficient of performance), compressor energy consumption and chilled water supply temperature for a vapor-compression liquid screw chiller. Mei and Levemore (2002) developed a NN-based fan model to simulate the pressure rise of a variable speed fan under steady state with experimental data. Compared with polynomial curve fitting model, NN-based model was more accurate. An evaporator was modeled by Nanayakkara et al. (2002) with a combination of lumped parameter model and a NN. Dynamic synaptic unit is proposed to enhance the information processing capacity of neurons. A NN controller was proposed to control the evaporator heat flow rate and secondary fluid outlet temperature while keeping the refrigerant superheat degree at the evaporator exit within a suitable range by manipulating

refrigerant and evaporator secondary fluid flow rates. Xu et al. (2005) developed a NN based dynamic model for air-conditioned zones and heat exchanger to realize the optimal control of the air handling unit. Zhang et al. (2005) developed a NN model to simulate the dynamic responses of an AHU, and another NN based controller was used to control the indoor temperature and maintain the indoor humidity less than 70% by adjusting the chilled water valve opening and supply fan speed.

2.1.4 Software Packages

Besides all kinds of models developed by individual researchers, there are also some simulation packages available to simulate HVAC&R systems, e.g. HVACSIM+ for HVAC system/component simulation plus HVAC controls, building envelope, and energy management and control system algorithms; TRNSYS for transient building and mechanical system simulation; BLAST for building load and system thermodynamics simulation; DOE-2 for building hourly energy consumption simulation; ESP-r for building energy consumption and environmental performance simulation and EE4 CBIP for building load calculation and energy consumption simulation (http://www.eere.energy.gov/buildings/tools_directory/ alpha_list.cfm; DOE-2, 1981; Klein et al., 1983; Park et al., 1985). Some of these simulation packages are based on sequential modeling technique, such as TRNSYS and DOE-2; some are modular based, such as EenergyPlus, HVACSIM+; computer codes are developed for standard HVAC components. Users can create their own component models and store them in the database to make the platform more suitable for their case as in the study by Garde (2001).

2.2 Uncertainty analysis

The accuracy of the model prediction directly relates to model based applications. However, existing theoretical HVAC&R system models exhibit more or less uncertainties coming from three facts: (1) inadequate knowledge about complicated HVAC&R process; (2) insufficient existing theories for describing HVAC&R process precisely; and (3) lack of accurate data of some model parameters. Correspondingly, there are two types of uncertainty, one type is model based uncertainty caused by neglecting and/or inaccurately describing the process, and the other type is parameter based uncertainty caused by uncertain model parameters. Although parameter based uncertainties can be partially avoided or reduced through system identification with experimental or operating data, there are still some parameters that cannot be determined either because the relating data is not available for measurement or the experimental data scatters in certain range and the scatter range is varied from case to case, such as refrigerant mean void fraction, heat transfer coefficients and cooling loads. As a consequence, simulation results obtained from solving model equations with parameters having predetermined fixed values cannot accurately represent the possible responses of the system. In other words, the model based predictions exhibit uncertainties. Investigating the possible range of the simulation results is very important to ensure the accuracy of the model predictions.

In the last decade, fuzzy-set based approach was proposed and used to study system uncertainties caused by uncertain parameters with satisfactory results, as shown in the studies by Abdel-Tawab and Noor (1999), Biondini (2004), Bondia and Pico (2004). In these studies, the uncertain parameters are treated as fuzzy-valued parameters, bounded

by suitable minimum and maximum extremes. The extremes and membership function $\mu(x) = [0 \quad 1]$, which represents the probability distribution, vagueness, ambiguity or imprecision of the parameter, are determined from experimental data or expert knowledge. The model is then expressed as fuzzy-valued equations and analyzed using fuzzy mathematics.

The foundation of the fuzzy mathematics is the extension principle introduced by Zadeh (1965). For a fuzzy mapping, $y = f(x_1, \cdots, x_n)$:

$$\mu(y) = \begin{cases} \sup(\min(\mu(x_1), \cdots, \mu(x_n))) & \text{if } f^{-1}(y) \text{ exist} \\ 0 & \text{otherwise} \end{cases} \qquad (2\text{-}1)$$

Based on the extension principle, a set of algebraic operations on a family of fuzzy sets are defined. Thus, standard mathematical concepts are extended to compute fuzzy-valued equations. But this method is not practical, especially for nonlinear problems, because of the significant computational time and expense it required (Bonarini and Nontempi, 1994).

More recent and practical method is based on α-cut concept and interval mathematics, in which the fuzzy-valued parameters are decomposed into intervals at different α-cut level and the fuzzy algebraic computations are therefore decomposed into interval calculus at each α-cut level. The results are the α-cut of the fuzzy results at the same α-cut level. But interval mathematics based fuzzy arithmetic has two main drawbacks. One is 'over-estimation', the range of solutions obtained are more or less wider than the correct one because the interactions between fuzzy-valued parameters are neglected; and the other is so called 'wrapping effects' arising from decomposing fuzzy parameters on the corresponding domain according to α-cut and express the fuzzy

numbers as a number of intervals, as shown in Biondini (2004), Hanss (2002, 2003), Bondia and Pico (2004).

Several algorithms were developed to reduce or minimize the solution range, such as the vertex method for monotonic functions proposed by Dong (1987) and interacting algorithm proposed by Bonarini and Nontempi (1994). Interacting algorithm aims at solving model equations described by ODEs with fuzzy parameters. Connection matrix between the solution and fuzzy parameters is constructed for every time step. The elements of the connection matrix represent the sensitivity of the solution with respect to small changes in the parameters. With this matrix, the directions of the tangents to the uncertainty region change in time can be computed, thus, the range of the solution based on interval mathematics is narrowed. Vertex method is further developed by Otto (1993), Yang (1993) and Hanss (2002, 2003). To reduce the computational expense, Hanss (2002, 2003) introduced a transformation method for both monotonic, non-monotonic and mixing problems. In this approach, fuzzy variables are classified into monotonic or non-monotonic type variable and treated differently to reduce the number of simulations. Klimke (2004) extended the vertex method to a sparse grid-based fuzzy arithmetic to further reduce the number of simulations while maintaining certain accuracy providing that the system is sufficiently smooth.

2.3 Optimal Control/Operation of HVAC&R Systems

With the increasing cost of energy, more and more attention has been paid to the energy consumption in buildings and therefore motivated intensive studies on efficient operation of different HVAC&R systems or components under different operating

conditions. As a consequence, various optimal or near-optimal operation schemes have been proposed. Braun et al. (1989A, 1990), Ahn and Mitchell (2001) investigated the optimal operation of chilled water systems on the supervisory level. In the study of Braun et al. the optimal set points of relative cooling tower airflow rate, supply air temperature, supply water temperature, relative condenser water flow rate and the number of chillers in operation were determined; in the study of Ahn and Mitchell, the optimal set points for supply air temperature, chilled water temperature and condenser water temperature were determined such that the energy consumption of the plant was minimized. Shelton (1991) and Kirsner (1996) investigated the optimization of the condenser water flow rates under varied operating conditions and stated that a high condenser water flow rate provided good performance under full load condition and a lower flow rate provided better performance under partial load conditions. Lu et al. (2004) presented a model-based optimization strategy for a condenser water loop. Their study illustrated that energy efficiency of condenser water loop can be maximized by regulating the water flow rate and fan air flow rate. Hugh and Crowther (2004) investigated the optimal operation of the chilled water and cooling tower at supervisory level. Austin (1993) studied partial load characteristics of individual chillers for a multi-chiller system, the operation of the system was optimized through maximizing the performance of individual chillers. Ke et al. (1997) simulated eight ventilation control strategies in a VAV system and concluded that the supply air temperature and supply air flow rate were two proper optimization parameters on the air side of the HVAC system. Engdahl and Johansson (2004) determined the optimal discharge air temperature with respect to the energy consumption of the HVAC unit and examined the proposed schemes on a VAV system with 100%

outdoor air. Zheng (1997) investigated the optimal operation of a multi-zone VAV system with multi-stage operating conditions, the optimal set points for the discharge air temperature, supply water temperature, flow rates of air entering zones were determined and examined through open-loop simulations. Cascia (2000) proposed a near-optimal control strategy to determine global set points for chilled water temperature, hot water temperature, coil discharge air temperature, variable speed fan static pressure and variable speed chilled water pump differential pressure based on data collected by EMS with the assumption of quasi-steady-state load, fixed chilled water temperature difference, and fixed enthalpy difference of the air leaving and entering the cooling coil during the optimization calculations. Wang and Jin (2000) realized on-line optimal control of a HVAC system which included CAV and VAV AHUs, a chiller, a pump, a supply fan and a return fan. Based on identification models, the optimal AHU supply air temperature, fresh air flow rate and chilled water supply temperature were determined. Lu et al. (2005) investigated the optimal operation of a HVAC&R system. With the assumption of constant mass flow rate of condenser water, constant supply temperature of condenser water and using the air temperature at the cooling coil inlet, the number of chillers, chilled water pumps and cooling coil fans in operation, air flow rate into each zone and chilled water supply temperature were determined to minimize the energy consumption of the chillers, fans and pumps. Simulation or experimental results from these studies all indicated significant energy savings through optimal operation of HVAC&R components or systems, such as simulation results of Lu et al. (2004) showed that compared to operation schemes with fixed condenser water flow, the optimal operation scheme saved nearly 50% and 10% energy for very low partial load conditions

and full load condition respectively. Energy saving was mainly from operating the condenser water pump and the cooling tower fans at low speeds. The study of Engdahl and Johansson (2004) showed that compared to the constant discharge air temperature scheme, at least 8% energy saving could be achieved by optimizing the discharge air temperature. A monthly saving of 3%-14% in KWH, with an average saving around 4.5% for a real plant was observed in the study by Cascia (2000).

The main difference between optimal control and conventional control is that in optimal control, a performance index or cost function is minimized or maximized over a given operation horizon through regulating controlled variables. A popular cost function is the total energy consumption of the system or operation cost during operation hours as the ones used by Braun et al. (1990), Zheng (1997), Cascia (2000) and Lu et al. (2004). Besides energy consumption, some studies also included system performance index, such as indoor thermal comfort and indoor air quality (IAQ), as part of the cost function as the performance functions used by Wang and Jin (2000) and Cui (2004).

One of the key issues in solving optimal control problems is how to find the solution(s) which minimize or maximize the cost function. In order to simplify the process of searching solutions, linear or quadratic cost functions were used in some studies for which analytical solutions exist. Cui (2004) expressed the energy consumption of an AHU as a linear function of outside air intake ratio. Linear optimization approach was used to identify the optimal outdoor air flow rate aiming at minimizing the energy consumption and improving IAQ for a laboratory AHU. Braun et al. (1990), Ahn and Mitchell (2001) assumed that total energy consumption of the system could be expressed as a quadratic function of controlled and uncontrolled variables. The analytical solutions

of quadratic optimization problems were applied directly to determine the optimal set points.

However, a nonlinear cost function is inevitable in most optimal control problems because energy consumption of HVAC&R systems cannot be accurately expressed as a quadratic function or linear function. Therefore, numerical methodologies for nonlinear optimization problems have to be used. For example, House and Smith (1995) optimized the operation of a two-zone VAV heating system using traditional derivative-based method. This approach became very complicated when the number of zones increased. Sun and Reddy (2005) employed sequential quadratic programming (SQP) method to find the optimal operation solutions for a HVAC&R system based on simulation results. Cumali (1988) adopted Pontryagin maximum principle to solve the optimization problems for several buildings in real time; same methodology was used by Zheng (1997) to find the optimal control set points for multi-stage operation of multi-zone VAV systems based on a full system dynamic model. Xu et al. (2005) presented a LR (Lagrangian relaxation, a decomposition and coordinated approach) based optimization method to find the near-optimal room temperature set point schedule. Chen et al. (2005) solved optimization problem for an ice-storage air conditioning system using dynamic programming method. This method is usually applied to multi-stage, sequential decision problems, particularly for optimization problems where the objective functions are undifferentiable.

Besides above mathematical methods, generic algorithm (GA) and NNs were used to find the optimization solutions as well. GA has great success in solving mixed integer constrained nonlinear optimization problems by incorporating the operation state of a

device into chromosome as 1 (represent device in operation) and 0 (represent device standby) and therefore has wide applications in optimal control of HVAC&R systems. Sakamoto et al. (1999) employed GA to determine the optimal operation of a electric-type district heating and cooling plant based on discrete system model. Chang (2005) adopted GA to decide the optimal chiller loading for multi-chiller system through maximizing every chiller's performance efficiency. Lu (2005) and Nassif et al. (2005) used GA to find solutions for global optimal control of HVAC systems. Integrated neural network and GA was employed by Chow (2002) to optimize the operation of absorption chiller systems. Ahmed and Al-Dajani (2000) used a multi-layer feed forward NN as feedback controller to realize the optimal control of nonlinear systems. The network was trained to directly minimize a cost function comprised of the system outputs, states and inputs. Plant states were fedback to the NN as part of NN inputs. By doing so, closed-loop control was realized. Compared to the conventional control strategies such as dynamic programming, this approach is more robust in term of reducing model error and handling uncertainties in initial conditions. Block partial derivatives instead of chain rule were used to calculate the gradient of the cost function with respect to the control signals and plant states such that the interconnections of control scheme and dynamics of the plant were taken into account. Massie et al. (2004) described a neural network based optimal controller for ice thermal storage systems. In his study, four neural networks were employed, three of them were used to model the chiller and ice tank; the last one acted as a global controller, which determined hourly controller settings that minimized the total cost over prediction horizon. The supervisory controller consisted of two networks, one for training and the other for the operation, working in parallel. The

training network learned the relationship between controlled variables, uncontrolled variables and plant characteristics. The weights of the training network were passed to the predictor network. For the predictor network, the weights of uncontrolled variables were fixed and the weights of the controlled variables were adjusted to minimize the cost function. Values of controlled variables can be calculated from the corresponding weights.

2.4 HVAC&R System Controller Design

PI/PID controllers have been the most popular controllers in industry because of the simple structure and reliable control performance. Considerable studies on PID controller tuning and applications have been done, e.g. Shavit and Brandt (1982), Nesler and Stoecker (1984), Ahmed (1991), Roberts and Oak (1991), Kamimura (1994, 2002), Krakow et al. (1995), Jette et al. (1998), Kasahara et al. (1998, 2000, 2001), Rahmati et al. (2003), Virk et al. (1991), Wang et al. (2001). Before applied to a real system, PI/PID controller needs to be tuned to ensure control performance, such as reduce overshoot and rise time. Tuning methods include Ziegler-Nichols method, the ultimate sensitivity method, step response method, frequency response method, partial model matching method, optimization method, and AI techniques such as neural network, fuzzy logic control (FLC), genetic algorithm and evolutionary algorithm.

One of the challenges in PID control applications is how to deal with the time-variant conditions because not only operating conditions are varied within a wide range, but also the dynamics of the HVAC&R system are changing with both time and operating conditions. PID control with fixed control gains cannot apply consistent control

performance, especially when the operation conditions are far away from the commissioning conditions. In order to solve the control problems caused by fixed control gains and variable operating conditions, adaptive controls have been proposed and implemented in HVAC&R industry since 1980s. For example, Kamimura et al. (1994) developed a computer-aided tuning software to tune PID controller parameters if the transfer function of the controlled process is known. Seem (1998) proposed a pattern recognition adaptive-control method which adjusted proportional gain on the basis of closed-loop responses to set-point changes or load disturbances. Chen (2002) proposed an improved general predictive control (GPC) algorithm to control a floor radiant heating system. GPC law was derived from minimizing an objective function comprised of tracking error and control cost. Simulation results demonstrated that GPC had better performance than on-off and PI control in term of reducing settling time and overshoot. Xu et al. (2005) developed a two-level controller to control the discharge air temperature in VAV systems. The lower level was a conventional PID control, initial gains of the controller were determined at the commissioning stage; the higher level updated the gains to minimize of the GPC criterion once the operating conditions had large deviation from the commissioning condition. Simulation and experiment results indicated that compared to a well-tuned conventional PID controller, the proposed controller had a faster setting time and a smaller overshoot. Neural network, fuzzy logic and genetic algorithm are all found applications in the adaptive controller design and controller gains tuning, e.g. adaptive controllers proposed by Curtiss et al. (1994, 1996), Dexter and Haves (1989), Shin (1995), Huang (1997), Huang and Nelson (1999), So et al. (1995), Zaheeruddin (2004). In general, the auto-tuning process can be summarized as follows:

(1) Develop a mathematical model that represents the controlled process. The common models are first-order plus dead time models, on-line identified models and dynamic models.

(2) Define a performance index to evaluate the control performance with different controller parameters, such as the integral mean square tracking error, overshoot, rising time and settling time.

(3) Derive a mathematical formula or regulation rule to compute the optimal controller parameters based on model predictions and performance index.

(4) Perform in-situ tests or simulations to evaluate the proposed tuning method and compare it with other tuning methods.

Although SISO (single-input single-output) controllers are dominant in HVAC&R system control, neglecting coupling effects between control loops is detrimental to their performance. Since control loops are interconnected, tuning one controller may deteriorate the performance of other controllers. Krakow et al. (1995) pointed out that in order to successfully control the zone air temperature and humidity at the same time, the compressor speed and evaporator fan speed should be adjusted simultaneously due to the adverse effects between the control loops. Jette et al. (1998) studied the effects of one poorly tuned controller on the performance of other control loops in a dual duct system. Experimental results showed that tuning one control loop had different effects on other control loops. To solve the problems brought by single loop control, MIMO (multi-input-multi-output) control was proposed. He et al. (1998) designed a MIMO controller for a vapor compression refrigeration system. The nonlinear refrigeration system model was linearized around different operating points. For each selected operating point, a MIMO

controller was designed offline using linear-quadratic Gaussian (LQG) technique. Control gains and corresponding operating points were stored in a lookup table. For online application, one set of controller gains was selected from lookup table according to the operating conditions to ensure MIMO controller adapt to different operating conditions. Anderson et al. (2002) designed a MIMO controller based on robust control theory to control hot water temperature, discharge air temperature and airflow rate for heating systems. Experimental tests showed that the MIMO controller significantly improved the transient behavior of the system compared to the conventional SISO control in term of reducing response time, rejecting disturbances and improving control stabilities. Semar et al. (2003) developed a MIMO controller for a single zone VAV HVAC system based on feedback linearization and back-stepping techniques. The mass flow rates of discharge air and chilled water were manipulated to maintain desired zone air temperature and discharge air temperature in the system. Simulation results showed that the MIMO controller was able to overcome the load disturbances and maintain good tracking performance.

Generally speaking, compared to controller design of SISO systems, the controller design of nonlinear MIMO systems is much more complicated due to the coupling nature of the nonlinear systems, especially when the coupling matrix contains uncertain parameters or even uncertain functions (Betzaida et al., 1995; Zhang et al., 2002). Therefore, much less studies are available in literature for broader class of nonlinear MIMO systems. Kokototic et al. (2001) reviewed the development of the controller design of nonlinear systems and Isidori (1995) discussed different controller design methods for different types of nonlinear systems.

The design of adaptive MIMO controller for nonlinear systems remains an open question due to the complexity of such systems. Even though back stepping and feedback linearization techniques have been used to design adaptive controllers for certain MIMO systems as in studies by Ge and Wang (2004), Tong et al. (2005), Zhang (2004), the extension of such techniques to HVAC&R system control is impractical because HVAC&R system cannot satisfy the strict limitation on the system, such as the model equations should be convertible into parametric strict feedback canonical form, without over simplification and neglecting lots of important dynamics.

2.5 Summary and Conclusions

From above review, we can conclude that in order to realize optimal operation of HVAC&R systems, following three steps are indispensable: (1) developing a system model to predict the system responses under different control schemes and operating conditions; (2) selecting an optimization method to find the optimal set points and (3) designing local control to implement the optimal operation. Furthermore, it is noted that previous studies on modeling, control and operation of HVAC&R systems have one or more of following limitations:

(1) Although extensive steady state and dynamic models were developed, most models were developed either for HVAC systems or refrigeration systems or individual components. The static and dynamic behavior of HVAC systems and refrigeration systems were well studied with the assumptions of constant inlet conditions, e.g. constant supply water temperature and flowrate for HVAC system modeling and constant return water temperature for refrigeration system modeling. The overall behavior of the

HVAC&R system is neglected. In other words, the interactions between HVAC system and refrigeration system are neglected.

(2) Most studies on optimal operation of HVAC&R systems were focused on component or subsystem level, the interactions between components, control loops and interactions between buildings and HVAC&R systems were ignored or over simplified.

(3) In order to simplify the optimization process, most optimal control studies employed steady state models or adaptive models based on identification techniques to predict system behavior. The steady state models may inaccurately predict the responses and energy consumption of the HVAC&R systems since the systems are working under time-variant operating conditions. Online identification model on one hand confines its application from the long term predictions, on the other hand may result in non-optimal solution because the termination criteria for simulation and optimization problem are different. The former is based on function values, while the later is based on the gradient of the objective function and constraints. Using simplified identification models for which performance function gradients may different from those of the rigorous models and may lead to a situation where the optimality conditions are satisfied at non-optimal points (Sun, 2005). It follows that the dynamic modeling is more suitable for the optimal control of HVAC&R systems.

(4) Most studies focused either on the supervisory level to determine global optimal set points or on the local controller design and tuning. There were not many studies covering the closed loop optimal control of HVAC&R systems. The open-loop optimal control may yield unacceptable or non optimal solutions for closed-loop systems.

(5) Although many adaptive controllers were designed to control HVAC&R

systems, most of them were focused on separate control loops without considering the dynamic effects of other loops. Being a system with high coupling effects, the performance of the overall system under adaptive control is worth studying. And the results will be more instructive for controlling and operation of the real systems.

From the view point of on-line prediction, the dynamic model should not only be able to capture process dynamics accurately but also need to be simple enough to save computational time. Thus lumped parameter models are preferred over distributed models since distributed models are computationally complex and finding realistic solutions within a reasonable period is not an easy task. Although the application of NN model is very simple, NN model is not suitable for optimal control because the accuracy of NN model is doubtful once the operating condition is beyond the training data range. Based on above analysis, the main objectives of this thesis for developing and realizing online optimal control strategies for HVAC&R system can be stated as follows:

(1) Develop a full scale dynamic model of a HVAC&R system. The system includes a water cooled variable speed vapor compression chiller and a two-zone VAV system. The model will be able to simulate the dynamics of overall HVAC&R system and will be used to evaluate the control strategies and calculate energy consumption of the system.

(2) Study the effects of uncertainties in modeling and operating parameters on the HVAC&R system responses.

(3) Develop a model based supervisory optimal control strategy for the HVAC&R system. Through minimizing the energy consumption of the system over a predefined prediction horizon, the optimal set points for controlled variables including chilled water

supply temperature, discharge air temperature and AHU fan static pressure will be determined. The interactions between different subsystems of the HVAC&R system will be taken into account when determining the optimal control strategy.

(4) Design an adaptive PI control system to implement the optimal set points. The parameters of the controllers will be computed and updated on line to minimize the tracking errors.

(5) Conduct simulation runs under different conditions to investigate the dynamic responses of the system and compare the optimal control with conventional control schemes.

Chapter 3 Dynamic Model of a VAV-HVAC System with Water-Cooled Vapor Compression Chiller

A good understanding of the performance of HVAC&R mechanical and control systems is the basis of developing successful operating and control strategies for the system. In this chapter, a dynamic model is developed for a two-zone VAV-HVAC&R system to simulate the dynamic responses of the system. The model is based on energy, momentum and mass balance principles. As a modular system model, the HVAC&R model is component based; dynamic model for each component is developed first and then connected to each other according to the physical layout and corresponding input and output information to form the integrated model for the whole system. The integrated HVAC & refrigeration system model is composed of a two-zone VAV system model and a water cooled vapor compression chiller (WCVCC) model. The two-zone VAV model includes a zone model, a cooling and dehumidifying coil model, a variable speed fan model, and an air duct model. The chiller model includes an evaporator model, a condenser model, a variable speed compressor model and a thermal expansion valve model.

Open-loop simulations are performed to investigate the dynamics of the VAV system, the chiller and the integrated system. The dynamic interactions between the chiller and the VAV system and the dynamic responses under step changes in cooling load and control inputs are also presented.

3.1 Description of a Two-Zone VAV-HVAC and Refrigeration System

Figure 3-1 illustrates the schematic of a typical two-zone VAV-HVAC & refrigeration system to be considered in this study. The system consists of a water-cooled vapor compression chiller and a two-zone VAV system. The VAV system includes a cooling and dehumidifying coil, a variable speed fan, two air-conditioned zones and connecting duct. One zone represents interior zone for which the cooling load is mainly affected by internal heat gain, and the other zone represents exterior zone for which the cooling load is directly affected by the outdoor conditions. The chiller, working with Freon 22 (R22), is composed of an evaporator, a condenser, a variable speed reciprocating compressor and a thermostatic expansion valve (TEV). The variable speed fan and variable speed compressor are run by DC motors. The speed of the motor varies with the energy input.

The VAV system and the chiller are connected through chilled water. Chilled water extracts the heat from the air when flowing through the cooling and dehumidifying coil and then sent to the evaporator where the heat is delivered to the refrigerant. The cooled air from cooling coil is delivered to the air-conditioned zones. Part of the return air is exhausted to the environment; and the rest is recirculated, mixed with outdoor fresh air and sent back to the cooling coil where it is cooled by the chilled water. At the same time, refrigerant in the evaporator absorbs the heat from the water and evaporates. Vapor refrigerant is delivered to the compressor where it is compressed. The high pressure and high temperature vapor refrigerant discharged from the compressor is sent to the condenser where it is cooled by the water and condenses. The condenser water gains heat from the refrigerant and sent to the cooling tower where it is cooled by air and

recirculated to the condenser. The refrigerant leaving the condenser flows through a thermal expansion valve which causes significant pressure loss and enters the evaporator at low pressure. This cycle is repeated and thus rejecting heat from indoor air to outdoor environment.

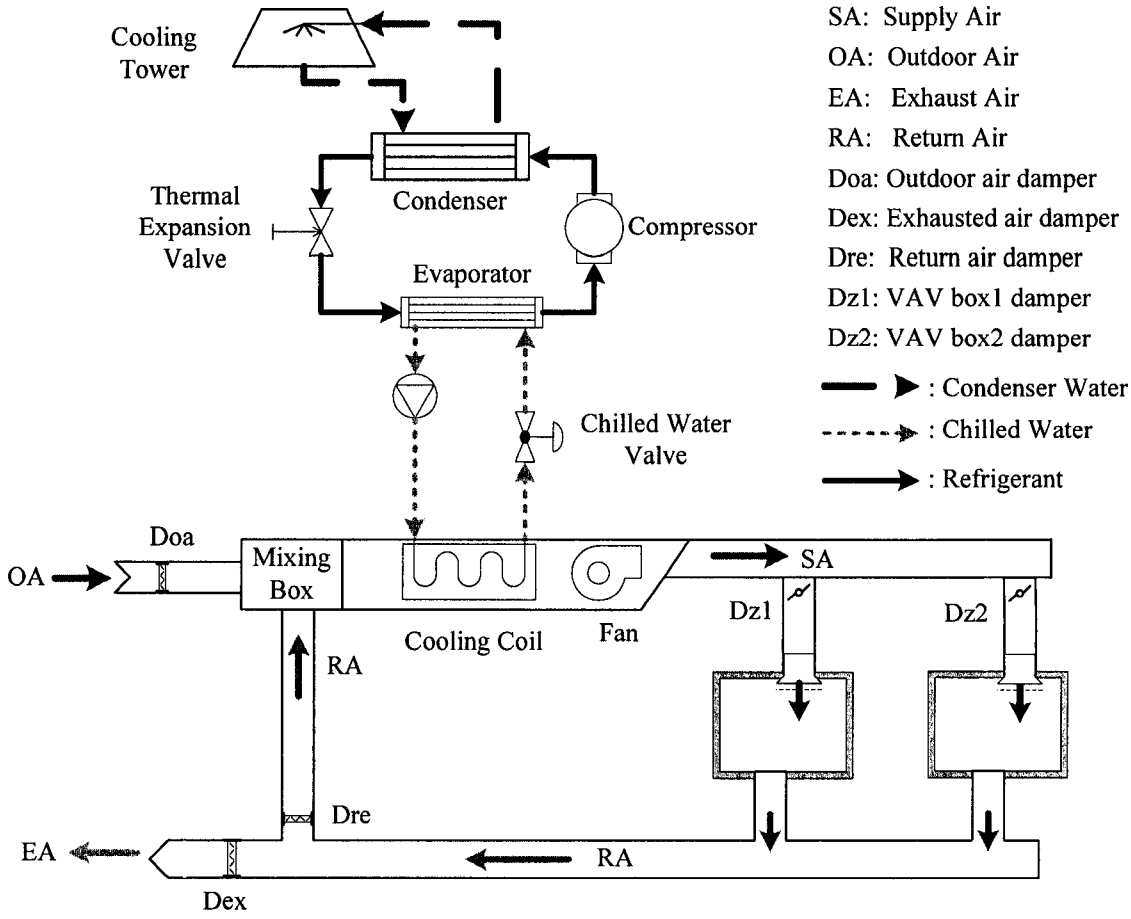

Figure 3-1 Schematic Diagram of a Typical Two-Zone VAV-HVAC&R System

In order to maintain desired indoor environment under variable operating conditions, the system has to be well controlled to operate properly and efficiently. Following controls are considered in this study:

- The AHU fan speed is controlled by modulating the normalized voltage input

to the fan motor to maintain certain static pressure at fan outlet and ensure enough air circulates in the system.

- The flow rate of the air entering each conditioned zone is controlled by modulating the corresponding VAV box damper opening to maintain the desired indoor temperature.
- The flow rate of chilled water entering the cooling coil is controlled by modulating the chilled water valve opening to maintain a given discharge/supply air temperature at the coil outlet.
- The compressor speed is controlled by modulating the normalized voltage input to the compressor motor to maintain a given supply chilled water temperature at the evaporator outlet.
- The outdoor air damper is maintained at desired opening to introduce enough fresh air into the system to satisfy the indoor air quality (IAQ) requirements.

3.2 Dynamic Model of a Two-Zone VAV System

A dynamic multi-zone VAV system model developed in an earlier study by Zheng (1997) is used to model the two-zone VAV system. The model includes a zone model, a cooling and dehumidifying coil model, an air flow model, a variable speed fan and DC motor model. The VAV system is divided into three subsystems, an airflow subsystem, a thermal subsystem and a water flow subsystem. The subsystems are modeled separately. Following assumptions are made to simplify the model development: (1) ideal gas behavior and perfect air mixing in the conditioned zones; (2) negligible infiltration and exfiltration effects; (3) no leakage from ductwork.

3.2.1 Airflow Subsystem Model

The airflow subsystem includes the variable speed fan and air duct. The airflow model describes the dynamics of the fan motor and the air flows. As illustrated in Figure 3-2, the representative air flows in the two-zone VAV system include outdoor fresh air, exhaust air, recirculated air, total supply air, return air, air entering zone1 and zone2. The corresponding mass flow rates are noted as $\dot{m}_{oa}$, $\dot{m}_{ex}$, $\dot{m}_{re}$, $\dot{m}_{a}$, $\dot{m}_{return}$, $\dot{m}_{z1}$ and $\dot{m}_{z2}$. Based on the assumption of no air leakage, and from the mass conservation principle, we have:

$$\dot{m}_{oa} = \dot{m}_{ex}, \quad \dot{m}_{ex} + \dot{m}_{re} = \dot{m}_{a} = \dot{m}_{return}, \quad \dot{m}_{z1} + \dot{m}_{z2} = \dot{m}_{a} \qquad (3\text{-}1)$$

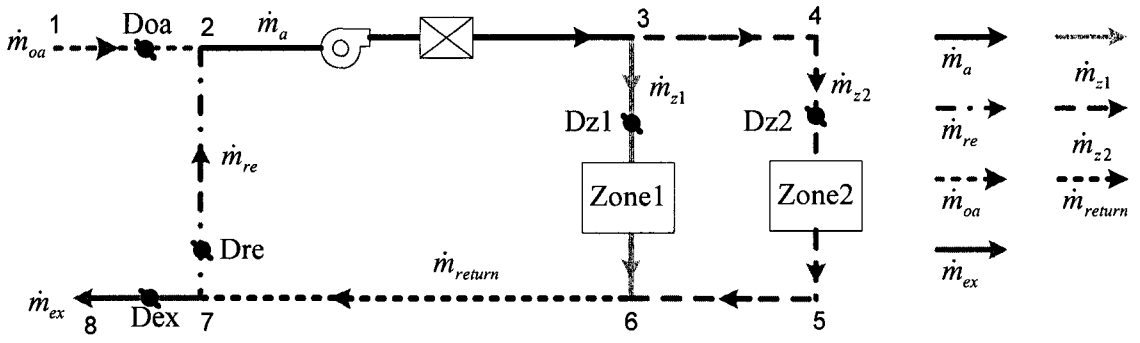

Figure 3-2 Air Flow Loops in a Two-Zone VAV-HVAC System

Therefore, three independent air flow loops are sufficient to describe the airflow characteristics of the two-zone system. Mass flow rate of the fresh air $\dot{m}_{oa}$, mass flow rate of the air entering into zone1 $\dot{m}_{z1}$ and zone2 $\dot{m}_{z2}$ and three circuits, loop1-2-7-8, loop 2-3-6-7-2 and loop 2-3-4-5-6-7-2 (Figure 3-2) are selected in this study. Governing equations for selected airflow loops are derived from principles of continuity, momentum conservation and pressure balance as follows:

$$\left(\sum_{1-2-7-8}\frac{L}{A_c}\right)\frac{d\dot{m}_{oa}}{dt}-\left(\sum_{2-7}\frac{L}{A_c}\right)\frac{d\dot{m}_{z1}}{dt}-\left(\sum_{2-7}\frac{L}{A_c}\right)\frac{d\dot{m}_{z2}}{dt} = -\sum_{1-2,7-8}\Delta P_{loss}+\sum_{2-7}\Delta P_{loss}-\Delta D_{oa}-\Delta D_{ex}+\Delta D_{re} \quad (3\text{-}2)$$

$$-\left(\sum_{7-2}\frac{L}{A_c}\right)\frac{d\dot{m}_{oa}}{dt}+\left(\sum_{2-3-6-7-2}\frac{L}{A_c}\right)\frac{d\dot{m}_{z1}}{dt}+\left(\sum_{2-3,6-7-2}\frac{L}{A_c}\right)\frac{d\dot{m}_{z2}}{dt} = \Delta P_{fan}-\sum_{2-3-6-7-2}\Delta P_{loss}-\Delta D_{z1}-\Delta D_{re} \quad (3\text{-}3)$$

$$-\left(\sum_{7-2}\frac{L}{A_c}\right)\frac{d\dot{m}_{oa}}{dt}+\left(\sum_{2-3,6-7-2}\frac{L}{A_c}\right)\frac{d\dot{m}_{z1}}{dt}+\left(\sum_{2-3-4-5-6-7-2}\frac{L}{A_c}\right)\frac{d\dot{m}_{z2}}{dt} = \Delta P_{fan}-\sum_{2-3-4-5-6-7-2}\Delta P_{loss}-\Delta D_{z2}-\Delta D_{re} \quad (3\text{-}4)$$

where, ΔD_{oa}, ΔD_{ex}, ΔD_{re}, ΔD_{z1} and ΔD_{z2} are pressure loss at outdoor air damper, exhaust air damper, return air damper, zone1 and zone2 VAV box damper respectively. Relationship of damper pressure loss and damper opening is derived from damper's characteristic curves. ΔP_{fan} is air pressure gain from fan; ΔP_{loss} is pressure losses when air flowing through corresponding duct; L is duct length and A_c is duct cross-sectional area.

The speed of the fan is modulated by regulating the input voltage to the motor. The governing equations for the motor are derived from torque balance, power balance and Kirchhoff's law, and they are given below.

$$\frac{dN_{fan}}{dt}=\frac{k_{i,fan}I_{fan}}{2\pi J_{eq,fan}}-\frac{B_{eq,fan}}{J_{eq,fan}}N_{fan}-\frac{\dot{m}_a\Delta P_{fan}}{(2\pi)^2\rho_a N_{fan}\eta_{fan}J_{eq,fan}} \quad (3\text{-}5)$$

$$\text{with } J_{eq,fan}=J_{m,fan}+J_{fan}(RN_{fan})^2;\quad B_{eq,fan}=B_{m,fan}+B_{fan}(RN_{fan})^2$$

$$L_{a,fan}\frac{dI_{fan}}{dt}=U_{fan}e-R_{a,fan}I_{fan}-2\pi k_{b,fan}N_{fan} \quad (3\text{-}6)$$

$$\Delta P_{fan}=C_h\rho_a {D_{fan}}^2 {N_{fan}}^2(RN_{fan})^2 \quad (3\text{-}7)$$

where N_{fan} is fan rotational speed; I_{fan} is motor current; U_{fan} is normalized voltage input to fan motor; D_{fan} is diameter of fan blades; η_{fan} is fan efficiency; C_h is fan pressure head coefficient; RN_{fan} is speed ratio of motor and fan; $k_{i,fan}$ is torque constant; $J_{eq,fan}$ is equivalent moment of inertia; $B_{eq,fan}$ is equivalent frictional factor; $L_{a,fan}$ is armature inductance; e is armature voltage, $R_{a,fan}$ is armature resistance, $k_{b,fan}$ is back emf constant; and ρ_a is air density.

3.2.2 Thermal Subsystem Model

The thermal subsystem includes the typical counter-cross-flow cooling and dehumidifying coil and two conditioned zones. Governing equations are derived from energy and mass conservation principles.

Cooling and Dehumidifying Model

Eq. (3-8)-(3-11) describe the dynamics of the cooling and dehumidifying coil, in which Eq. (3-8) and (3-9) describe dynamics of discharge air temperature and humidity; Eq. (3-10) describes time responses of mean tube wall temperature; Eq.(3-11) describes dynamics of return water temperature.

$$\begin{aligned} m_{a,cc}c_{a,v}\frac{dT_{a,\sup}}{dt} = &-\dot{m}_a c_{a,p}(T_{a,\sup} - T_{a,cc,in}) - h_{a,cc}\eta_{s,ov}A_{a,cc}(\overline{T}_{a,cc} - \overline{T}_{t,cc}) \\ &-(c_{a,p} - c_{a,v})\dot{m}_a\overline{T}_{a,cc}(W_{a,\sup} - W_{a,cc,in}) \\ &+h_{m,cc}\eta_{m,ov}A_{a,cc}(c_w + c_{a,v} - c_{a,p})\overline{T}_{a,cc}(\overline{W}_{a,cc} - \overline{W}_{t,sat})f_{w,t} \end{aligned} \quad (3\text{-}8)$$

$$m_{a,cc}\frac{dW_{a,\sup}}{dt} = -\dot{m}_a(W_{a,cc,out} - W_{a,cc,in}) - h_{m,cc}\eta_{m,ov}A_{a,cc}(\overline{W}_{a,cc} - \overline{W}_{t,sat})f_{w,t} \quad (3\text{-}9)$$

$$\frac{d\overline{T}_{t,cc}}{dt} = \frac{1-\eta_s}{\eta_s + \frac{m_{t,cc}c_t}{m_{fin,cc}c_{fin}}}\left(\left(\frac{1}{m_{a,cc}c_{a,v}} + \frac{1}{m_{fin,cc}c_{fin}(1-\eta_s)}\right)\eta_{s,ov}h_{a,cc}A_{a,cc}(\overline{T}_{a,cc} - \overline{T}_{t,cc})\right.$$
$$- \frac{h_{w,cc}A_{w,cc}}{m_{fin,cc}c_{fin}(1-\eta_s)}(\overline{T}_{t,cc} - \overline{T}_{w,cc}) + \frac{\dot{m}_a c_{a,p}}{m_{a,cc}c_{a,v}}(T_{a,\sup} - T_{a,cc,in})$$
$$+ \frac{(c_{a,p} - c_{a,v})\,\dot{m}_a \overline{T}_{a,cc}}{m_{a,cc}c_{a,v}}(W_{a,\sup} - W_{a,cc,in})$$
$$\left. + \left((c_{a,p} - c_{a,v} - c_w)\frac{\overline{T}_{a,cc}}{m_{a,cc}c_{a,v}} + \frac{i_{fg,w}}{m_{fin,cc}c_{fin}(1-\eta_s)}\right)h_{m,cc}\eta_{m,ov}A_{a,cc}(\overline{W}_{a,cc} - \overline{W}_{t,sat})f_{w,t}\right) \quad (3\text{-}10)$$

$$m_{w,cc}c_w\frac{dT_{w,re}}{dt} = \dot{m}_{w,cc}c_w(T_{w,\sup} - T_{w,re}) + h_{w,cc}A_{w,cc}(\overline{T}_{t,cc} - \overline{T}_{w,cc}) \quad (3\text{-}11)$$

where, $T_{w,\sup}$ and $T_{w,re}$ are chilled water supply temperature and return temperature, they are same as water temperature at the coil inlet and outlet; $T_{a,cc,in}$, $W_{a,cc,in}$, $T_{a,\sup}$, and $W_{a,\sup}$ are temperature and humidity ratio of the air entering and leaving the coil; $\overline{T}_{a,cc}$, $\overline{T}_{w,cc}$ and $\overline{T}_{t,cc}$ are mean temperature of air, water, tube wall and fins in the coil; $\overline{W}_{a,cc}$ is mean humidity ratio of the air in the coil; $\overline{W}_{t,sat}$ is humidity ratio of saturated air at wall temperature; $\dot{m}_a$ and $\dot{m}_{w,cc}$ are mass flow rates of the air and the water flowing into the coil; $m_{a,cc}$ and $m_{w,cc}$ are mass of the air and the water contained in the coil; $m_{t,cc}$ and $m_{fin,cc}$ are mass of tubes and fins of the coil; $c_{a,v}$ and $c_{a,p}$ are specific heat of air under constant volume and constant pressure respectively; c_w, c_t and c_{fin} are specific heat of water, tube material and fin material; $h_{a,cc}$ and $h_{w,cc}$, $A_{a,cc}$ and $A_{w,cc}$ are heat transfer coefficients and total heat transfer areas at coil air-side and water-side respectively; $h_{m,cc}$ is mass transfer coefficient; η_s and $\eta_{s,ov}$ are fin efficiency and coil surface effectiveness

in sensible heat transfer;, $\eta_{m,ov}$ is coil surface effectiveness in mass transfer; $i_{fg,w}$ is water latent heat of vaporization; $f_{w,t}$ accounts for whether moisture condensation occurs on the tube and fin surface or not:

$$f_{w,t} = \begin{cases} 1 & \overline{W}_{a,cc} \geq \overline{W}_{t,st} \text{ condensation occures} \\ 0 & \text{otherwise} \end{cases}.$$

Equations for calculations of heat transfer coefficients, fin efficiency and surface effectiveness were adapted from McQuiston (2000).

Environmental Zone Model

The following equations describe the time rate of changes in zone air temperature and humidity ratio.

$$\rho_a V_{zi} c_{a,p} \frac{dT_{zi}}{dt} = \dot{m}_{zi} c_{a,p} (T_{a,\text{sup}} - T_{zi}) + q_{si} \quad (i = 1,2) \qquad (3\text{-}12)$$

$$\rho_a V_{zi} \frac{dW_{zi}}{dt} = \dot{m}_{zi} (W_{a,\text{sup}} - W_{zi}) + \frac{q_{li}}{i_{fg,w}} \quad (i = 1,2) \qquad (3\text{-}13)$$

where, T_{zi} and W_{zi} are temperature and humidity ratio of the i^{th} zone; q_{si} and q_{li} are sensible and latent load of the zone; V_{zi} is the volume of the zone and $i_{fg,w}$ is water latent heat of vaporization.

3.2.3 Water Flow Subsystem Model

The mass flow rate of the chilled water circulating in the system is determined by the chilled water valve opening. The relationship between water flow rate and valve opening is derived from valve characteristic curves through polynomial curving fitting as follows:

$$\dot{m}_w = \dot{m}_{w,\max}(a_0 + a_1 U_{val}^1 + a_2 U_{val}^2 + a_3 U_{val}^3) \quad (3\text{-}14)$$

where $\dot{m}_w$ is chilled water mass flow rate; $\dot{m}_{w,\max}$ is water flow rate when chilled water valve is fully open; U_{val} is normalized valve opening; and $a_0 \ldots a_3$ are fitting parameters.

3.2.4 VAV System Model

The two zone VAV system is described by Eq.(3-2)–(3-14). After establishing the geometrical parameters through steady state calculations, the dynamics of the two air conditioned zones and VAV system can be simulated by solving model equations for a given set of inputs, including control inputs such as normalized voltage input to the fan, normalized opening of air dampers and normalized chilled water valve opening; working conditions like cooling loads profiles and supply water temperature and initial conditions. Model dynamic responses include time responses of fan motor current and speed, air flow rates in the system, temperature and humidity ratio of the discharge air, chilled water flow rate, return water temperature, zone air temperature and humidity ratio. Open-loop simulation results are presented in section 3.4.

3.3 Dynamic Model of a Water Cooled Vapor Compression Chiller

The water-cooled vapor compression chiller works with R22 and is composed of a variable speed reciprocating compressor, a thermostatic expansion valve (TEV) and two heat exchangers, one is evaporator and the other is condenser. Same as the variable speed fan, motivated by a DC motor, the speed of the compressor is adjustable by modulating the energy input to the motor. The condenser and the evaporator are shell and tube type heat exchangers. In the evaporator, the refrigerant flows inside the tubes, the water flows

in the shell. In the condenser, the refrigerant flows in the shell and the condenser water flows inside the tubes.

The condenser and evaporator are modeled using the moving boundary approach. The condenser and evaporator are divided into super-heated (SH) section, two-phase (TP) section and sub-cooled (SC) section according to the exhibited refrigerant states. The length of each section varies with time since the saturated liquid and vapor boundaries move during transients. Governing equations for each section are derived from mass and energy conservation principles.

Following assumptions are made to simplify the real process: (1) one dimensional fluid flow in heat exchangers; (2) negligible pressure drop along heat exchangers; (3) negligible heat conduction along axial direction in heat exchangers; (4) uniform physical properties of fluids along transversal direction; (5) mean void fraction remains invariant in two-phase section during transient; (6) uniform tube wall temperature; (7) perfect compressor shell insulation; (8) negligible density variations of superheated vapor and sub-cooled liquid refrigerant with the change of refrigerant temperature.

3.3.1 Evaporator Model

Refrigerant enters evaporator as mixture of vapor and liquid, where it is heated by the chilled water and evaporates inside the tube. According to the refrigerant state inside the tube, the evaporator is divided into *TP* section where liquid and vapor refrigerant co-exist and *SH* section where only vapor refrigerant exists. The boundary between the *TP* and *SH* section moves with the evaporation of liquid refrigerant. Figure 3-3 illustrates refrigerant phase change and heat flow direction within the evaporator.

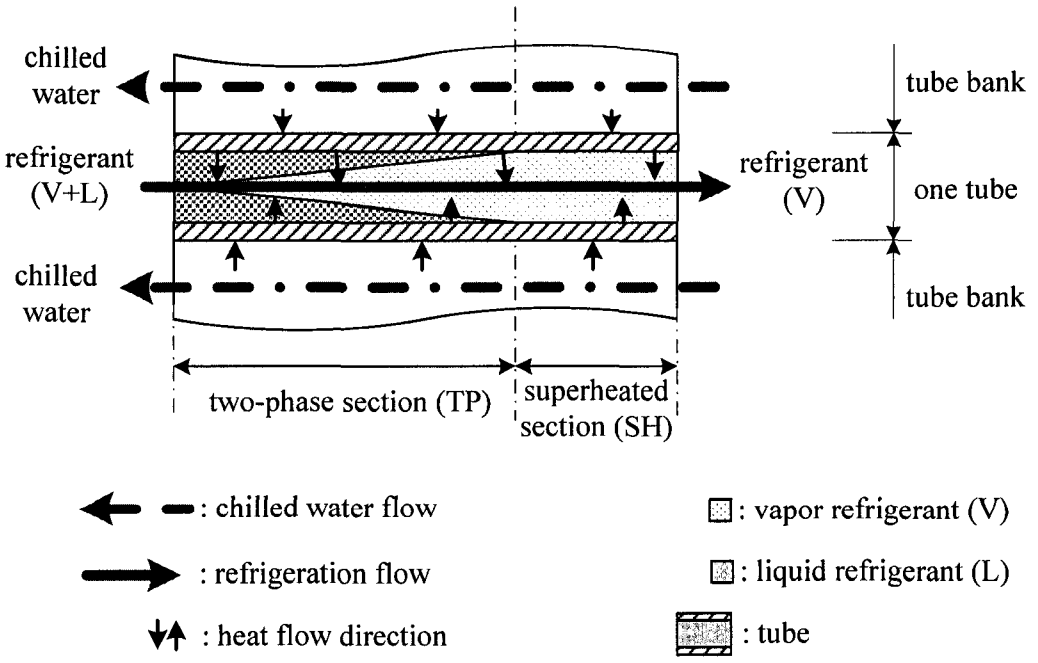

Figure 3-3 Refrigerant Phase Change and Heat Flow Direction within Evaporator

Evaporator Refrigerant Side Equations

From the mass conservation principle, for refrigerant flowing in the evaporator, following equation holds,

$$\begin{aligned} \dot{m}_{r,eva,in} - \dot{m}_{r,eva,out} &= \int_0^{Ltp,e} A_{c,r,eva} \frac{\partial \rho_r}{\partial t} dx + \int_{Ltp,e}^{Le} A_{c,r,eva} \frac{\partial \rho_r}{\partial t} dx \\ &= \int_0^{Ltp,e} A_{c,r,eva} \frac{\partial(\gamma_e \rho_{r,satv,Pe} + (1-\gamma_e)\rho_{r,satl,Pe})}{\partial t} dx + \int_{Ltp,e}^{Le} A_{c,r,eva} \frac{\partial \rho_r}{\partial t} dx \end{aligned} \quad (3\text{-}15)$$

where, $L_{tp,e}$ is length of *TP* section in the evaporator; $A_{c,r,eva}$ is inside cross-sectional area of evaporator tube; γ_e is refrigerant void fraction; $\rho_{r,satv,Pe}$ and $\rho_{r,satl,Pe}$ are densities of saturated vapor refrigerant and saturated liquid refrigerant at evaporator pressure P_e respectively. Assuming there is no accumulator in the system, refrigerant leaving the evaporator enters the condenser, vice versa. Therefore, the refrigerant mass flow rate at

the evaporator inlet $\dot{m}_{r,eva,in}$, mass flow rate of refrigerant passing through the TEV $\dot{m}_{r,TEV}$ and refrigerant mass flow rate at the condenser outlet $\dot{m}_{r,con,out}$ are equal. Mass flow rate of refrigerant at the evaporator outlet $\dot{m}_{r,eva,out}$ is equal to the mass flow rate of the refrigerant compressed by the compressor $\dot{m}_{r,COM}$, and is equal to the refrigerant mass flow rate at the condenser inlet $\dot{m}_{r,con,in}$.

Eq.(3-15) involves integration of time-dependent variable $L_{tp,e}$. Assume the density of superheated vapor refrigerant $\rho_{r,v}$ is equal to the density of saturated vapor refrigerant $\rho_{r,satv}$ under same pressure, $\rho_{r,v} = \rho_{r,satv}$, based on Leibniz integral rule:

$$\frac{d}{dz}\left(\int_{x_1(z)}^{x_2(z)} f(x,z)dx\right) = \int_{x_1(z)}^{x_2(z)} \frac{\partial f}{\partial z}dx + f(x_2(z),z)\frac{dx_2}{dz} - f(x_1(z),z)\frac{dx_1}{dz} \qquad (3\text{-}16)$$

Eq.(3-15) is rewritten as:

$$\begin{aligned}\dot{m}_{r,TEV} - \dot{m}_{r,COM} &= A_{c,r,eva}\left(\frac{d}{dt}\left(\int_0^{Ltp,e}(\gamma_e\rho_{r,satv,Pe} + (1-\gamma_e)\rho_{r,satl,Pe})dx\right) - \rho_{r,satv,Pe}\frac{dL_{tp,e}}{dt}\right) \\ &\quad + A_{c,r,eva}\left(\frac{d}{dt}\left(\int_{Ltp,e}^{Le}\rho_{r,v}dx\right) + \rho_{r,satv,Pe}\frac{dL_{tp,e}}{dt}\right) \\ &= A_{c,r,eva}(1-\bar{\gamma}_e)(\rho_{r,satl,Pe} - \rho_{r,satv,Pe})\frac{dL_{tp,e}}{dt} \\ &\quad + A_{c,r,eva}\left((L_{sh,e} + \bar{\gamma}_e L_{tp,e})\frac{d\rho_{r,satv,Pe}}{dt} + (1-\bar{\gamma}_e)L_{tp,e}\frac{d\rho_{r,satl,Pe}}{dt}\right)\end{aligned} \qquad (3\text{-}17)$$

where $L_{sh,e} = L_e - L_{tp,e}$ is length of evaporator *SH* section, $\bar{\gamma}_e$ is mean void fraction of refrigerant in evaporator *TP* section.

With chain rule $\frac{d\rho_{r,satv,Pe}}{dt} = \frac{d\rho_{r,satv,Pe}}{dP_e}\frac{dP_e}{dt}$ and $\frac{d\rho_{r,satl,Pe}}{dt} = \frac{d\rho_{r,satl,Pe}}{dP_e}\frac{dP_e}{dt}$, Eq.(3-17) is rewritten as,

$$\dot{m}_{r,TEV} - \dot{m}_{r,COM} = A_{c,r,eva}(1-\bar{\gamma}_e)(\rho_{r,satl,Pe} - \rho_{r,satv,Pe})\frac{dL_{tp,e}}{dt} + A_{c,r,eva}\left((L_{sh,e} + \bar{\gamma}_e L_{tp,e})\frac{d\rho_{r,satv,Pe}}{dP_e} + (1-\bar{\gamma}_e)L_{tp,e}\frac{d\rho_{r,satl,Pe}}{dP_e}\right)\frac{dP_e}{dt} \quad (3\text{-}18)$$

Similarly, we have following mass conservation equation for the refrigerant flowing in the evaporator *SH* section:

$$\dot{m}_{r,v,Ltp,e} - \dot{m}_{r,COM} = \int_{Ltp,e}^{Le} A_{c,r,eva}\frac{\partial \rho_r}{\partial t}dx = A_{c,r,eva}\left(\frac{d}{dt}\left(\int_{Ltp,e}^{Le}\rho_{r,v}dx\right) + \rho_{r,satv,Pe}\frac{dL_{tp,e}}{dt}\right) = A_{c,r,eva}L_{sh,e}\frac{d\rho_{r,satv,Pe}}{dP_e}\frac{dP_e}{dt} \quad (3\text{-}19)$$

where, $\dot{m}_{r,v,Ltp,e}$ is mass flow rate of the refrigerant passing through the boundary of *TP* section and *SH* section.

In addition, from the energy conservation principle, for refrigerant flowing through the evaporator *TP* section, we have following energy equation:

$$\int_0^{Ltp,e}\frac{\partial(\rho_r i_r)}{\partial t}A_{c,r,eva}dx + \int_0^{Ltp,e}\frac{\partial \dot{m}_r i_r}{\partial x}dx - \int_0^{Ltp,e}\dot{q}_{tr,eva,tp}dx = 0 \quad (3\text{-}20)$$

equivalent to:

$$\dot{m}_{r,TEV}i_{r,eva,in} - \dot{m}_{r,v,Ltp,e}i_{r,satv,Pe} + Q_{tr,eva,tp} = A_{c,r,eva}\left(\frac{d}{dt}\left(\int_0^{Ltp,e}\rho_r i_r dx\right) - \rho_{r,satv,Pe}i_{r,satv,Pe}\frac{dL_{tp,e}}{dt}\right) \quad (3\text{-}21)$$

where $i_{r,eva,in}$ is enthalpy of the refrigerant at the evaporator inlet which is equal to the enthalpy of the refrigerant leaving the TEV; $i_{r,satv,Pe}$ is enthalpy of saturated vapor refrigerant at evaporator pressure. $Q_{tr,eva,tp}$ is the total heat transferred from tube wall to the refrigerant in *TP* section, given as,

$$Q_{tr,eva,tp} = h_{r,eva} A_{r,eva} (\overline{T}_{t,e} - T_{r,sat,Pe}) L_{tp,e} \quad (3\text{-}22)$$

where $A_{r,eva}$ is heat transfer area per unit length between the refrigerant and tube wall; $\overline{T}_{t,e}$ is mean temperature of tube wall; $T_{r,sat,Pe}$ is refrigerant saturation temperature at evaporator pressure. $h_{r,eva}$ is refrigerant evaporating heat transfer coefficient, which is calculated with following equation for forced convection evaporation in tubes (ASHRAE, 2005):

$$h = 1.8\left(C_o (0.38 Fr_l^{-0.3})^n\right)^{-0.8} h_f$$

$$with \quad C_o = \left(\frac{1-x}{x}\right)^{0.8} \left(\frac{\rho_l}{\rho_v}\right)^{0.5}$$

$$Fr_l = \frac{G^2}{\rho_l g d}$$

$$n = \begin{cases} 0 & if\ Fr_l > 0.04 \\ 1 & if\ Fr_l < 0.04 \end{cases}$$

$$h_f = \begin{cases} \dfrac{\mathrm{Re}_l \mathrm{Pr}_l \left(\frac{f}{2}\right)\left(\frac{k_l}{d}\right)}{1.07 + 12.7\left(\mathrm{Pr}_l^{2/3} - 1\right)\left(\frac{f}{2}\right)^{0.5}} & if\ 0.5 \le \mathrm{Pr}_l \le 2000,\ 10^4 \le \mathrm{Re}_l \le 5*10^6 \\ \dfrac{(\mathrm{Re}_l - 1000)\mathrm{Pr}_l \left(\frac{f}{2}\right)\left(\frac{k_l}{d}\right)}{1 + 12.7\left(\mathrm{Pr}_l^{2/3} - 1\right)\left(\frac{f}{2}\right)^{0.5}} & if\ 0.5 \le \mathrm{Pr}_l \le 2000,\ 2300 \le \mathrm{Re}_l \le 10^4 \end{cases}$$

$$with \quad f = \left(1.58 \ln(\mathrm{Re}_l) - 3.28\right)^{-2}$$

(3-23)

where x is refrigerant quality, G is mass velocity, g is gravitational acceleration, d is tube internal diameter, Re_l, Pr_l, ρ_l and k_l are Reynolds number, Prandtl number, density and thermal conductivity of the liquid refrigerant, ρ_v is density of vapor refrigerant.

By substituting $\dot{m}_{r,v,Ltp,e}$ from Eq.(3-19) into Eq.(3-21), and rearranging the

equation yields,

$$\begin{aligned}
&\dot{m}_{r,TEV} i_{r,eva,in} - \dot{m}_{r,COM} i_{r,satv,Pe} + Q_{tr,eva,tp} \\
&\quad = A_{c,r,eva} \frac{d}{dt}\left(\int_0^{Ltp,e} (\gamma_e \rho_{r,satv,Pe} i_{r,satv,Pe} + (1-\gamma_e)\rho_{r,satl,Pe} i_{r,satl,Pe}) dx \right) \\
&\qquad - A_{c,r,eva} \rho_{r,satv,Pe} i_{r,satv,Pe} \frac{dL_{tp,e}}{dt} + A_{c,r,eva} L_{sh,e} i_{r,satv,Pe} \frac{d\rho_{r,satv,Pe}}{dP_e} \frac{dP_e}{dt} \qquad (3\text{-}24) \\
&\quad = A_{c,r,eva}(1-\bar{\gamma}_e)(\rho_{r,satl,Pe} i_{r,satl,Pe} - \rho_{r,satv,Pe} i_{r,satv,Pe}) \frac{dL_{tp,e}}{dt} \\
&+ A_{c,r,eva} \left(\begin{array}{c} \bar{\gamma}_e L_{tp,e} \rho_{r,satv,Pe} \dfrac{di_{r,satv,Pe}}{dP_e} + i_{r,satv,Pe}(L_{sh,e} + \bar{\gamma}_e L_{tp,e}) \dfrac{d\rho_{r,satv,Pe}}{dP_e} \\ + (1-\bar{\gamma}_e) L_{tp,e} \left(i_{r,satl,Pe} \dfrac{d\rho_{r,satl,Pe}}{dP_e} + \rho_{r,satl,Pe} \dfrac{di_{r,satl,Pe}}{dP_e} \right) \end{array} \right) \frac{dP_e}{dt}
\end{aligned}$$

Similarly, following energy equation holds for the refrigerant flowing through evaporator *SH* section:

$$\int_{Ltp,e}^{Le} \frac{\partial(\rho_r i_r)}{\partial t} A_{c,r,eva} dx + \int_{Ltp,e}^{Le} \frac{\partial \dot{m}_r i_r}{\partial x} dx - \int_{Ltp,e}^{Le} \dot{q}_{tr,eva,sh} dx = 0 \qquad (3\text{-}25)$$

equivalent to:

$$\begin{aligned}
&\dot{m}_{r,Ltp,e} i_{r,v,Pe} - \dot{m}_{r,COM} i_{eva,out} + Q_{tr,eva,sh} = \\
&\qquad A_{c,r,eva} \left(\frac{d}{dt}\left(\int_{Ltp,e}^{Le} \rho_{r,satv,Pe} i_{r,v,Pe} dx \right) + \rho_{r,satv,Pe} i_{r,satv,Pe} \frac{dL_{tp,e}}{dt} \right) \qquad (3\text{-}26)
\end{aligned}$$

where $i_{r,v,Pe}$ is enthalpy of superheated refrigerant at evaporator pressure; $Q_{tr,eva,sh}$ is total heat transferred from tube wall to the refrigerant in *SH* section, given as,

$$Q_{tr,eva,sh} = h_{r,v,e} A_{r,eva} (\overline{T}_{t,e} - \overline{T}_{r,eva,sh}) L_{sh,e} \qquad (3\text{-}27)$$

where $\overline{T}_{r,eva,sh}$ is mean temperature of the refrigerant in *SH* section, approximated as,

$$\overline{T}_{r,eva,sh} = 0.5(T_{r,sat,Pe} + T_{r,eva,out}) \qquad (3\text{-}28)$$

and $h_{r,v,e}$ is refrigerant side heat transfer coefficient in *SH* section, which is computed

with Eq.(3-28) for fully developed turbulent flow inside tubes given by Dittus and Boelter (ASHRAE, 1993):

$$h = 0.023\left(\frac{k_l}{d}\right)\mathrm{Re}^{0.8}\,\mathrm{Pr}^{n} \qquad (n = 0.4\ \textit{for heating and}\ n = 0.3\ \textit{for cooling}) \qquad (3\text{-}29)$$

where Re, Pr and k_l are Reynolds number, Prandtl number and thermal conductivity of the fluid, evaluated at mean bulk temperature. d is tube inside diameter.

By substituting $\dot{m}_{r,v,Ltp,e}$ from Eq.(3-19) and $Q_{tr,eva,sh}$ from Eq.(3-27) into Eq.(3-26), and rearranging the equation yields,

$$\begin{aligned}
&\dot{m}_{r,COM}(i_{r,satv,Pe} - i_{r,eva,out}) + \dot{Q}_{tr,eva,sh} \\
&= A_{c,r,eva}\left(\frac{d}{dt}\left(\rho_{r,satv,Pe}\bar{i}_{r,v,Pe}(L_e - L_{tp,e})\right) + \rho_{r,satv,Pe} i_{r,satv,Pe}\frac{dL_{tp,e}}{dt} - L_{sh,e} i_{r,satv,Pe}\frac{d\rho_{r,satv,Pe}}{dt}\right) \\
&= -A_{c,r,eva}\rho_{r,satv,Pe}(i_{r,satv,Pe} - \bar{i}_{r,sh,Pe})\frac{dL_{tp,e}}{dt} \\
&\qquad + A_{c,r,eva}L_{sh,e}\left((\bar{i}_{r,sh,Pe} - i_{r,satv,Pe})\frac{d\rho_{r,satv,Pe}}{dt} + \rho_{r,satv,Pe}\frac{d\bar{i}_{r,sh,Pe}}{dt}\right)
\end{aligned} \qquad (3\text{-}30)$$

where $\bar{i}_{r,sh,Pe}$ is mean enthalpy of the refrigerant in evaporator *SH* section, approximated as:

$$\bar{i}_{r,sh,Pe} = i_{r,satv,Pe} + c_{p,r,v,Pe}(\bar{T}_{r,eva,sh} - T_{r,sat,Pe}) \qquad (3\text{-}31)$$

where $c_{p,r,v,Pe}$ is specific heat of vapor refrigerant at evaporator pressure.

Substituting Eq.(3-31) into Eq.(3-30) yields,

$$\dot{m}_{r,COM}(i_{r,satv,Pe}-i_{r,eva,out})+Q_{tr,eva,sh}$$
$$=-A_{c,r,eva}\rho_{r,satv,Pe}(i_{r,satv,Pe}-\bar{i}_{r,sh,Pe})\frac{dL_{tp,e}}{dt}+0.5A_{c,r,eva}L_{sh,e}\rho_{r,satv,Pe}c_{p,r,v,Pe}\frac{dT_{r,eva,out}}{dt}$$
$$+A_{c,r,eva}L_{sh,e}\left(\begin{array}{l}(\bar{i}_{r,sh,Pe}-i_{r,satv,Pe})\dfrac{d\rho_{r,satv,Pe}}{dP_e}+\rho_{r,satv,Pe}\dfrac{di_{r,satv,Pe}}{dP_e}\\ +0.5\rho_{r,satv,Pe}\left((T_{r,eva,out}-T_{r,sat,Pe})\dfrac{dc_{p,r,v,Pe}}{dP_e}-c_{p,r,v,Pe}\dfrac{dT_{r,sat,Pe}}{dP_e}\right)\end{array}\right)\frac{dP_e}{dt} \quad (3\text{-}32)$$

Refrigerant thermal properties are evaluated at evaporator pressure with polynomial functions. Coefficients of the polynomial functions are derived through curve fitting with published ASHRAE data. With these polynomial equations, the derivatives of the thermal properties with respect to the pressure are computable.

Evaporator Tube Wall Equations

Based on the assumption of uniform tube wall temperature, the dynamics of tube wall temperature is formulated from energy conservation principle as,

$$C_{t,eva}\frac{d\bar{T}_{t,e}}{dt}=Q_{wt,eva}-Q_{tr,eva,tp}-Q_{tr,eva,sh} \quad (3\text{-}33)$$

where $C_{t,eva}$ is thermal capacity of tubes; $Q_{wt,eva}$ is total heat transferred from chilled water to tube wall in the evaporator, given as,

$$Q_{wt,eva}=h_{w,eva}A_{w,eva}(\bar{T}_{w,e}-\bar{T}_{t,e})L_e \quad (3\text{-}34)$$

where $A_{w,eva}$ is heat transfer area per unit length in the evaporator water side; $\bar{T}_{w,e}$ is mean temperature of water in the evaporator; $h_{w,eva}$ is water side heat transfer coefficient and computed with Eq. (3-35) for fluid flowing across tube banks (ASHRAE, 1993).

$$h=0.33\left(\frac{k}{d}\right)\mathrm{Re}_{\max}^{\ 0.6}\,\mathrm{Pr}^{0.36}\left(\frac{\mathrm{Pr}}{\mathrm{Pr}_{\infty}}\right)^{0.25} \quad (3\text{-}35)$$

where Pr and Pr_{∞} are fluid Prandtl numbers evaluated with fluid mean temperature and inlet temperature respectively; Re_{max} is fluid Reynolds number evaluated with maximum velocity; k is fluid thermal conductivity; and d is tube outside diameter.

Evaporator Water Side Equations

For the water flowing through the evaporator, from the energy conservation principle, we can derive following equation:

$$C_{w,eva}\frac{d\overline{T}_{w,e}}{dt} = \dot{m}_{w,eva}(T_{w,eva,in} - T_{w,eva,out}) - \dot{Q}_{wt,eva} \qquad (3\text{-}36)$$

where $C_{w,eva}$ is thermal capacity of the water contained in the evaporator; $\dot{m}_{w,eva}$ is chilled water mass flow rate, $T_{w,eva,in}$ and $T_{w,eva,out}$ is temperature of the water at the evaporator inlet and outlet respectively.

The evaporator is then described by Eqs.(3-18), (3-24), (3-32), (3-33) and (3-36). Given chilled water mass flow rate, temperature of water and refrigerant at the evaporator inlet, we can simulate the dynamics of the evaporator, which include the evaporator pressure, length of *TP* and *SH* sections, temperature of the refrigerant and water at the evaporator outlet, and mean temperature of the tube wall.

3.3.2 Condenser Model

The high pressure and high temperature vapor refrigerant discharged by the compressor is cooled by the water in the condenser and condenses at tube outside surface. According to the refrigerant state, the condenser is divided into two to three sections depending on cases, a *SH* section, a *TP* section and a *SC* section, if exists. In the *SC* section, only liquid refrigerant exists. Figure 3-4 illustrates refrigerant phase change and

heat flow directions within the condenser.

Following the same procedure used in deriving the evaporator model, the governing equations for the condenser model are derived as follows with the assumption that density of sub-cooled liquid refrigerant and superheated vapor refrigerant is equal to the density of saturated liquid and saturated vapor at the same pressure respectively: $\rho_{r,l} = \rho_{r,satl}$, $\rho_{r,v} = \rho_{r,satv}$.

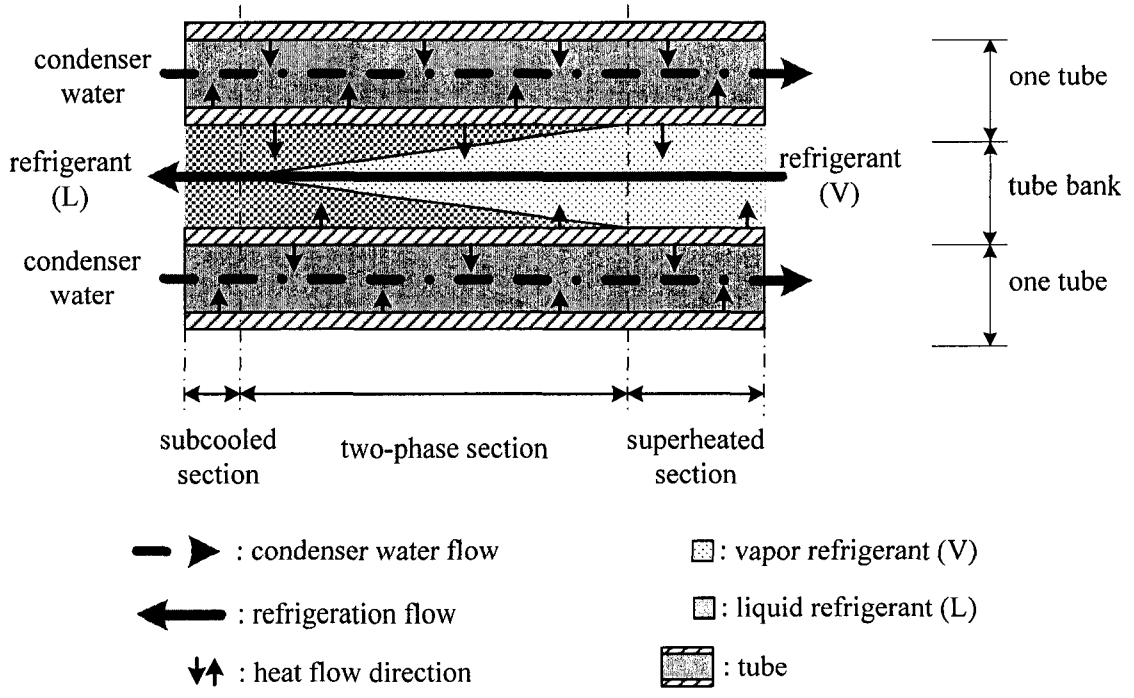

Figure 3-4 Refrigerant Phase Change and Heat Flow Directions within Condenser

Condenser Refrigerant Side Equations

According to the mass conservation principle, we have following three mass equations for the refrigerant flowing through the condenser *SH* section, *SC* section and entire condenser respectively:

$$\dot{m}_{r,COM} - \dot{m}_{r,v,con} = \int_o^{Lsh,c} A_{c,r,con} \frac{\partial \rho_r}{\partial t} dx$$
$$= A_{c,r,con}\left(\frac{d}{dt}\left(\int_o^{Lsh,c} \rho_{r,v} dx \right) - \rho_{r,satv,Pc} \frac{dL_{sh,c}}{dt} \right) = A_{c,r,con} L_{sh,c} \frac{d\rho_{r,satv,Pc}}{dP_c} \frac{dP_c}{dt} \quad (3\text{-}37)$$

$$\dot{m}_{r,l,con} - \dot{m}_{r,TEX} = \int_{Ltp-sh,c}^{Lc} A_{c,r,con} \frac{\partial \rho_r}{\partial t} dx$$
$$= A_{c,r,con}\left(\frac{d}{dt}\left(\int_{Ltp-sh,c}^{Lc} \rho_{r,l} dx \right) - \rho_{r,satl,Pc} \frac{dL_{tp-sh,c}}{dt} \right) = A_{c,r,con} L_{sc,c} \frac{d\rho_{r,satl,Pc}}{dP_c} \frac{dP_c}{dt} \quad (3\text{-}38)$$

$$\dot{m}_{r,COM} - \dot{m}_{r,TEV} = A_{c,r,con}\left(\begin{array}{l} \int_o^{Lsh,c} \frac{\partial \rho_{r,satv,Pc}}{\partial t} dx + \int_{Lsh,c}^{Ltp-sh,c} \frac{\partial (\gamma_c \rho_{r,satv,Pc} + (1-\gamma_c)\rho_{r,satl,Pc})}{\partial t} dx \\ + \int_{Ltp-sh,c}^{Lc} \frac{\partial \rho_{r,satl,Pc}}{\partial t} dx \end{array} \right)$$
$$= A_{c,r,con}(1-\bar{\gamma}_c)(\rho_{r,satv,Pc} - \rho_{r,satl,Pc}) \frac{dL_{sh,c}}{dt} + A_{c,r,con}\bar{\gamma}_c(\rho_{r,satv,Pc} - \rho_{r,satl,Pc}) \frac{dL_{tp-sh,c}}{dt}$$
$$+ A_{c,r,con}\left((L_{sh,c} + \bar{\gamma}_c L_{tp,c}) \frac{d\rho_{r,satv,Pc}}{dP_c} + ((1-\bar{\gamma}_c)L_{tp,c} + L_{sc,c}) \frac{d\rho_{r,satl,Pc}}{dP_c} \right) \frac{dP_c}{dt} \quad (3\text{-}39)$$

where $\dot{m}_{r,v,con}$ is mass flow rate of the refrigerant passing through the boundary of *SH* section and *TP* section, where the refrigerant starts to condense; $\dot{m}_{r,l,con}$ is mass flow rate of the refrigerant passing through the boundary of *TP* section and *SC* section, where all refrigerant is condensed. $A_{c,r,con}$ is inside cross-sectional area of condenser tube; $L_{sh,c}$ is length of condenser *SH* section; $L_{tp\text{-}sh,c}$ is total length of condenser *SH* section and *TP* section; $L_{tp,c} = L_{tp-sh,c} - L_{sh,c}$ is length of *TP* section; and $L_{sc,c} = L_c - L_{tp-sh,c}$ is length of condenser *SC* section; P_c is condenser pressure; $\rho_{r,satv,Pc}$ and $\rho_{r,satl,Pc}$ are density of saturated vapor refrigerant and saturated liquid refrigerant at condenser pressure; $\bar{\gamma}_c$ is refrigerant mean void fraction in condenser *TP* section.

According to the energy conservation principle, following energy equation holds

for the refrigerant flowing through condenser *SH* section:

$$\dot{m}_{r,COM} i_{r,con,in} - \dot{m}_{r,v,con} i_{r,satv,Pc} - Q_{rt,con,sh} = \int_0^{Lsh,c} \frac{d(\rho_r i_r dx)}{dt}$$
$$= A_{c,r,con}\left(\frac{d}{dt}(\rho_{r,satv,Pc}\bar{i}_{r,v,con,sh}L_{sh,c}) - \rho_{r,satv,Pc} i_{r,satv,Pc}\frac{dL_{sh,c}}{dt}\right) \quad (3\text{-}40)$$

where $i_{r,con,in}$ is enthalpy of refrigerant at the condenser inlet, which is equal to the enthalpy of refrigerant discharged by the compressor, $\bar{i}_{r,v,con,sh}$ is mean enthalpy of refrigerant in condenser *SH* section and approximated as:

$$\bar{i}_{r,v,con,sh} = i_{r,satv,Pc} + c_{p,r,v,Pc}(\bar{T}_{r,con,sh} - T_{r,sta,Pc}) \quad (3\text{-}41)$$

where $i_{r,satv,Pc}$ and $c_{p,r,v,Pc}$ are enthalpy and specific heat of saturated vapor refrigerant at condenser pressure. $\bar{T}_{r,con,sh}$ is mean temperature of refrigerant in *SH* section and approximated as,

$$\bar{T}_{r,con,sh} = 0.5(T_{r,con,in} + T_{r,sat,Pc}) \quad (3\text{-}42)$$

where $T_{r,con,in}$ is temperature of the refrigerant at the condenser inlet, and $T_{r,sat,Pc}$ is refrigerant saturation temperature at condenser pressure; $Q_{rt,con,sh}$ is total heat transferred from refrigerant to tube wall in condenser *SH* section:

$$Q_{rt,con,sh} = h_{r,con,sh} A_{r,con}(\bar{T}_{r,con,sh} - \bar{T}_{t,c}) L_{sh,c} \quad (3\text{-}43)$$

where $A_{r,con}$ is condenser refrigerant side heat transfer area per unit length; $\bar{T}_{t,c}$ is mean temperature of condenser tube wall; and $h_{r,con,sh}$ is condenser refrigerant side mean heat transfer coefficient in *SH* section, and is calculated with Eq.(3-35).

By substituting $\dot{m}_{r,v,con}$ from Eq.(3-37) into Eq.(3-40), and rearranging the equation yields,

$$\dot{m}_{r,COM}(i_{r,con,in}-i_{r,satv,Pc})-Q_{rt,con,sh}=A_{c,r,con}\rho_{r,satv,Pc}(\bar{i}_{r,v,con,sh}-i_{r,satv,Pc})\frac{dL_{sh,c}}{dt}$$
$$+A_{c,r,con}L_{sh,c}\left((\bar{i}_{r,v,con,sh}-i_{r,satv,Pc})\frac{d\rho_{r,satv,Pc}}{dP_c}+\rho_{r,satv,Pc}\frac{di_{r,satv,Pc}}{dP_c}\right. \quad (3\text{-}44)$$
$$\left.+\rho_{r,satv,Pc}(\bar{T}_{r,con,sh}-T_{r,sat,Pc})\frac{dc_{p,r,v,Pc}}{dP_c}-0.5\rho_{r,satv,Pc}c_{p,r,v,Pc}\frac{dT_{r,sat,Pc}}{dP_c}\right)\frac{dP_c}{dt}$$

Similarly, the following energy equation holds for the refrigerant flowing through the condenser *TP* section:

$$\dot{m}_{r,v,con}i_{r,satv,Pc}-\dot{m}_{r,l,con}i_{r,satl,Pc}-Q_{rt,con,tp}=\int_{Lsh,c}^{Ltp-sh,c}\frac{d(\rho_r i_r dx)}{dt}$$
$$=A_{c,r,con}\frac{d}{dt}(\bar{\gamma}_c\rho_{r,satv,Pc}i_{r,satv,Pc}+(1-\bar{\gamma}_c)\rho_{r,satl,Pc}i_{r,satl,Pc}(L_{tp-sh,c}-L_{sh,c})) \quad (3\text{-}45)$$
$$+A_{c,r,con}\rho_{r,satl,Pc}i_{r,satl,Pc}\frac{dL_{tp-sh,c}}{dt}-A_{c,r,con}\rho_{r,satv,Pc}i_{r,satv,Pc}\frac{dL_{sh,c}}{dt}$$

where $i_{r,satl,Pc}$ is enthalpy of saturated refrigerant liquid at condenser pressure; $Q_{rt,eva,tp}$ is total heat transfer from refrigerant to condenser tube wall in condenser *TP* section:

$$Q_{rt,eva,tp}=h_{r,con}A_{r,con}(T_{r,sat,Pc}-\bar{T}_{t,c})L_{tp,c} \quad (3\text{-}46)$$

where $h_{r,con}$ is condensation heat transfer coefficient computed with following equation for film type condensation (Stoecker and Jones, 1989):

$$h=0.725\left(\frac{k_l^{\,3}\rho_l^{\,2}g}{\mu_l}\right)^{0.25}\left(\frac{i_{fg}}{Nd\Delta t}\right)^{0.25} \quad (3\text{-}47)$$

where, k_l, ρ_l and μ_l are thermal conductivity, density and dynamic viscosity of the liquid fluid; i_{fg} is latent heat of vaporization; N is number of tubes in vertical row; d is outside diameter of tube; g is gravitational acceleration; Δt is temperature difference between tube wall and the fluid.

By substituting $\dot{m}_{r,v,con}$ from Eq.(3-37) and $\dot{m}_{r,l,con}$ from (3-38) into Eq.(3-45), and

rearranging the equation yields,

$$\begin{aligned}
&\dot{m}_{r,COM} i_{r,satv,Pc} - \dot{m}_{r,TEX} i_{r,satl,Pc} - Q_{rt,con,tp} \\
&= A_{c,r,con}(1-\bar{\gamma}_c)(\rho_{r,satv,Pc} i_{r,satv,Pc} - \rho_{r,satl,Pc} i_{r,satl,Pc}) \frac{dL_{sh,c}}{dt} \\
&\quad + A_{c,r,con}\bar{\gamma}_c(\rho_{r,satv,Pc} i_{r,satv,Pc} - \rho_{r,satl,Pc} i_{r,satl,Pc}) \frac{dL_{tp-sh,c}}{dt} \\
&\quad + A_{c,r,con}\left(\begin{array}{l} i_{r,satv,Pc}(L_{sh,c} + L_{tp,c}\bar{\gamma}_c)\dfrac{d\rho_{r,satv,Pc}}{dP_c} + i_{r,satl,Pc}(L_{sh,c} + (1-\bar{\gamma}_c)L_{tp,c})\dfrac{d\rho_{r,satl,Pc}}{dP_c} \\ + L_{tp,c}\left(\bar{\gamma}_c \rho_{r,satv,Pc} \dfrac{di_{r,satv,Pc}}{dP_c} + (1-\bar{\gamma}_c)\rho_{r,satl,Pc} \dfrac{di_{r,satl,Pc}}{dP_c} \right) \end{array} \right) \frac{dP_c}{dt}
\end{aligned} \tag{3-48}$$

Again, for the refrigerant flowing through condenser *SC* section, we have the following energy equation:

$$\begin{aligned}
\dot{m}_{r,l,con} i_{r,satl,Pc} - \dot{m}_{r,TEV} i_{r,con,out} - Q_{rt,con,sc} &= \int_{Ltp-sh,c}^{Lc} \frac{d(\rho_r i_r dx)}{dt} \\
&= A_{c,r,con}\left(\frac{d}{dt}\left(\rho_{r,satl,Pc} \bar{i}_{r,l,con,sc}(L_c - L_{tp,con})\right) - \rho_{r,satl,Pc} i_{r,satl,Pc} \frac{dL_{tp,con}}{dt} \right)
\end{aligned} \tag{3-49}$$

where $i_{r,con,out}$ is enthalpy of the refrigerant leaving condenser; $\bar{i}_{r,l,con,sc}$ is mean enthalpy of the refrigerant contained in condenser *SC* section, approximated as:

$$i_{r,con,out} = i_{r,satl,Pc} + c_{p,r,l,Pc}(T_{r,con,out} - T_{r,sat,Pc}) \tag{3-50}$$

$$\bar{i}_{r,l,con,sc} = i_{r,satl,Pc} + c_{p,r,l,Pc}(\bar{T}_{r,con,sc} - T_{r,sat,Pc}) \tag{3-51}$$

where i_{satl} and $c_{p,r,l}$ are enthalpy and specific heat of saturated liquid refrigerant at constant pressure, T_{sat} is saturation temperature, $T_{r,con,out}$ is temperature of the refrigerant leaving the condenser, and $\bar{T}_{r,con,sc}$ is mean temperature of refrigerant contained in *SC* section, approximated as,

$$\overline{T}_{r,con,sc} = 0.5(T_{r,con,out} + T_{r,sat,Pc}) \quad (3\text{-}52)$$

$Q_{rt,con,sc}$ is the total heat transferred from refrigerant to tube wall in condenser *SC* section,

$$Q_{rt,con,sc} = h_{r,con,sc} A_{r,con} (\overline{T}_{r,con,sc} - \overline{T}_{t,c}) L_{sc,c} \quad (3\text{-}53)$$

where $h_{r,con,sc}$ is refrigerant side heat transfer coefficient of in condenser *SC* section, which is computed with Eq.(3-35).

By substitute $\dot{m}_{r,l,con}$ from Eq.(3-38) into Eq.(3-49), and rearranging the equation yields,

$$\begin{aligned} &\dot{m}_{r,TEV}(i_{r,satl,Pc} - i_{r,con,out}) - Q_{rt,con,sc} \\ &= A_{c,r,con}\rho_{r,satl,Pc}(\bar{i}_{r,l,con,sc} - i_{r,satl,Pc})\frac{dL_{tp-sh,c}}{dt} + 0.5A_{c,r,con}L_{sc,c}c_{p,r,l,Pc}\frac{dT_{r,con,out}}{dt} \\ &+ 0.5A_{c,r,con}L_{sc,c}\rho_{r,satl,Pc}\left(\frac{di_{r,satl,Pc}}{dP_c} + (\overline{T}_{r,con,sc} - T_{r,sat,Pc})\frac{dc_{p,r,l,Pc}}{dP_c} - 0.5c_{p,r,l,Pc}\frac{dT_{r,sat,Pc}}{dP_c}\right)\frac{dP_c}{dt} \end{aligned} \quad (3\text{-}54)$$

Condenser Tube Wall Equations

Assuming uniform tube temperature, we have the following energy equation holds for tubes:

$$C_{t,con}\frac{d\overline{T}_{t,c}}{dt} = Q_{rt,con,sh} + Q_{rt,con,tp} + Q_{rt,con,sc} - Q_{tw,con} \quad (3\text{-}55)$$

where $C_{t,con}$ is thermal capacity of condenser tubes; $Q_{tw,con}$ is total heat transferred from tubes to the water in the condenser:

$$Q_{tw,con} = h_{w,con} A_{w,con} (\overline{T}_{t,c} - \overline{T}_{w,c}) L_c \quad (3\text{-}56)$$

where $A_{w,con}$ is condenser water side heat transfer area per unit length; $\overline{T}_{w,c}$ is mean water

temperature in the condenser; $h_{w,con}$ is condenser water side heat transfer coefficient, calculated with Eq.(3-29).

Condenser Water Side Equations

For the water flowing through the condenser, we have the following energy equation holds:

$$C_{w,con}\frac{d\overline{T}_{w,c}}{dt} = Q_{tw,con} - \dot{m}_{w,con}(T_{w,con,in} - T_{w,con,out}) \qquad (3\text{-}57)$$

where $C_{w,con}$ is thermal capacity of the water contained in the condenser; $\dot{m}_{w,con}$ is condenser water mass flow rate, $T_{w,con,in}$ and $T_{w,con,out}$ are temperatures of the water at the condenser inlet and outlet respectively.

The condenser model is described by Eqs.(3-39), (3-44), (3-48), (3-54), (3-55) and (3-57). For a given mass flow rate and temperature of the water and refrigerant at the condenser inlet, we can simulate the dynamics of the condenser with this model. The dynamic outputs include the time variation of the condenser pressure, length of *TP*, *SH* and *SC* sections, temperature of the refrigerant and the water at the condenser outlet, and mean tube wall temperature.

3.3.3 Thermal Expansion Valve (TEV) Model

TEV is a pressure reducing component, which connects condenser and evaporator. The main functions of TEV include: (1) regulate the flow rate of the liquid refrigerant entering the evaporator to match the rate of evaporation in the evaporator and (2) maintain certain pressure difference between the condenser and the evaporator. The flow through the TEV can be simplified as orifice flow. Based on Bernoulli and continuity

equations, the mass flow rate of the refrigerant flowing through the TEV $\dot{m}_{r,TEV}$ is modeled as:

$$\dot{m}_{r,TEV} = C_v(SH - SH_{ss})\left(\sqrt{\rho_{r,TEV,in}(P_c - P_e)}\right) \quad (3\text{-}58)$$

where, C_v is orifice coefficient of the TEV, $\rho_{r,TEV,in}$ is density of the refrigerant at the TEV inlet. SH_{ss} is static superheat degree required to overcome the spring force, which is one of TEV characteristic parameter and is assumed equal to 4°C in this study. SH is refrigerant degree of superheat at the evaporator outlet:

$$SH = T_{r,eva,out} - T_{r,sat,pe} \quad (3\text{-}59)$$

Based on the assumption of isenthalpic flow in TEV, we have:

$$h_{r,TEV,out} = h_{r,TEV,in} \quad (3\text{-}60)$$

3.3.4 Variable Speed Compressor Model

Assuming isentropic compression process, neglecting refrigerant mass variations in the compressor and heat transfer between the shell and environment, the refrigerant mass flow rate at the compressor inlet and outlet is modeled as:

$$\dot{m}_{r,COM} = N_{com}\rho_{r,suc}V_{com}\eta_{v,com} \quad (3\text{-}61)$$

where N_{com} is compressor rotational speed; V_{com} is piston displacement volume, $\rho_{r,suc}$ is density of the refrigerant at suction condition, $\eta_{v,com}$ is volumetric efficiency of the cylinder, which accounts for the re-expansion effect of the refrigerant vapor trapped in the clearance volume and is calculated as follows:

$$\eta_{v,com} = 1 + CL\left(\left(\frac{P_{r,suc}}{P_{r,dis}}\right)^{\frac{1}{K}} - 1\right) \quad (3\text{-}62)$$

where $CL = \frac{V_{clearance}}{V_{com} - V_{clearance}}$ is clearance volume ratio, assumed to be equal to 5%.

$K = \frac{c_p}{c_v}$ is effective cylinder isentropic exponent and is evaluated at inlet condition. $P_{r,suc}$ and $P_{r,dis}$ are compressor suction and discharge pressure, which are assumed to be equal to evaporator pressure P_e and condenser pressure P_c respectively.

As mentioned before, the variable speed compressor is run by a D.C. motor. By regulating the voltage applied to the motor, the motor speed is modulated, which in turn causes the variations in refrigerant mass flow rate and refrigerant cooling capacity. Therefore, the chiller cooling capacity is regulated to match the cooling load requirement by modulating the voltage input. Governing equations for the compressor motor are the same as governing equations for the variable speed fan motor described earlier and given as:

$$\frac{dN_{com}}{dt} = \frac{k_{i,com} I_{com}}{2\pi J_{eq,com}} - \frac{B_{eq,com}}{J_{eq,com}} N_{com} - \frac{W_{com}}{(2\pi)^2 N_{com}} \quad (3\text{-}63)$$

$$\text{with } J_{eq,com} = J_{m,com} + J_{com}(RN_{com})^2; \quad B_{eq,com} = B_{m,com} + B_{com}(RN_{com})^2$$

$$L_{a,com} \frac{dI_{com}}{dt} = U_{com} e - R_{a,com} I_{com} - 2\pi k_{b,com} N_{com} \quad (3\text{-}64)$$

where I_{com} is input current of motor; U_{com} is normalized input voltage to the motor; RN_{com} is speed ratio of motor and compressor; $k_{i,com}$ is compressor motor torque constant; $J_{eq,com}$ and $B_{eq,com}$ are equivalent moment of inertia and equivalent frictional factor of the

motor; $L_{a,com}$ is armature inductance; e is armature voltage, $R_{a,com}$ is armature resistance, $k_{b,com}$ is back emf constant; and W_{com} is the compressor work:

$$W_{com} = \dot{m}_{r,COM}(i_{out} - i_{in})/\eta_{com} \quad (3\text{-}65)$$

where, η_{com} is adiabatic efficiency of the compressor, accounts for the deviation of real compression process from the ideal adiabatic one, which is assumed to be equal to 80%; i_{out} and i_{in} are enthalpy of the refrigerant at the compressor inlet and outlet, which are assumed to be equal to the enthalpy of the refrigerant discharged from the evaporator and entering the condenser.

In addition, refrigerant discharge temperature is calculated based on the assumption of isentropic compression as:

$$T_{r,dis} = T_{r,suc}\left(\frac{P_{r,suc}}{P_{r,dis}}\right)^{\frac{K-1}{K}} \quad (3\text{-}66)$$

3.3.5 Water Cooled Vapor Compression Chiller Model

The chiller model is described by Eqs.(3-18), (3-24), (3-32), (3-33), (3-36), (3-39), (3-44), (3-48), (3-54), (3-55), (3-57), (3-58), (3-61), (3-63) and (3-64). Chiller's geometric parameters were established through steady state calculations. By solving above equations together, we can simulate the chiller dynamics under a set of operating conditions, which include the normalized voltage input to the compressor motor, water mass flow rate and temperature at the condenser and evaporator inlet. The dynamic outputs include condenser and evaporator pressure, refrigerant mass flow rate through the TEV and compressor, refrigerant superheat degree at the evaporator outlet, water temperature at the evaporator and condenser outlet, length of *SH*, *TP* and *SC* sections in

the evaporator and condenser; and speed of the compressor. Simulation results are presented in section 3.4.

3.4 Combined System Model and Open-Loop Simulation Results

After establishing the two-zone VAV system model and the chiller model, the integrated system model is obtained by connecting the VAV model and the chiller model together through the chilled water circuit. We assume:

(1) There is no bypass chilled water loop, therefore, the mass flow rate of the chilled water flowing through the cooling coil is equal to the mass flow rate of water flowing through the evaporator, and is determined by the chilled water valve opening.

(2) There is no heat loss during water transportation. Water temperature at the evaporator inlet is equal to the water temperature at the cooling coil outlet (return water temperature) and water temperature at the cooling coil inlet is equal to the water temperature at the evaporator outlet (supply water temperature).

Model equations are programmed using Matlab 6.0 and solved with ODE solver - ODE15s with given control inputs, loads profiles, outdoor air temperature profile and initial conditions.

Simulations were performed to investigate the HVAC & chiller dynamics under different inputs and the dynamic interactions between the chiller and VAV system. Two simulation results are presented in this section. CASE 1 focuses on the interactions between the chiller system and the VAV system. CASE 2 focuses on the dynamic responses of the system under step changes in cooling loads and control inputs.

3.4.1 Simulation - CASE 1

Chiller receives water with higher temperature from the cooling and dehumidifying coil and supplies the same amount of chilled water with lower temperature to the coil. The changes in one system affect the other through the chilled water circuit. In order to investigate the interactions between the chiller and the VAV system, three simulations were performed. The chiller and the two-zone VAV system were simulated independently first and then the integrated system was simulated with the same operation conditions. Simulation results from the integrated system and individual systems are presented and compared in this section.

Chiller Simulation

Chiller start-up process under full load condition was simulated with fully open chilled water valve, fixed water temperature and mass flow rate at the condenser inlet and fixed water temperature at the evaporator inlet as:

- $U_{com} = 1$, $U_{val} = 1$
- $T_{w,re} = 12.32\ °C$
- $T_{w,con,in} = 28\ °C$,
- $\dot{m}_{w,con} = 0.6\ kg/s$

Simulation results including the responses of compressor speed, chilled water mass flow rate, water temperature at the condenser and evaporator outlet, refrigerant mass flow rate, evaporator and condenser pressure, superheated degree, length of *SH*, *TP* and *SC* sections in the condenser and evaporator are presented in Figure 3-5.

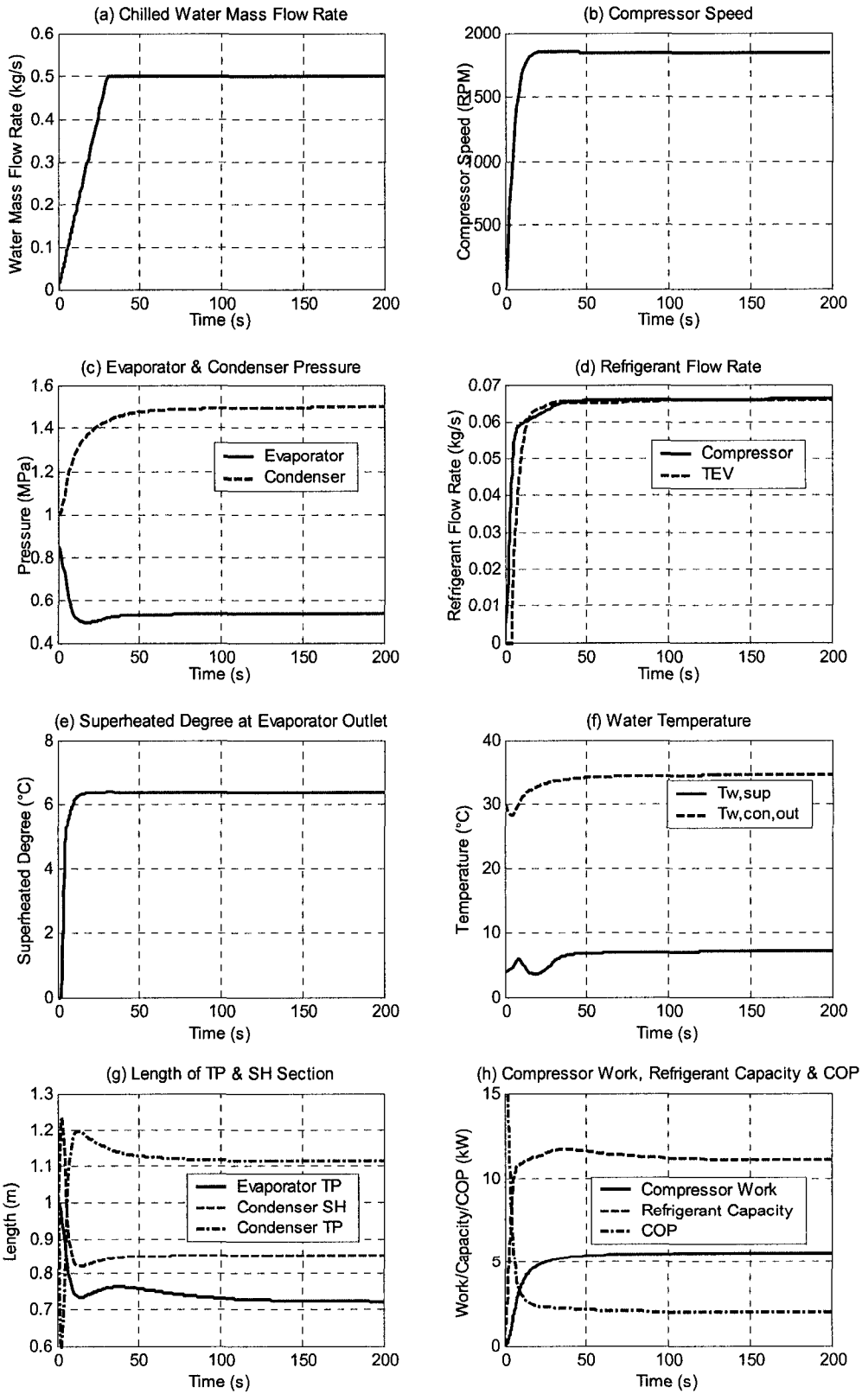

Figure 3-5 Open-Loop Simulation Results of Chiller

From Figure 3-5, we note that:

(1) With the opening of chilled water valve, the water mass flow rate increases from zero to the steady state value in 30 seconds (Figure 3-5 (a)). The steady state value is determined by the chilled water valve opening and the dynamics is related to the characteristics of the valve and the actuator. A linear valve with time constant equal to 30 seconds was assumed.

(2) Soon after the system start up, the compressor motor speed increases very fast from 0 to 1854 rpm in about 25 seconds (Figure 3-5 (b)). The mass flow rate of the refrigerant flowing through the compressor is directly related to the compressor speed, compression ratio and refrigerant states at the evaporator outlet, soon after the compressor start-up, with the increase of the compressor speed, more refrigerant is drawn into the compressor, compressed and delivered to the condenser. The mass flow rate of the refrigerant flowing through the compressor increases and reaches the steady state in about 40 seconds (Figure 3-5 (d)). With refrigerant flowing out of the evaporator and entering the condenser, the pressure and temperature of the refrigerant increase in the condenser while decrease in the evaporator. The evaporator and condenser pressure reaches steady state in about 50 seconds (Figure 3-5 (c)).

(3) The mass flow rate of the refrigerant flowing through the TEV is directly related to the degree of superheat at the evaporator outlet (Figure 3-5 (e)) and the pressure difference between the condenser and the evaporator. At the beginning, the refrigerant superheat degree is not high enough (less than SH_{ss}) to overcome the spring force and TEV remains closed and no refrigerant enters the evaporator. With the evaporation of the refrigerant, the mass, temperature and pressure of the refrigerant in the

evaporator decrease, the superheat degree at the evaporator outlet and the pressure difference between the evaporator and the condenser increase; the TEV starts to open. With the opening of the TEV, more refrigerant enters the evaporator. The mass flow rate of the refrigerant flowing through the TEV reaches steady state in about 75 seconds (Figure 3-5 (d)).

(4) As the refrigerant temperature decreases in the evaporator, the chilled water is cooled and the water temperature decreases exponentially. The heat is transferred to the condenser water through the circulation of refrigerant such that the condenser water temperature increases. Water temperature reaches steady state in about 100 seconds (Figure 3-5 (f)). The fast responses result from the high heat transfer coefficients.

(5) Figure 3-5 (g) is the changes of length of *TP* and *SH* sections with time in the evaporator and the condenser. Figure 3-5 (h) shows the calculated system performance parameters, including the refrigerant capacity ($CAPACITY$), compressor work (W_{com}) and COP (coefficient of performance) defined as:

$$CAPACITY = \dot{m}_{r,COM}(i_{eva,out} - i_{eva,in}) \qquad (3\text{-}67)$$

$$COP = \frac{CAPACITY}{W_{com}} \qquad (3\text{-}68)$$

Two-Zone VAV System Simulation

For better comparison, in VAV system simulation, the water temperature at the cooling coil inlet was set to be equal to the steady state value of the water temperature at the evaporator outlet from above chiller simulation; at the same time, the cooling loads were selected such that the steady state value of the chilled water temperature at the coil outlet was close to the water temperature at the evaporator inlet in the chiller simulation.

Chilled water valve was kept fully open. Simulation results, including dynamics of airflows in the system, fan speed, air and water temperatures at the coil outlet, and the air temperature in two zones, under following operating conditions are presented in Figure 3-6:

- $U_{val} = 1$, $U_{fan} = 1$, $U_{z1} = 1$, $U_{z2} = 1$
- $T_{w,\sup} = 7.1\,°C$
- $T_{oa} = 28\,°C$
- $Q_{s1} = 4.5\,kW$, $Q_{l1} = 1\,kW$
- $Q_{s2} = 3.6\,kW$, $Q_{l2} = 0.8\,kW$

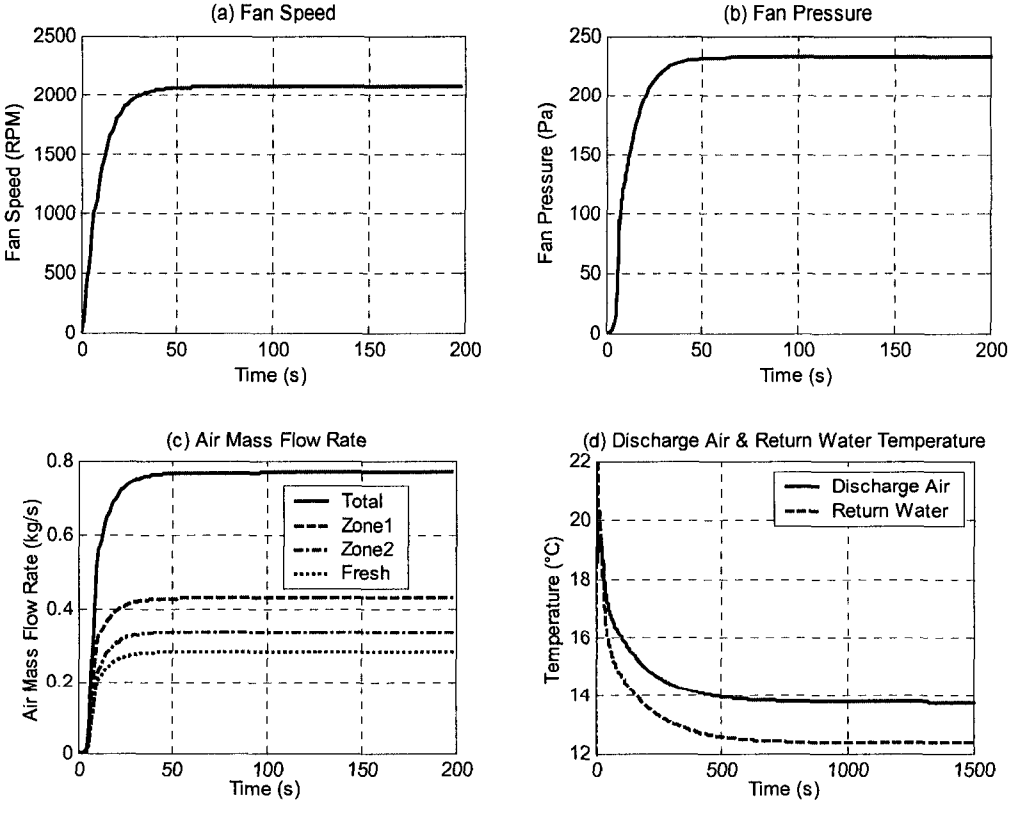

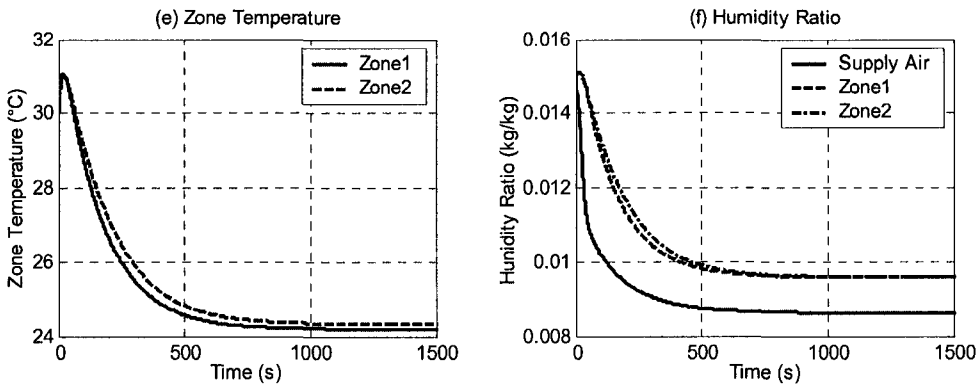

Figure 3-6 Open-Loop Simulation Results of VAV System

From Figure 3-6, we note that:

(1) Soon after the start-up, the fan motor speed increases very fast from 0 to 2070 rpm in 50 seconds (Figure 3-6 (a)). With the increase of fan speed, the fan pressure increases (Figure 3-6 (b)) causing air circulation in the duct. The dynamics of air flow follow the fan dynamics but the magnitudes are dependent on dampers' position and fan pressure gain (Figure 3-6 (c)).

(2) With the chilled water flowing through the coil, the air is cooled; the temperature and the humidity ratio of the air start to decrease while the temperature of the water increases exponentially. The magnitude of the decrease in air temperature and humidity ratio depends on the cooling capacity of the chilled water and coil efficiency. The time rate of change of air temperature and humidity ratio is determined by the coil characteristics. The steady state is reached in about 500 seconds (Figure 3-6 (d)).

(3) With the cold and dry air flowing into the air conditioned zones, the temperature and humidity ratio of zone air decrease and reach the steady states in about 1000 seconds (Figure 3-6 (e) and (f)). The dynamics depend on the zone air capacity; the higher zone air capacity, the longer it will take for the zone air to reach the steady state.

(4) The results show that there are two time scales involved in the VAV system dynamics, the dynamic responses of the fan and air flows (tens of seconds) are much faster than the responses of the coil and zone (thousands of seconds). Therefore, the dynamics of the VAV system is determined by the dynamics of the cooling coil and the air-conditioned zone.

Integrated System Simulation

In order to investigate the interactions between the VAV system and the chiller, the integrated system responses were examined with the same control inputs, initial conditions, outdoor air temperature profile and loads profiles as used in the individual systems simulations. Simulation results are presented in Figure 3-7 and Figure 3-8.

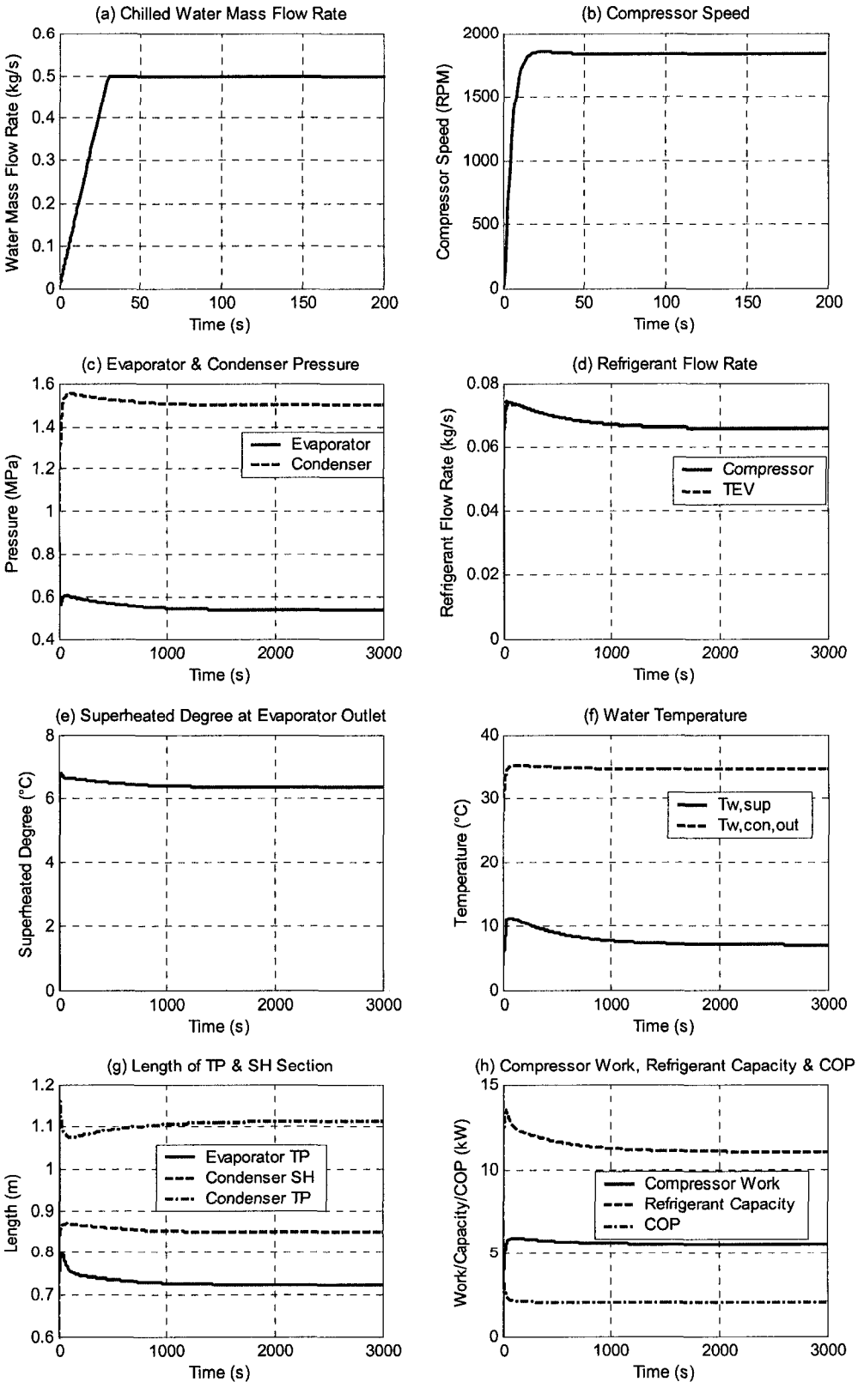

Figure 3-7 Open-Loop Simulation Results of Integrated System – Chiller

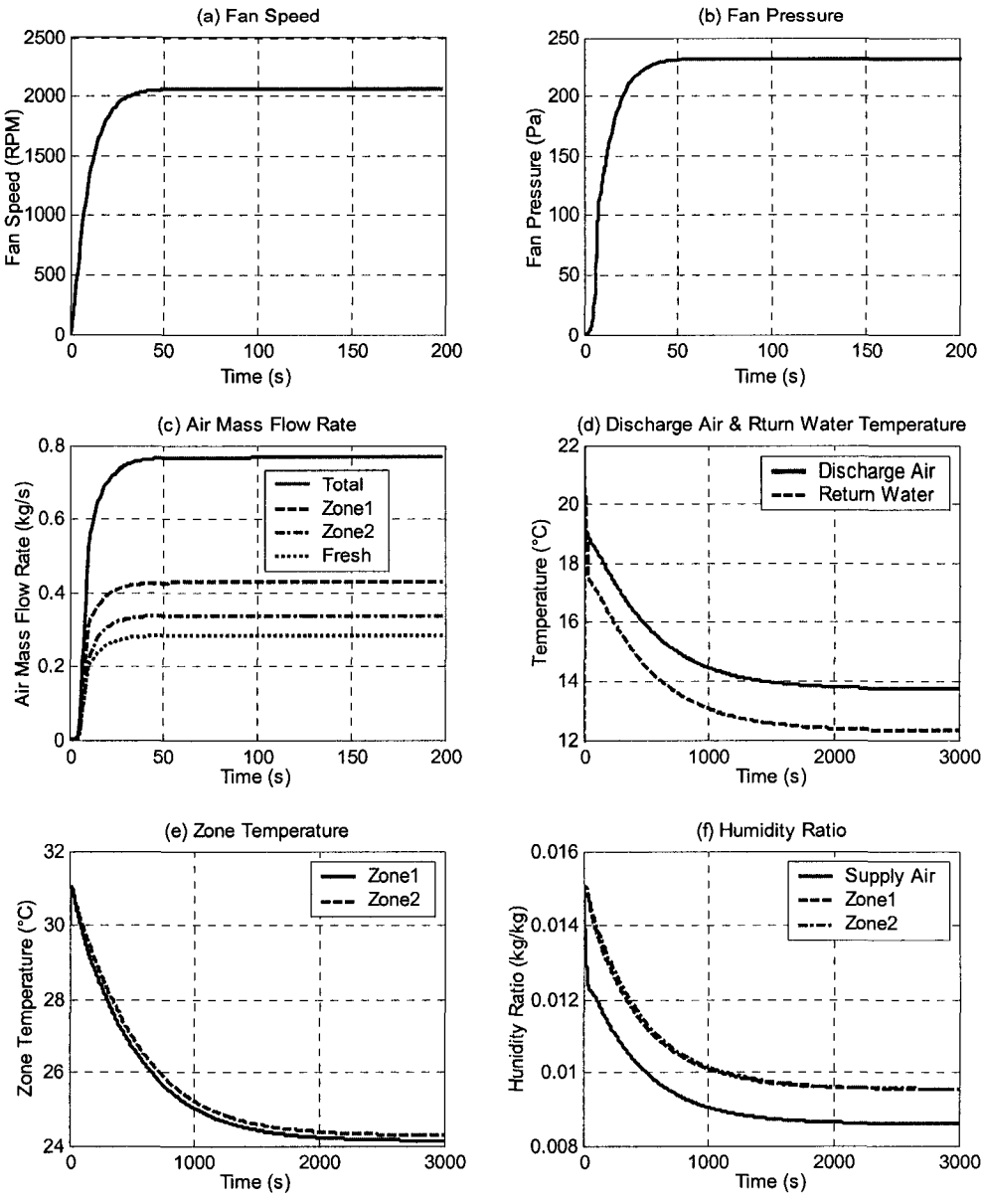

Figure 3-8 Open-Loop Simulation Results of Integrated System – VAV System

By comparing Figure 3-5 with Figure 3-7, Figure 3-6 with Figure 3-8, results reveal that:

(1) There are no significant variations in the final steady state values before and after system integration.

(2) The integrated system responses also show a two-time scale property in that

the responses of compressor speed, airflow rate, chilled water flow rate, and condenser water are much faster than the responses of chilled water, discharge air and zone air temperature. However, compared to individual systems, the ratio of time-scale in the integrated system is found to be larger.

(3) Dynamics of the compressor and the fan remain the same before and after integration because motor's dynamics are independent from the rest of the system. Consequently, there is no change in the dynamic responses of air flows. So does the responses of the chilled water flow rate which is determined by the chilled water valve and actuator, and is independent of the rest of the system.

(4) The responses of the evaporator are comparatively slower after the system integration. Compared tens of seconds before integration, chilled water supply temperature and evaporator pressure reach steady state in about 1000 second after integration. This is because the dynamics of the chilled water leaving the cooling coil affects the dynamics of the evaporator.

(5) Consequently, the responses of the refrigerant mass flow rates in the chiller are much slower after integration, reach steady state in about 1000 seconds, since refrigerant flow rate through the compressor and the TVE are directly related to the pressure difference between the condenser and the evaporator.

(6) On the other hand, dynamics of the evaporator affects the coil dynamics also. The responses of the discharge air are slower after integration, discharge air temperature and return water temperature reach steady state in about 1500 seconds.

(7) The responses of the condenser pressure and the length of *TP* and *SH* sections are slower after integration also because of the impact of the dynamics of the refrigerant

discharged from the evaporator. However, the responses of the condenser water remain fast without showing significant changes before and after integration because of the small impact of the dynamics of the evaporator and the VAV system on condenser dynamics. Compared to the evaporator and the VAV system, condenser water loop is more dependent on the cooling tower.

Above results are of interest in designing control systems. First, discharge air temperature control loop will not only be influenced by airflow and water flow modulations in the VAV system but also influenced by the compressor speed modulation in the chiller through chilled water loop, which make it more susceptible to load changes in the integrated system. Second, the condenser control loop is expected to be more stable compared to the evaporator control loop in the integrated system and therefore it is justified to decouple it in the optimization analysis. Third, the long time lags have to be compensated to improve regulation properties of controllers.

3.4.2 Simulation - CASE 2

In real buildings, the cooling load changes all the time. Consequently, in order to maintain a desired indoor environment, the operation of the HVAC&R system has to be adjusted to match the load variations. The classic on-off control usually impairs the performance of the system and increases the energy consumption. Varying the power input to the system by regulating the motor voltage input to the fan and compressor to match cooling requirements and maintain indoor temperature not only improves the performance of the system but also reduces the energy consumption at the same time.

In this section, simulations are performed to investigate the system responses under time-changing operating conditions. These simulations represent a practical operation

situation in which the cooling loads decrease and therefore the HVAC&R system is controlled to respond to the load change in one of the following three schemes:

- increase supply water temperature by reducing the energy input to the compressor U_{com};
- increase discharge air temperature by reducing the chilled water mass flow rate flowing through the cooling coil through reducing the chilled water valve opening U_{val}
- decrease the air mass flow rates to the zones by reducing energy input to the fan U_{fan} and VAV boxes damper opening U_{z1} and U_{z2}

The simulation conditions are noted below:

for $t < 2500s$:

- $\dot{m}_{w,con} = 0.6\ kg/s$, $T_{w,con,in} = 28\ °C$
- $Q_{s1} = 4.2\ kW$, $Q_{l1} = 1\ kW$
- $Q_{s2} = 3.4\ kW$, $Q_{l2} = 0.8\ kW$
- $U_{com} = 1$, $U_{val} = 1$, $U_{fan} = 1$, $U_{z1} = 1$ and $U_{z2} = 1$

for $t >= 2500s$:

- $\dot{m}_{w,con} = 0.6\ kg/s$, $T_{w,con,in} = 28\ °C$
- $Q_{s1} = 3.9\ kW$, $Q_{l1} = 0.8kW$
- $Q_{s2} = 3.1\ kW$, $Q_{l2} = 0.7kW$
- One of the following operation schemes:
  - Scheme 1: $U_{com} = 0.9$, $U_{val} = 1$, $U_{fan} = 1$, $U_{z1} = 1$, $U_{z2} = 1$

- Scheme 2: $U_{com}=1$, $U_{val}=0.5$, $U_{fan}=1$, $U_{z1}=1$, $U_{z2}=1$

- Scheme 3: $U_{com}=1$, $U_{val}=1$, $U_{fan}=0.5$, $U_{z1}=0.8$, $U_{z2}=0.7$

Simulation results of three operation schemes are illustrated in Figure 3-9, Figure 3-10 and Figure 3-11 respectively. In Table 3–1 list of steady state responses of the system before and after step changes in loads and control inputs is given. 'Base Case' indicates the steady states of the system before the step change.

Table 3–1 Effects of Step Variations of Control Inputs and Loads on System Responses

	Base Case	Scheme 1 (U_{com})	Scheme 2 (U_{val})	Scheme 3 (U_{fan} / U_{z1} / U_{z2})
T_{z1} / T_{z2} (°C)	**22.7 / 23**	22.6 /22.7	22.6 /22.7	22.5 / 22.8
Total Energy (kW)	**6.8**	6	7	6.1
Refrigeration Capacity (kW)	**10.8**	10	10	9.5
$\dot{m}_r$ (kg/s)	**0.065**	0.06	0.06	0.057
$\dot{m}_w$ (kg/s)	**0.5**	0.5	0.18	0.5
$\dot{m}_{z1}$ / $\dot{m}_{z2}$ (kg/s)	**0.43 / 0.34**	0.43 / 0.34	0.43 / 0.34	0.26 / 0.21
$T_{a,sup}$ (°C)	**13**	13.6	13.6	8.1
$T_{w,sup}$ (°C)	**6.3**	7.4	0.8	2
$T_{w,re}$ (°C)	**11.6**	12.2	14.42	6.5
Superheated Degree (°C)	**6.3**	6.2	6.14	6
P_e / P_c (Mpa)	**0.52/1.49**	0.54 / 1.44	0.49 / 1.46	0.46 / 1.43

a

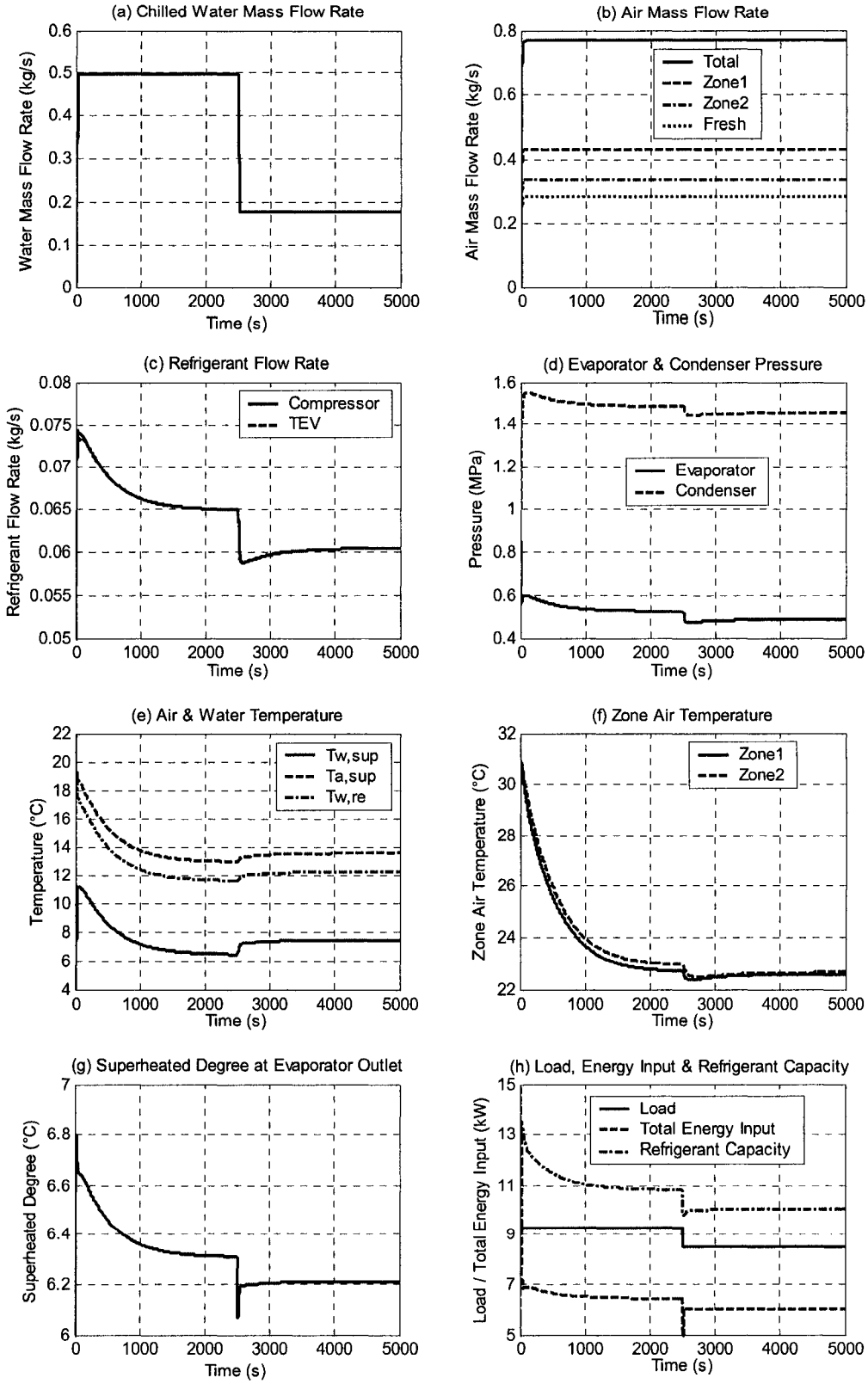

Figure 3-9 Open-Loop Simulation Results Due to a Step Change in Load & Ucom

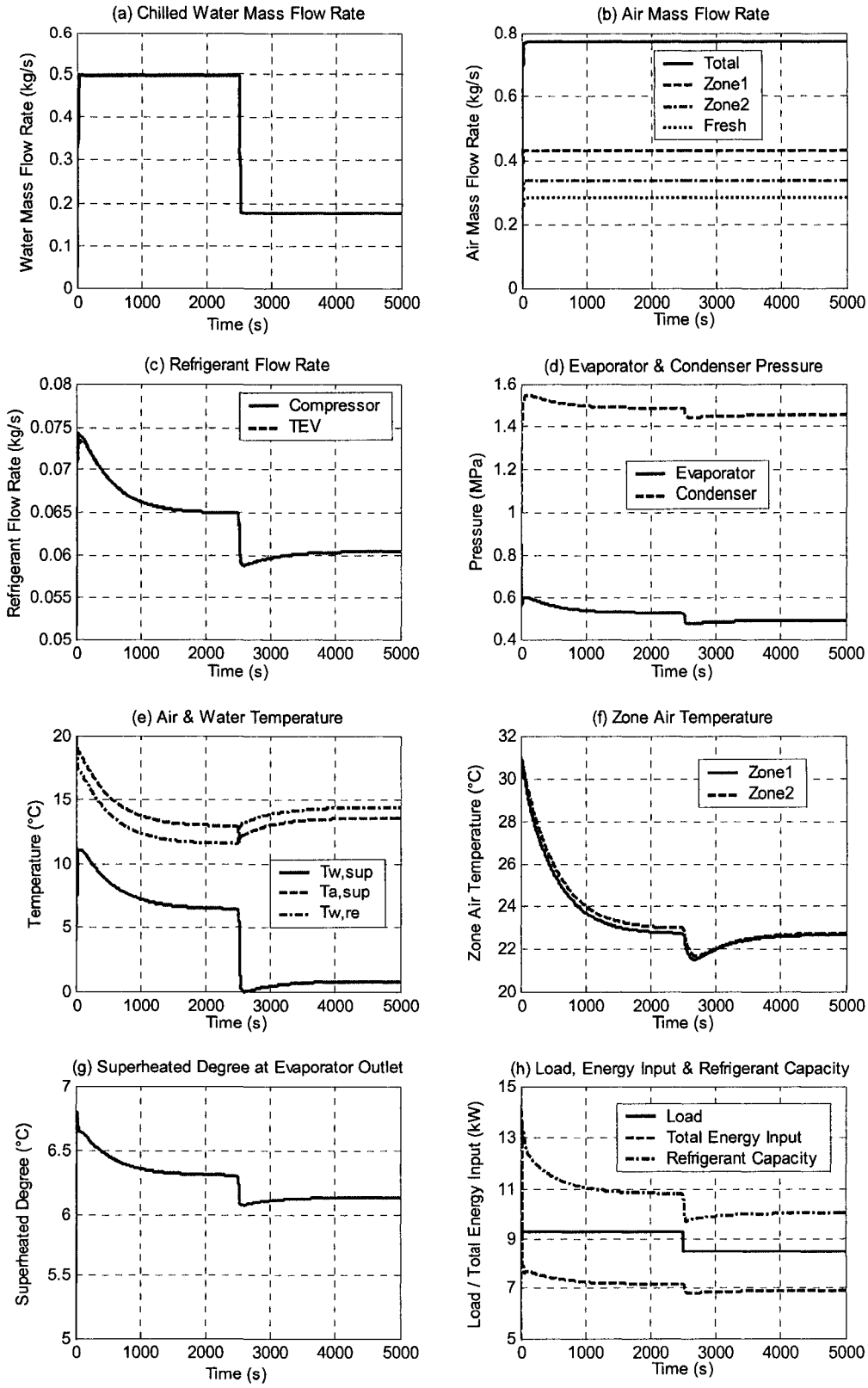

Figure 3-10 Open-Loop Simulation Results Due to a Step Change in Load & Uval

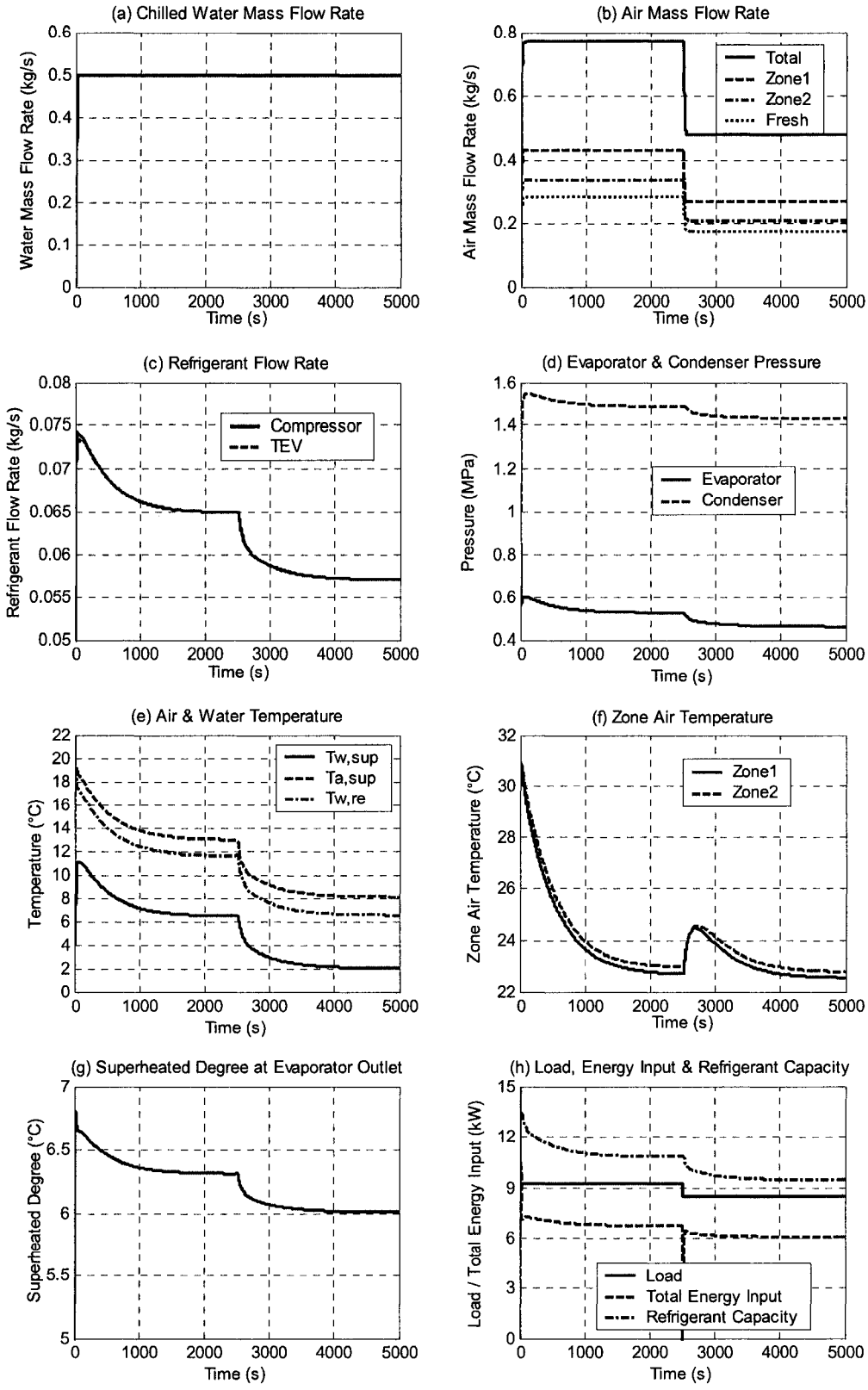

Figure 3-11 Open-Loop Simulation Results Due to a Step Change in Load, Uz1, Uz2 & Ufan

From Figure 3-9 to Figure 3-11 we note that:

(1) All of the three schemes can maintain zone1 air temperature around 22.5°C and zone2 air temperature around 22.8°C. In three cases, the refrigerant mass flow rate decreases and causes the reduction in the refrigeration capacity and therefore matches the reduced cooling requirement. In the case of U_{com} control (scheme1), the reduction of the refrigerant mass flow rate is caused by the decrease of the compressor speed, while in the cases of U_{val} control (scheme2) and $U_{fan}/U_{z1}/U_{z2}$ control (scheme3), the reduction of the refrigerant mass flow rate is caused by the lower refrigerant density at lower evaporator pressure.

(2) In the case of U_{com} control, the chilled water temperature at the evaporator outlet $T_{w,\text{sup}}$ increases because the reduction of the refrigeration capacity causes the increase in the evaporating temperature. And the temperature of the return water $T_{w,re}$ and supply air temperature T_{dis} increase consequently since the mass flow rates of the chilled water and the air are unchanged. In this scheme, zone air temperature is maintained through regulating the supply air temperature.

(3) In the case of U_{val} control, with the decrease of U_{val}, less chilled water enters the cooling coil which causes the increase in discharge air temperature. With the same energy input to the compressor, the reduction in the chilled water flow rate causes the decrease of chilled water temperature as well. In this scheme, zone air temperature is maintained through regulating the supply air temperature also.

(4) In the case of $U_{fan}/U_{z1}/U_{z2}$ control, with the reduction of U_{fan}, U_{z1} and U_{z2}, less air circulates in the system. The reduction in air flow rate causes the decrease of

discharge air temperature and chilled water temperature as well. In this scheme zone air temperature is maintained through regulating the air flow rate.

(5) By comparing the refrigeration capacity and total energy consumption of the three cases, we can see that, scheme 2 consumed more energy than scheme 1 and scheme 3 because of the higher energy inputs to the fan and the compressor in scheme 2.

Above results also indicate that there is always more than one operation scheme that can achieve the same control objectives, however, the energy consumption could be different. Therefore, it is possible to reduce the total energy consumption by designing good control strategies while maintaining desired indoor air conditions.

Chapter 4 Fuzzy-Set Based HVAC&R Model Uncertainty and Sensitivity Analysis

As mentioned before, existing theoretical HVAC&R system models exhibit more or less uncertainties coming from neglecting and inaccurate description of the dynamic processes and the use of inaccurate model parameters. And therefore, simulation results obtained from traditional methods by which model equations are solved with predetermined crisp numbers cannot accurately represent the possible responses of the system. Since the accuracy of the model prediction plays an important role in model based applications, investigating the possible ranges of the simulation results and evaluating the uncertainties of the results are very important to ensure the accuracy of the model predictions.

In addition, since HVAC&R systems have strong coupling effects among subsystems and control loops, the conventional method of designing controllers independently as separate loops could seriously limit the regulation properties and control performance of local loop controllers. The effects of individual control variables on the controlled variables and on the dynamic responses of the system are worth to be investigated. Such information is helpful for designing and tuning the control system.

In this chapter, a fuzzy-set based extended transformation approach proposed by Hanss (2002, 2003) is employed to investigate the uncertainties of the proposed model caused by pre-selected uncertain parameters and the sensitivities of the control inputs. The uncertain parameters are treated as fuzzy-valued numbers and the propagation of the uncertain parameters is assessed using fuzzy arithmetic. The probability distributions of

HVAC&R model outputs are constructed based on simulation results. The upper and lower bounds of model dynamic outputs are functions of the fuzziness in selected uncertain parameters. These bounds can help achieve better predictions of the responses of the HVAC&R system by quantifying the range within which the responses fall and provide potential variations in measurements under parameter uncertainties.

4.1 Background of Fuzzy-Set Theory

In fuzzy set theory, a variable with probability distributions is considered as a fuzzy-valued parameter, and the characteristics of the distribution or uncertain information of the variable is described by its membership function, $\mu_F(u)$, which is a curve that defines how each point in the input space is mapped to a membership value between 0 and 1. Zadeh (1978) interprets the fuzzy sets in terms of probability as: F is the set of possible values of a variable p, and $\mu_F(u)$ is the grade of probability of choosing u as a suitable value for p. Obviously, the construction of the membership function depends on the context of the problem. The membership function can be any arbitrary curve. The most commonly used membership functions include triangular function, the Gaussian distribution function, sigmoid function and polynomial functions.

In order to use extended interval mathematics to evaluate fuzzy-valued functions, the continuous fuzzy-valued variable is decomposed into a set of intervals based on the α-cut concept. An α-cut of a fuzzy variable p at membership level μ^j $(0 \le \mu^j \le 1)$ is represented by the interval $\left[a^{(j)}\ \ b^{(j)}\right](a^{(j)} \le b^{(j)})$, in which the probability of p is at least equal to μ^j. Assume a fuzzy number p is described by a symmetric triangular membership function, according to the α-cut concept, p can be decomposed into a family

of $m+1$ intervals as shown in Figure 4-1. p is now expressed as:

$$p = \left\{ \left[a^{(0)},\ b^{(0)}\right], \cdots, \left[a^{(j)},\ b^{(j)}\right], \cdots, \left[a^{(m)},\ b^{(m)}\right] \right\}$$
$$\text{with} \quad \text{membership level } \mu^j = \frac{j}{m} \quad (j = 0, 1 \cdots m) \qquad (4\text{-}1)$$
$$a^{(0)} = p_l \ \text{ and } \ b^{(0)} = p_u$$

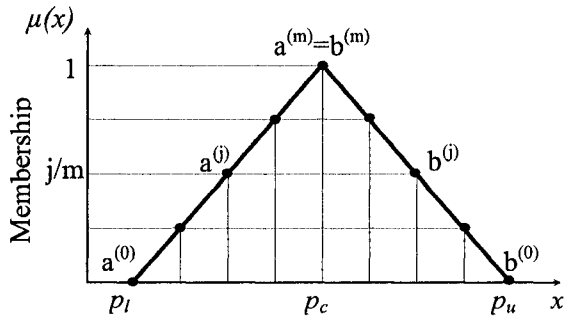

Figure 4-1 α-cut Decomposition of a Fuzzy Parameter with Triangular Membership Functions

Using α-cut, all fuzzy variables appearing in the fuzzy-valued function are decomposed into intervals at different α-cut levels and the fuzzy algebraic computations are therefore decomposed into interval calculus at each α-cut level. The results are the α-cut decomposing of the fuzzy results at the same level. (Bonarini and Bontempi, 1994)

4.2 The Transformation Method

The transformation method is one of the methods used to evaluate fuzzy valued functions. Transformation method has two forms, one is general form used to evaluate non-monotonic fuzzy-valued functions; the other is reduced form used to evaluate monotonic functions where the function is monotonic with respect to all fuzzy parameters. A brief description of the transformation method is given in this section, detailed description is given in Hanss (2002, 2003).

Assume a model having n independent uncertain parameters, represented by n

fuzzy variables $p_1, p_2, \cdots p_n$, is represented by following equation:

$$y = F(p_1, p_2, \cdots p_n) \qquad (4\text{-}2)$$

where y is fuzzy-valued output of the model. The implementation of the transformation method is described in the following three steps.

STEP 1: Parameter Decomposition

Given a refinement number *m*, decompose every fuzzy variable into a set of *m*+1 intervals using the α-cut concept. For the i^{th} fuzzy variable p_i, the family of intervals is expressed as:

$$p_i = \left\{ \left[a_i^{(0)} \;\; b_i^{(0)}\right], \cdots, \left[a_i^{(j)} \;\; b_i^{(j)}\right], \cdots, \left[a_i^{(m)} \;\; b_i^{(m)}\right] \right\} \quad (i = 1, \cdots, n \;\; and \;\; a_i^{(j)} \le b_i^{(j)}) \qquad (4\text{-}3)$$

STEP 2: Construct Transformation Matrix

Case 1 - Transformation Matrix in General Form

In general form of the transformation method, at every membership level μ^j, in addition to the boundary points $a_i^{(j)}$ and $b_i^{(j)}$, point(s) $c_{i,l}^{(j)}$ given in Eq.(4.4) are added to each intervals because for non-monotonic problems, besides the boundary points, the extreme point may exist inside the argument domain. Figure 4-2 illustrates the decomposition of a fuzzy parameter by inserting additional points for each interval.

$$c_{i,l}^{(j)} = \begin{cases} a_i^{(j)} & j = 0,1 \cdots m \;\; and \;\; l = 1 \\ \dfrac{c_{i,l-1}^{(j+1)} + c_{i,l}^{(j+1)}}{2} & j = 0,1 \cdots m-2 \;\; and \;\; l = 2,3, \cdots m-j \\ b_i^{(j)} & j = 0,1 \cdots m \;\; and \;\; l = m-j+1 \end{cases} \qquad (4\text{-}4)$$

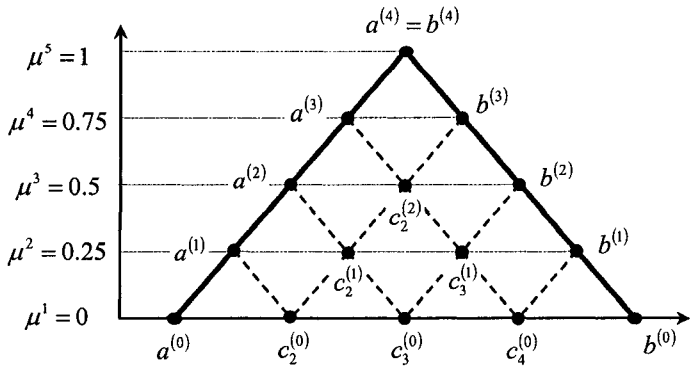

Figure 4-2 Insertion of Additional Point(s) in General Transformation Method (m=4)

The corresponding transformation vector of p_i at membership level μ^j, $P_i^{(j)}$, is composed of $(m+1-j)^i$ repeated sets of tuples $\left(\gamma_{i,1}^{(j)}, \gamma_{i,2}^{(j)}, \cdots \gamma_{i,(m+1-j)}^{(j)}\right)$, each tuple is composed of $(m+1-j)^{n-i}$ repeated elements $c_{i,l}^{(j)}$. In all, $P_i^{(j)}$ contains $(m+1-j)^n$ elements as:

$$P_i^{(j)} = \underbrace{\left[\left(\gamma_{i,1}^{(j)}, \gamma_{i,2}^{(j)}, \cdots \gamma_{i,(m+1-j)}^{(j)}\right), \cdots, \left(\gamma_{i,1}^{(j)}, \gamma_{i,2}^{(j)}, \cdots \gamma_{i,(m+1-j)}^{(j)}\right)\right]}_{(\text{m+1-j})^i \text{ tuples}}$$

$$\text{with } \gamma_{i,l}^{(j)} = \underbrace{\left(c_{i,l}^{(j)}, c_{i,l}^{(j)}, \cdots c_{i,l}^{(j)}\right)}_{(m+1-j)^{n-i} \text{ elements}}, \quad l = 1, 2, \cdots m+2-j \qquad (4\text{-}5)$$

The transformation matrix P^j at membership level μ^j is composed of the transformation vectors of all fuzzy variables: the i^{th} row of P^j is the transformation vector of the i^{th} fuzzy variable at the same membership level, $P_i^{(j)}$.

$$P^j = \begin{bmatrix} P_1^{(j)} \\ P_2^{(j)} \\ \vdots \\ P_n^{(j)} \end{bmatrix} \qquad (4\text{-}6)$$

Each column of the transformation matrix P^j represents one of the possible

combination of the possible extreme points of all uncertain parameters, geometrically corresponds to a vertex point or an extrama.

For example, for three independent fuzzy variables, p_1, p_2, p_3, assume $m = 4$, at membership level $\mu = 0.5$ with $j = 2$, as shown in Figure 4-2, intervals of the fuzzy variables are:

$$p_1^{(2)} = \left[a_{1,1}^{(2)}\ c_{2,1}^{(2)}\ b_{1,1}^{(2)}\right];\quad p_2^{(2)} = \left[a_{1,2}^{(2)}\ c_{2,2}^{(2)}\ b_{1,2}^{(2)}\right];\quad p_3^{(2)} = \left[a_{1,3}^{(2)}\ c_{2,3}^{(2)}\ b_{1,3}^{(2)}\right] \qquad (4\text{-}7)$$

simply denoted as: $p_1^{(2)} = [d_1\ d_2\ d_3];\quad p_2^{(2)} = [e_1\ e_2\ e_3];\quad p_3^{(2)} = [f_1\ f_2\ f_3]$

The corresponding transformation vectors (each contains $3^3 = 27$ elements) are:

$$P_1^{(2)} = [d_1\ d_1\ d_1\ d_1\ d_1\ d_1\ d_1\ d_1\ d_1\ d_2\ d_2\ d_2\ d_2\ d_2\ d_2\ d_2\ d_2\ d_2\ d_3\ d_3\ d_3\ d_3\ d_3\ d_3\ d_3\ d_3\ d_3]$$
$$P_2^{(2)} = [e_1\ e_1\ e_1\ e_2\ e_2\ e_2\ e_3\ e_3\ e_3\ e_1\ e_1\ e_1\ e_2\ e_2\ e_2\ e_3\ e_3\ e_3\ e_1\ e_1\ e_1\ e_2\ e_2\ e_2\ e_3\ e_3\ e_3]$$
$$P_3^{(2)} = [f_1\ f_2\ f_3\ f_1\ f_2\ f_3\ f_1\ f_2\ f_3\ f_1\ f_2\ f_3\ f_1\ f_2\ f_3\ f_1\ f_2\ f_3\ f_1\ f_2\ f_3\ f_1\ f_2\ f_3\ f_1\ f_2\ f_3]$$

and the transformation matrix is:

$$P^{(2)} = \begin{bmatrix} d_1\ d_1\ d_1\ d_1\ d_1\ d_1\ d_1\ d_1\ d_1\ d_2\ d_2\ d_2\ d_2\ d_2\ d_2\ d_2\ d_2\ d_2\ d_3\ d_3\ d_3\ d_3\ d_3\ d_3\ d_3\ d_3\ d_3 \\ e_1\ e_1\ e_1\ e_2\ e_2\ e_2\ e_3\ e_3\ e_3\ e_1\ e_1\ e_1\ e_2\ e_2\ e_2\ e_3\ e_3\ e_3\ e_1\ e_1\ e_1\ e_2\ e_2\ e_2\ e_3\ e_3\ e_3 \\ f_1\ f_2\ f_3\ f_1\ f_2\ f_3\ f_1\ f_2\ f_3\ f_1\ f_2\ f_3\ f_1\ f_2\ f_3\ f_1\ f_2\ f_3\ f_1\ f_2\ f_3\ f_1\ f_2\ f_3\ f_1\ f_2\ f_3 \end{bmatrix}$$

(4-8)

Case 2 - Transformation Matrix in Reduced Form

For monotonic problems, the extreme point is one of the boundary points. Thus the transformation vector in reduced form is composed of 2^{i-1} repeated pair $\left(\alpha_i^{(j)}\ \beta_i^{(j)}\right)$, each pair contains 2^{n-i+1} elements; the first 2^{n-i} elements are equal to the lower boundary $a_i^{(j)}$ and the second 2^{n-i} elements are equal to the other boundary $b_i^{(j)}$. All together, $P_i^{(j)}$ contains 2^n elements:

$$p_i^{(j)}=\underbrace{\left[(\alpha_i^{(j)}\ \beta_i^{(j)}),\cdots,(\alpha_i^{(j)}\ \beta_i^{(j)})\right]}_{\text{total } 2^{i-1} \text{ pairs}}$$

$$\text{with } \alpha_i^{(j)}=\underbrace{\left(a_i^{(j)},\cdots a_i^{(j)}\right)}_{2^{n-i} \text{ elements}},\ \beta_i^{(j)}=\underbrace{\left(b_i^{(j)},\cdots b_i^{(j)}\right)}_{2^{n-i} \text{ elements}} \qquad (4\text{-}9)$$

For three fuzzy variables p_1, p_2, p_3, $m=4$ and $j=2$, the intervals of the fuzzy variables in reduced form are:

$$p_1^{(2)}=\left[a_{1,1}^{(2)}\ b_{1,1}^{(2)}\right];\quad p_2^{(2)}=\left[a_{1,2}^{(2)}\ b_{1,2}^{(2)}\right];\quad p_2^{(2)}=\left[a_{1,2}^{(2)}\ b_{1,2}^{(2)}\right] \qquad (4\text{-}10)$$

Simply denoted as: $p_1^{(2)}=[a_1\ b_1];\quad p_2^{(2)}=[a_2\ b_2];\quad p_3^{(2)}=[a_3\ b_3]$

The transformation vectors (contains $2^3=8$ elements) are:

$$P_1^{(2)}=[a_1\ a_1\ a_1\ a_1\ b_1\ b_1\ b_1\ b_1]\ P_2^{(2)}=[a_2\ a_2\ b_2\ b_2\ a_2\ a_2\ b_2\ b_2]\ P_3^{(2)}=[a_3\ b_3\ a_3\ b_3\ a_3\ b_3\ a_3\ b_3]$$

and the corresponding transformation matrix is:

$$P^{(2)}=\begin{bmatrix} a_1\ a_1\ a_1\ a_1\ b_1\ b_1\ b_1\ b_1 \\ a_2\ a_2\ b_2\ b_2\ a_2\ a_2\ b_2\ b_2 \\ a_3\ b_3\ a_3\ b_3\ a_3\ b_3\ a_3\ b_3 \end{bmatrix} \qquad (4\text{-}11)$$

STEP 3: Model Evaluation and Outputs Retransformation:

At each α-cut level, evaluate the model with every column of the corresponding transformation matrix using the conventional arithmetic for crisp numbers and construct the outputs in the format:

$$Y^{(j)}=\begin{cases}\left[Y_1^{(j)},\ Y_2^{(j)},\cdots,Y_z^{(j)}\right] & j=0,1,\cdots m-1;\ z=\begin{cases}(m+1-j)^n & \text{in general form}\\ 2^n & \text{in reduced form}\end{cases}\\ Y_1^{(m)} & j=m\end{cases} \qquad (4\text{-}12)$$

The minimum and maximum extremes of the outputs at each α-cut level are given as:

$$\text{For } j = m: \quad a^{(m)} = b^{(m)} = Y_1^{(m)}$$

$$\text{For } j = 0, 1, \cdots m\text{-}1: \begin{cases} a^{(j)} = \min\limits_k \left(a^{(j+1)},\ Y_k^{(j)} \right) \\ b^{(j)} = \max\limits_k \left(b^{(j+1)},\ Y_k^{(j)} \right) \end{cases} \qquad (4\text{-}13)$$

$$\text{with } k = 1, 2, \cdots (m+1-j)^n \quad \text{in general form}$$

$$k = 1, 2, \cdots 2^n \quad \text{in reduced form}$$

4.3 The Extended Transformation Method

By comparing transformation vector in general form (Eq.(4-5)) and in reduced form (Eq.(4-9)), we can see that the general transformation matrix for non-monotonic problem has much larger scale than the reduced transformation matrix for monotonic problem and therefore causing much more computations. With the increase of the number of uncertain variables, the difference can be huge. In order to reduce the computational cost, the reduced transformation approach is always preferred whenever it is applicable. To handle the problems containing both monotonic and non-monotonic parameters, Hanss (2003) extended the transformation method by combining the reduced transformation method with the general transformation method. In the extended method, fuzzy-valued parameters are classified into general type ('G-type') and reduced type ('R-type'). Parameter which causes monotonic behavior with respect to all interested outputs is classified as R-type parameter; otherwise, it is classified as G-type parameter. Transformation vectors and transformation matrix are then constructed according to the types of the fuzzy parameters. The extended transformation fuzzy analysis is briefly described in the following four steps.

STEP 1: Parameter Decomposition

Given a refinement number m, every continuous fuzzy variable is decomposed

into $m+1$ intervals as in Eq.(4-3).

STEP 2: Parameter Classification

In order to determine the type of the fuzzy-valued parameter, all fuzzy parameters are assumed to be G-type first and transformation matrix is constructed according to Eq. (4-5) and Eq.(4-6). Evaluate the fuzzy function with every column of the transformation matrix P^0 with membership level $\mu = 0$. Express the results in the format:

$$[Y_1^{(0)}, Y_2^{(0)}, \cdots, Y_{(m+1)^n}^{(0)}]$$

The i^{th} parameter is classified as 'R-type' parameter if it satisfies the following criteria; otherwise, it is classified as 'G-type' parameter:

$$\tau_i = \frac{\min(T_i)\max(T_i)}{m(m+1)^{n-1}(b_i^{(0)} - a_i^{(0)})} > \varepsilon$$
$$\text{with } T_i = \left\{ t_i(1,1,1), \cdots, t_i((m+1)^{n-i}, (m+1)^{i-1}, m) \right\} \qquad (4\text{-}14)$$
$$t_i(k,l,r) = Y_{s(k,l,r+1)}^{(0)} - Y_{s(k,l,r)}^{(0)}$$
$$s(k,l,r) = k + \left[(m+1)(l-1) + r - 1\right](m+1)^{n-i}$$

where $\varepsilon > 0$ is a small threshold value.

STEP 3: Construct Transformation Matrix

At each α level, construct the transformation vectors for every fuzzy variable according to its type. Assume there are '*ng*' G-type parameters and '(*n-ng*)' R-type parameters.

The transformation vector for G-type parameter in the extended method is still composed of $(m+1-j)^i$ repeated sets of tuples $\left(\gamma_{i,1}^{(j)}, \gamma_{i,2}^{(j)}, \cdots \gamma_{i,(m+1-j)}^{(j)}\right)$; and each tuple is composed of $2^{n-ng}(m+1-j)^{ng-i}$ repeated elements $c_{i,l}^{(j)}$. In all, $P_i^{(j)}$ contains

$2^{n-ng}(m+1-j)^{ng}$ elements as:

$$P_i^{(j)} = \underbrace{\left[(\gamma_{i,1}^{(j)}, \gamma_{i,2}^{(j)}, \cdots \gamma_{i,(m+1-j)}^{(j)}), \cdots, (\gamma_{i,1}^{(j)}, \gamma_{i,2}^{(j)}, \cdots \gamma_{i,(m+1-j)}^{(j)})\right]}_{\text{(m+1-j)}^{\,i} \text{ tuples}} \qquad (i = 1 \cdots ng)$$

$$\text{with } \gamma_{i,l}^{(j)} = \underbrace{(c_{i,l}^{(j)}, c_{i,l}^{(j)}, \cdots c_{i,l}^{(j)})}_{2^{n-ng}\text{(m+1-j)}^{\,ng-i} \text{ elements}}, \quad l = 1, 2, \cdots m+2-j \qquad (4\text{-}15)$$

The transformation vector for R-type parameter in the extended method is composed of $(m+1-j)^{ng}\ 2^{\text{i-ng-1}}$ repeated pair $\left(\alpha_i^{(j)}\ \beta_i^{(j)}\right)$, each pair contains 2^{n-i+1} elements. All together, $P_i^{(j)}$ contains $(m+1-j)^{ng}\ 2^{\text{n-ng}}$ elements also:

$$P_i^{(j)} = \underbrace{\left[(\alpha_i^{(j)}\ \beta_i^{(j)}), \cdots, (\alpha_i^{(j)}\ \beta_i^{(j)})\right]}_{\text{total } (m+1-j)^{\,ng}\ 2^{\text{i-ng-1}} \text{ pairs}} \qquad (i = ng+1 \cdots n)$$

$$\text{with } \alpha_i^{(j)} = \underbrace{(a_i^{(j)}, \cdots, a_i^{(j)})}_{2^{\text{n - i}} \text{ elements}},\ \beta_i^{(j)} = \underbrace{(b_i^{(j)}, \cdots, b_i^{(j)})}_{2^{\text{n - i}} \text{ elements}} \qquad (4\text{-}16)$$

The transformation matrix P^i is constructed as follows: the first '*ng*' rows are transformation vectors of the G-type parameters and the last '(*n-ng*)' rows are transformation vectors of the R-type parameters. Each transformation vector contains $(\text{m}+1-\text{j})^{ng}\ 2^{\text{n-ng}}$ elements.

$$P^i = \begin{bmatrix} P_1^{(j)} \\ \vdots \\ P_{ng}^{(j)} \\ P_{ng+1}^{(j)} \\ \vdots \\ P_n^{(j)} \end{bmatrix} \qquad (4\text{-}17)$$

STEP4: Model Evaluation and Outputs Retransformation

At each α-cut level, evaluate the model with every column of the transformation

matrix, construct the outputs in the format of Eq.(4-12). The minimum and maximum extremes of the outputs at each α-cut level are:

$$\text{For } j=m: \quad a^{(m)}=b^{(m)}=Y_1^{(m)}$$

$$\text{For } j=0,1,\cdots m\text{-}1: \begin{cases} a^{(j)}=\min\limits_k(a^{(j+1)},\ Y_k^{(j)}) \\ b^{(j)}=\max\limits_k(b^{(j+1)},\ Y_k^{(j)}) \end{cases} \quad k=1,2,\cdots(m+1-j)^{ng}2^{n-ng} \qquad (4\text{-}18)$$

Thus, the outputs of the model are expressed in the decomposed and transformed forms. The probability distributions of the fuzzy-valued function outputs can thus be constructed by sweeping a set of α-cuts at different membership levels ranging from 0 to 1. The accuracy of the distributions is directly related to the number of α-cuts employed.

4.4 Fuzzy-Set Based HVAC&R System Model Uncertainty Analysis

4.4.1 Uncertain Parameter Analysis

The majority of parameters appearing in HVAC&chiller model equations given in Chapter 3 are uncertain variables. These parameters include (1) system configuration parameters, i.e. size of heat exchangers and air duct; (2) operation conditions, i.e. cooling load and outdoor air temperature; and (3) parameters which can only be calculated using empirical equations or derived from experience or experimental data, i.e. mean void fraction, heat transfer coefficients. In theory, all uncertain parameters could be treated as fuzzy variables with membership functions describing the probability distributions of the uncertainties in certain range. However, considering the computational cost, it is impractical and unnecessary to include too many uncertain parameters in the uncertainty analysis because the significance of different uncertain parameters on model outputs is different and the influence of some uncertain parameters can be neglected. In this study,

only those parameters which have significant impacts on system behavior or model predictions are considered and treated as fuzzy variables.

The objective of HVAC&R system is to remove the heat from the air-conditioned areas; therefore, the cooling load directly affects the operation of the system. However, the predictions of the cooling load hardly represent the real operating conditions because too many unpredictable factors affect the actual load. To account for the influence of uncertain cooling load on system responses, the sensible loads of both zones are included in the uncertainty analysis.

Since the air-conditioning process is basically a heat transfer process, the performance of the heat exchangers, including cooling and dehumidifying coil, evaporator and condenser, has profound effect on the performance of the system. For a heat exchanger with given size and working fluids, the heat transfer rate depends on fluid mass flow rates and temperature difference of two fluids. To account for the effects of uncertainties in the heat exchangers, chilled water mass flow rate $\dot{m}_{w,chi}$, cooling coil air side heat transfer coefficient $h_{a,cc}$ and condenser water mass flow rate $\dot{m}_{w,con}$ are selected. $\dot{m}_{w,chi}$ is selected because chilled water connects the chiller and the VAV system and the variations in $\dot{m}_{w,chi}$ affect the performance of both cooling coil and evaporator. $h_{a,cc}$ is selected because on one hand, compared to cooling coil water side heat transfer coefficient, the air side heat transfer coefficient $h_{a,cc}$ is much smaller, and therefore the performance of the cooling coil is dominated by $h_{a,cc}$; on the other hand, $h_{a,cc}$ could represent the overall effects of the air flow rate and fin efficiency of the coil. The condenser water mass flow rate $\dot{m}_{w,con}$ is selected to represent the effects of the

uncertainties in the condenser on the overall system behavior.

Meanwhile, the indoor heat is discharged to the environment through condenser water loop. The performance of the cooling tower affects the performance of the HVAC&R system. Therefore, the water temperature at the condenser inlet $T_{w,con,in}$ is selected to include the influence of the performance and uncertainties of the cooling tower on the performance of the HVAC&R system. In summery, all together six uncertain parameters were selected for the uncertainty analysis, they are:

- mass flow rate of condenser water, $\dot{m}_{w,con}$, denoted as p_1
- mass flow rate of chilled water $\dot{m}_{w,chi}$, denoted as p_2
- water temperature at the condenser inlet, $T_{w,con,in}$, denoted as p_3
- cooling coil air side heat transfer coefficient, $h_{a,cc}$, denoted as p_4
- sensible cooling load of zone1, Q_{s1}, denoted as p_5
- and sensible cooling load of zone2, Q_{s2}, denoted as p_6.

Since we don't have sufficient data and knowledge to establish the probability distributions of above uncertain parameters, for simplicity, we assume that the probability distributions of p_1 - p_6 can be represented by symmetric triangular membership functions, as shown in Figure 4-1, with p_c equal to the nominal value (most likely value) and interval base is ±20% of the p_c (worst deviations from the nominal value), that is to say, $p_u = 120\% p_c$ and $p_l = 80\% p_c$.

4.4.2 Numerical Results

By replacing $\dot{m}_{w,con}$, $\dot{m}_{w,chi}$, $T_{w,con,in}$, $h_{a,cc}$, Q_{s1} and Q_{s2} appeared in model

equations given in the previous chapter with fuzzy-valued parameters $p_1 - p_6$, we have the system model described by fuzzy-valued ODEs. The extended transformation approach is now applied to evaluate the uncertainties in the model outputs. The outputs of interest include the air temperature in both zones T_{z1} and T_{z2}; discharge air temperature $T_{a,\text{sup}}$; chilled water temperature $T_{w,\text{sup}}$ and $T_{w,re}$; water temperature at the condenser outlet $T_{w,con,re}$. Both nominal values and variations of fuzzy variables are assumed to be constant throughout the simulation process.

The application of the extended transformation method starts with the decomposition of the fuzzy-valued parameters. Given refinement number $m = 3$, the corresponding membership level is equal to $\mu = 0, 0.33, 0.67, and\ 1$, which means the variation of the uncertain parameters are equal to ±20%, ±13%, ±7% and 0% of the corresponding nominal values respectively. And then the types of uncertain parameters are determined as described in Section 4.3 STEP 2. The resulting time histories of the effectiveness of every fuzzy variable on interested outputs are plotted in Figure 4-3. τ_i^j is scaled as follows for better fitting in the same figure: $\tau_1^2/100$, $\tau_2^1/10$, $\tau_2^2 * 10$, $\tau_2^4 * 10$, $\tau_3^2 * 100$, $\tau_4^2 * 100$, $\tau_5^2 * 100$, $\tau_5^5/10$, $\tau_6^2 \times 100$, and $\tau_6^6/100$. Subscript 'i' represents the i^{th} fuzzy variable, superscript 'j' represents the j^{th} interested output:

- $j = 1$ for chilled water supply temperature, $T_{w,\text{sup}}$;
- $j = 2$ for water temperature at the condenser outlet, $T_{w,con,re}$;
- $j = 3$ for discharge air temperature, $T_{a,\text{sup}}$;
- $j = 4$ for chilled water return temperature, $T_{w,re}$;

- $j = 5$ for zone1 air temperature, T_{z1}
- $j = 6$ for zone2 air temperature, T_{z2}.

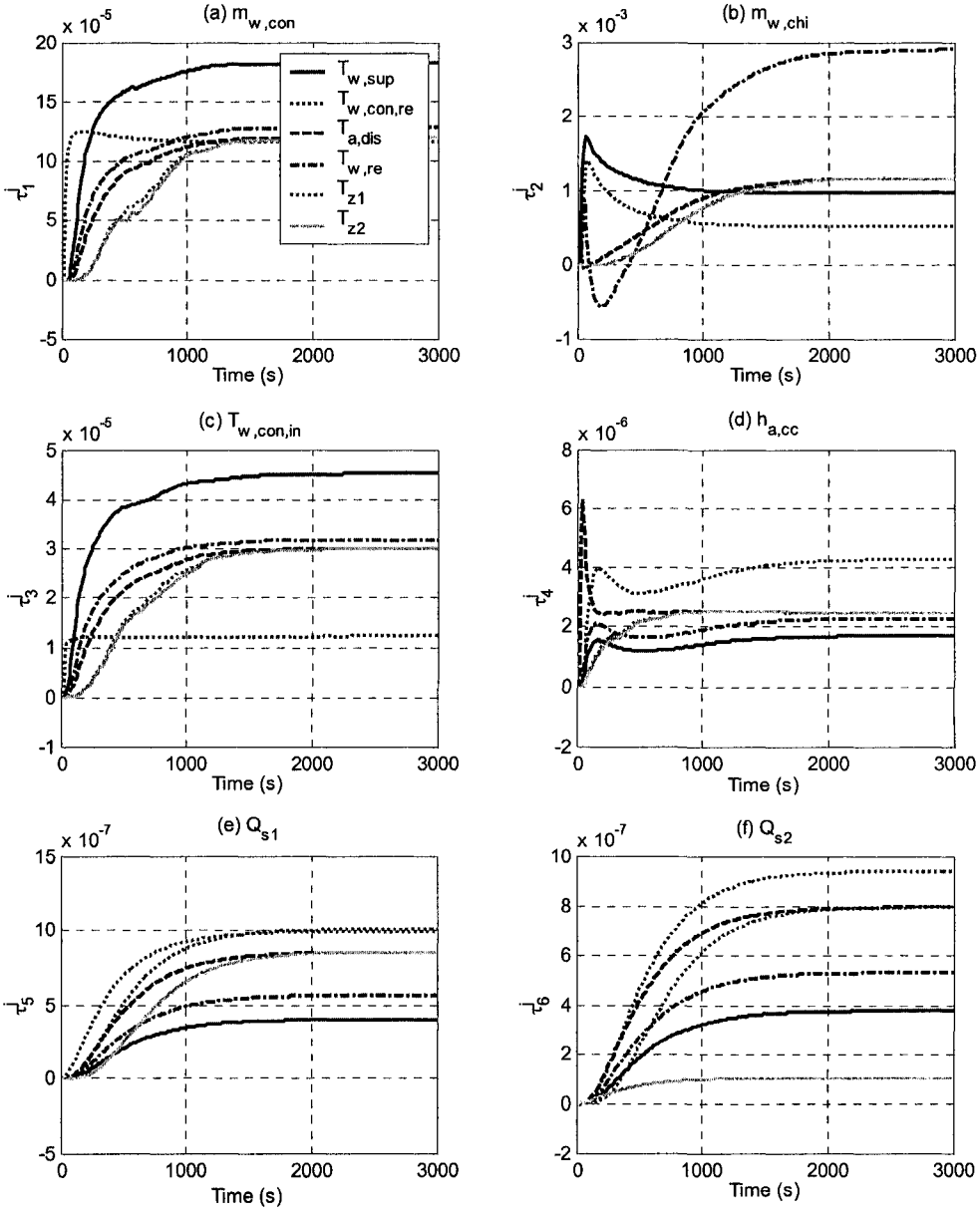

Figure 4-3 Results of Classification of Uncertain Parameters -- $\tau_1 - \tau_6$ V.S. Model Predictions

Since system dynamics in first few seconds are mostly dependent on the initial conditions used to solve model equations, it is justified to neglect early dynamics in the uncertainty analysis. Neglecting dynamics of the interested outputs for $t \leq 40s$, from

Figure 4-3, we note that, when $t > 40s$, $\tau_2^3(t)$ and $\tau_2^4(t)$ experience sign changes, and all other remain positive: $\tau_i^j(t) \geq 10^{-10}$ for $i, j = 1, 2, \cdots 6$. According to the classification criteria Eq. (4-12), p_2 chilled water mass flow rate $\dot{m}_{w,chi}$ is classified as G-type parameter, while the rest parameters p_1, $p_3 - p_6$, condenser water mass flow rate $\dot{m}_{w,con}$, water temperature at the condenser inlet $T_{w,con,in}$, cooling coil air side heat transfer coefficient $h_{a,cc}$, zone loads Q_{s1} and Q_{s2} are classified as R-type parameters.

This result is consistent with theoretical analysis. For example, providing other conditions are kept unchanged except the cooling load, the higher cooling load causes higher return air temperature; which in turn causes higher discharge air temperature, higher water temperature at the evaporator inlet and condenser outlet. If cooling coil air side heat transfer coefficient $h_{a,cc}$ is the only changing parameter, with the increase of $h_{a,cc}$, more heat is transferred from the air to the water in the coil, therefore, the discharge air temperature decreases; which in turn causes decrease in zone air temperature and increase in return water temperature. Since other working conditions of the chiller remain unchanged, with the increase of return water temperature, the supply water temperature and water temperature in the condenser increase.

After the types of fuzzy variables are determined, the transformation matrix at each α-level are constructed according to Eq.(4.15) – (4-17). The model equations are then solved with the same initial conditions, control inputs and every column of the transformation matrix at different membership levels.

Given $m = 3$, the upper and lower bounds of the possible distributions of the model dynamic responses (preclude some impractical results, e.g. chilled water supply

temperature $\leq 0°C$) at $\mu = 0, 1/3, 2/3$ *and* 1 are shown in Figure 4-4 (left column).

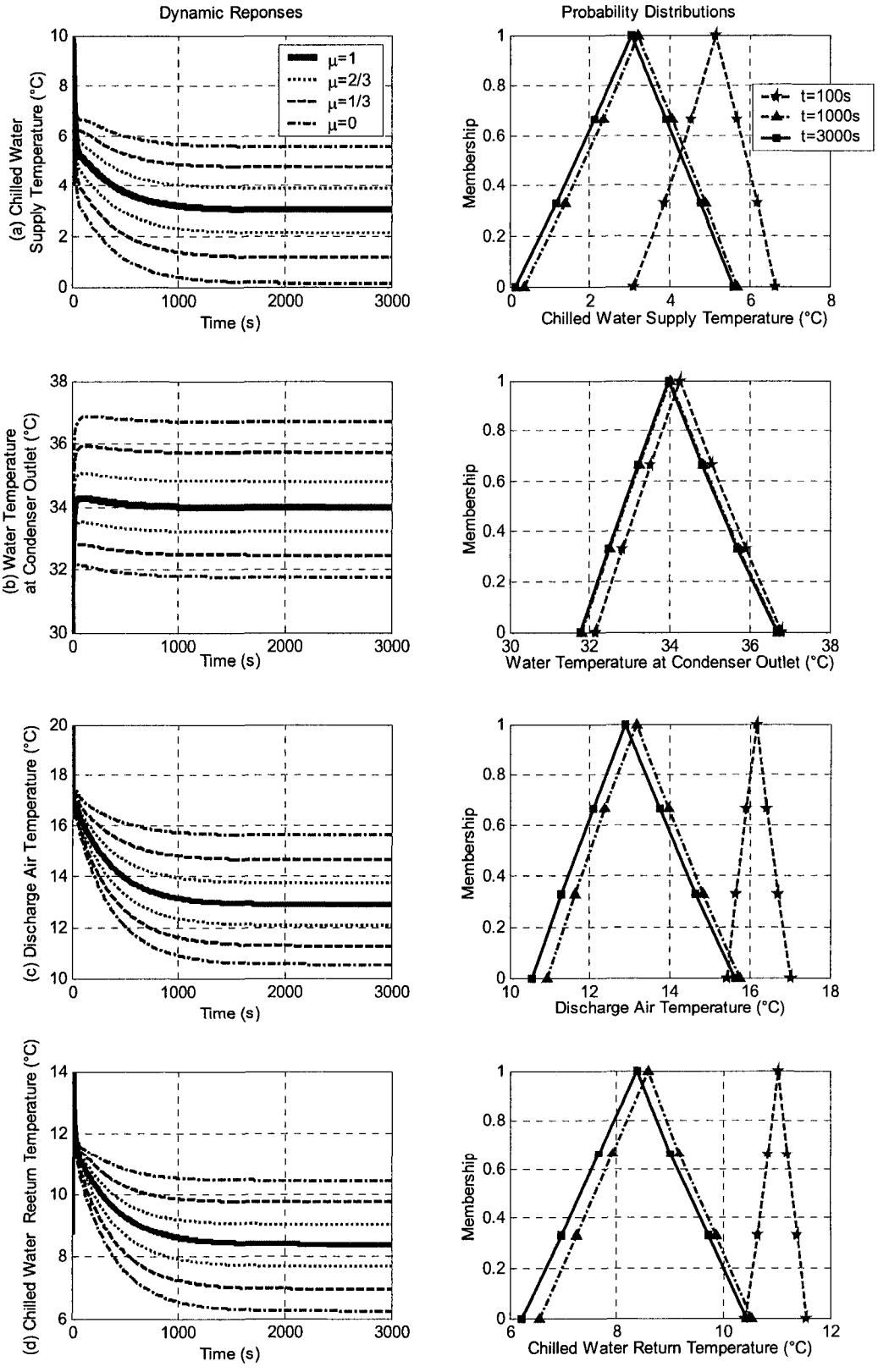

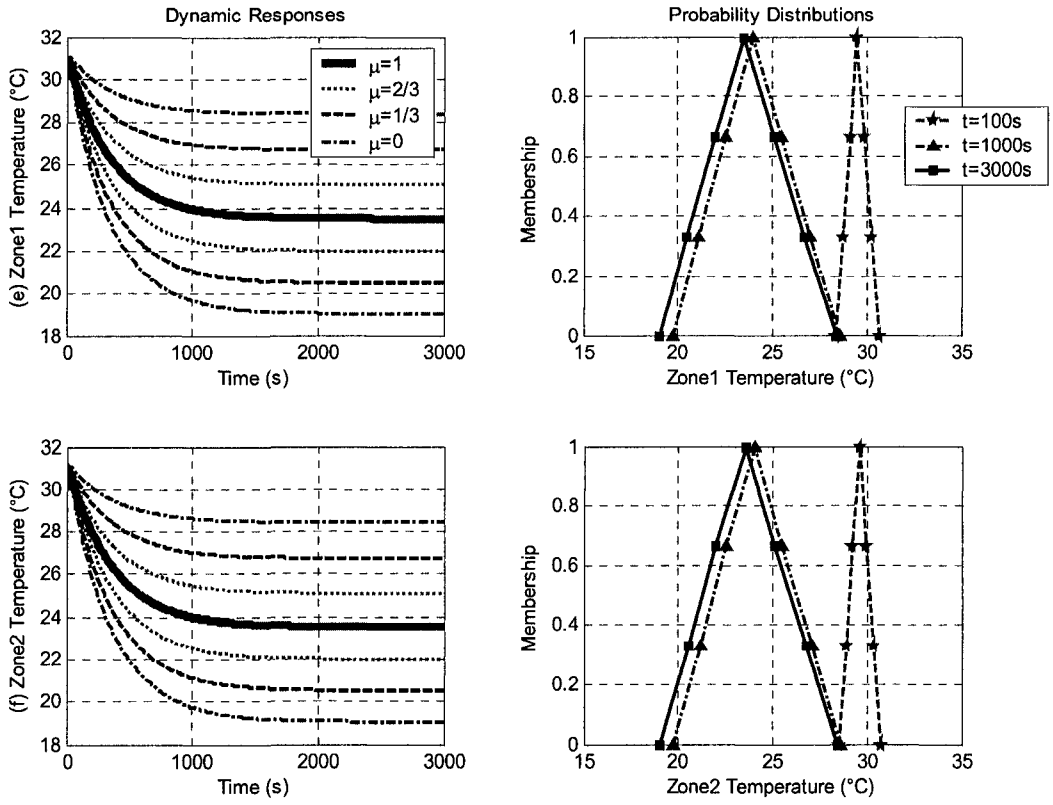

Figure 4-4 System Dynamic Responses and Approximate Distributions under Uncertain Model Parameters

At any given time, approximate distributions of the responses can be constructed by connecting the upper and lower bounds of the responses for that time at different α-cut levels. The probability distributions at $t = 100s, 1000s \; and \; 3000s$ (steady state) are illustrated in Figure 4-4 (right column). With this information, the approximate distributions of outputs at other membership levels are derivable. For example, if uncertain parameters under consideration have a variation range of ±10% of corresponding nominal values, in other words, the membership level is $\mu = 0.5$, the approximate distribution range of the supply water temperature under steady state is derived as follows:

- In the probability distributions figure, draw a horizontal line from $\mu = 0.5$,
- This line intersects with the profile of the probability distributions of $T_{w,sup}$ at $t = 3000s$.
- Get the readings from x axis of the intersections. They are lower and upper limits of the range of supply water temperature falls.

From Figure 4-5, we know that the steady state value of the supply water temperature is in the range [1.64°C, 4.33°C] if the uncertainties of the uncertain parameters are ±10% of corresponding nominal values.

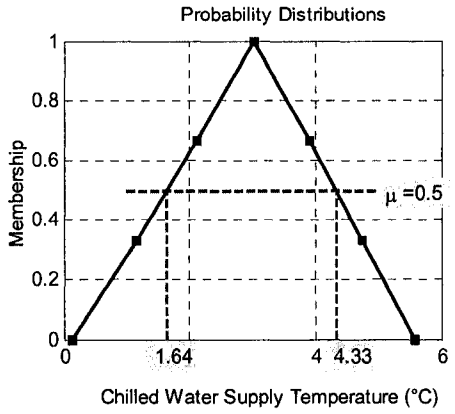

Figure 4-5 Derive Approximate Distributions from Distribution Figure

From Figure 4-4 we can state the following:

(1) The overall impacts of the uncertain parameters on different outputs are different, for example, the steady state supply water temperature falls in the range [0.1°C, 5.6°C], with nominal value equal to 3.0°C, the variation base is [-2.9°C, 2.6°C] of the nominal value; the steady state zone1 air temperature falls in the range [19°C, 28.4°C] with nominal value equal to 23.5°C, the variation base is [-4.5°C, 4.9°C] of the nominal value. The nominal value, lower and upper bounds of the interested outputs under steady

state and corresponding variability are summarized in Table 4–1.

Table 4–1 Model Steady State Prediction Variations with Uncertain Parameters

	Norminal Value (°C)	Upper Bound (°C)		Lower Bound (°C)	
		Value	Deviation	Value	Deviation
$T_{w,sup}$	3.0	5.6	2.6	0.1	-2.9
$T_{w,con,re}$	34.0	36.7	2.7	31.8	-2.2
$T_{ea,sup}$	13.1	15.9	2.8	10.7	-2.4
$T_{w,re}$	8.5	10.6	2.1	6.4	-2.1
T_{z1}	23.5	28.4	4.9	19.0	-4.5
T_{z2}	23.5	28.4	4.9	19.0	-4.5

(2) Comparing the probability distributions at $t = 100s, 1000s$ *and* $3000s$, we can see that the distribution ranges of the dynamic responses tend to increase with time, and reach the maximum variations when the system reaches steady state ($t = 3000s$). The variations of distribution ranges of a specific output are directly related to the dynamics of the output. For an output with fast response, such as condenser water outlet temperature, the distribution range at $t = 100s$ and membership level $\mu = 0$ is [32.1°C, 36.8°C], which is rather close to the distribution range of [31.8°C, 36.7°C] at $t = 1000s$ and $\mu = 0$. Since condenser water reaches the steady state around $t = 400s$, the profiles of the membership function of the condenser water outlet temperature at $t = 1000s$ and $t = 3000s$ almost overlap with each other. However, for an output with slow response, such as discharge air temperature, compared to the distribution range of [11°C, 16°C] at $t = 1000s$ and $\mu = 0$, the distribution range [15.3°C, 17°C] at $t = 100s$ and $\mu = 0$ is much smaller. Since discharge air temperature reaches steady state around $t = 1500s$, the

distribution range at $t = 1000s$ is much closer to the distribution range of [10.7°C, 15.9°C] at $t = 3000s$ and $\mu = 0$.

Above results reflect the integrated effects of the six uncertain parameters. In order to find the contribution of individual uncertain parameter to the variation of a specific model output, following sensitivity coefficient is computed:

for G - type parameter, $i = 1, 2, \cdots, ng$

$$\left(s_i^j\right)_p = \frac{1}{2^{n-ng}(m+1-j)^{ng-1}(b_i^{(j)} - a_i^{(j)})} \sum_{k=1}^{2^{n-ng}(m+1-j)^{ng-i}} \sum_{l=1}^{(m+1-j)^{i-1}} \left({y_p}^j{}_{d(k,l)} - {y_p}^j{}_{c(k,l)} \right)$$

$$\text{with} \quad c(k,l) = k + (l-1)2^{n-ng}(m+1-j)^{ng-i+1}$$

$$d(k,l) = k + \left[(m+1-j)l - 1\right]2^{n-ng}(m+1-j)^{ng-i}$$

for R - type parameter, $i = ng+1, ng+2, \cdots, n$

$$\left(s_i^j\right)_p = \frac{1}{2^{n-ng-1}(m+1-j)^{ng}(b_i^{(j)} - a_i^{(j)})} \sum_{k=1}^{2^{n-i}} \left(\sum_{l=1}^{(m+1-j)^{ng}2^{i-ng-1}} \left({y_p}^j{}_{d(k,l)} - {y_p}^j{}_{c(k,l)} \right) \right)$$

$$\text{with} \quad c(k,l) = k + (l-1)2^{n-i+1}$$

$$d(k,l) = k + \left[2l - 1\right]2^{n-i}$$

(4-19)

where $\left(s_i^j\right)_p$ represents the impact of the i^{th} uncertain parameter on the p^{th} output y_p at membership level of μ_j; $b_i^{(j)}$ and $a_i^{(j)}$ are upper and lower bounds of the intervals of the i^{th} parameter at the same membership level of μ_j; ${y_p}^j{}_{c(k,l)}$ and ${y_p}^j{}_{d(k,l)}$ are the c^{th} and the d^{th} element of the output array $Y_p^{(j)}$ as illustrated in Eq. (4-18). The second term of Eq.(4-19) computes cumulative differences between two outputs y_p for all possible $(m+1-j)^{n-1}$ combinations of uncertain parameters: $p_1, p_2, \ldots, p_{i-1}, p_{i+1}, \ldots, p_n$. This cumulative differences divided by $2^{n-ng}(m+1-j)^{ng-1}$ or $2^{n-ng-1}(m+1-j)^{ng}$ yields mean difference, which is then divided by $b_i^{(j)} - a_i^{(j)}$, the difference of maximal value and

minimal value of the i^{th} parameter p_i. Therefore, $(s_i^j)_p$ can also be interpreted as mean gradient or mean sensitivity of the i^{th} parameter with respect to the p^{th} interested model output at membership level of μ_j. The overall effects $(s_i^j)_p$ for all membership levels S_i^p is weighted average of $(s_i^j)_p$, the higher the membership level, the greater the weight is.

$$S_i^p = \frac{1}{m+1}\sum_{j=0}^{m}\left|(s_i^j)_p\right|\frac{j+1}{m} \qquad (4\text{-}20)$$

To evaluate the relative significance of the influence of individual uncertain parameters on a certain model output, the normalized effect of uncertain parameter is computed as:

$$NS_i^p = \frac{S_i^p}{\sum_{i=1}^{n} S_i^p} \qquad (4\text{-}21)$$

where subscript 'i' represents the i^{th} uncertain parameter, and superscript 'p' represents the p^{th} output. Normalized effects of every uncertain parameter with respect to all interested outputs are computed and depicted in Table 4–2.

Table 4–2 Normalized Effects of Uncertain Parameters on Model Predictions

	$T_{w,sup}$	$T_{w,con,re}$	$T_{a,sup}$	$T_{w,re}$	T_{z1}	T_{z2}
$m_{w,con}$	5%	45%	4%	6%	2%	2%
$m_{w,chi}$	45%	4%	19%	12%	10%	10%
$T_{w,con,in}$	7%	42%	6%	8%	4%	4%
$h_{a,cc}$	7%	2%	10%	12%	6%	6%
Q_{s1}	19%	4%	31%	32%	61%	17%
Q_{s2}	17%	3%	30%	30%	17%	60%

By comparing the values in the same row in Table 4–2, we can see the effects of individual uncertain parameters on different outputs:

(1) Uncertainties in condenser water flow rate $\dot{m}_{w,con}$ and inlet temperature $T_{w,con,in}$ have great impact on the variations of the condenser water temperature prediction, accounts for 45% and 42% of the variation respectively, while have very small effects on other model predictions.

(2) Uncertainties in chilled water flow rate $\dot{m}_{w,chi}$ has great impact on the variation of the water supply temperature prediction, accounts for 45% of the variation. $\dot{m}_{w,chi}$ also affects the variations in the discharge air temperature, return water temperature and air temperature in zones, while has small effect on the condenser water temperature.

(3) Uncertainties in the cooling coil air side heat transfer coefficient $h_{a,cc}$ affects the predictions of discharge air temperature, chilled water temperature and air temperature in both zones. However, compared to other parameters, its effects are not significant.

(4) Uncertainties in the zone loads, Q_{s1} and Q_{s2}, have significant impacts on corresponding zone air temperature, discharge air temperature and return water temperature, accounts for 60% of the zone air temperature variation, 30% of the discharge air temperature variation and 30% of the return water temperature variation. Q_{s1} and Q_{s2} also affect the supply water temperature and the air temperature of another zone. Again, their impacts on the condenser water temperature prediction are small.

In addition, by comparing the values in the same column of Table 4–2, the significance of uncertainties in model parameters with respect to the variations in the

interested model predictions can be ranked as follows:

(1) Supply water temperature variation is mainly caused by the uncertainties in the chilled water mass flow rate, and also affected by the uncertainties in cooling loads. The effects of variations in air side heat transfer coefficient, condenser water temperature and mass flow are insignificant.

(2) Variations in water temperature at condenser outlet are mainly caused by variations in the condenser water mass flow rate and condenser water inlet temperature. Variations in other parameters don't affect it much.

(3) Discharge air temperature variation is mainly caused by the variations in the cooling loads and the second most significant impact is coming from the variations in chilled water mass flow rate. Air side transfer coefficient also affects its distribution. But the impacts of condenser water temperature and flow rate are not significant.

(4) Variations in return water temperature is mainly caused by the cooling loads. The other significant sources causing its variations are chilled water mass flow rate and cooling coil air side transfer coefficient. The impacts of condenser water temperature and condenser water flow rate are not significant either.

(5) Zone air temperature variations are mainly caused by the variations in the cooling loads of that zone; and the variations in cooling load of the other zone is the second main sources causing the zone air temperature variations. The mass flow rate of the chilled water also affects zone air temperature distributions through the discharge air.

In addition, from Table 4–1 and Table 4–2, we can see that the variations in the condenser water temperature are mainly caused by the variations in the condenser water mass flow rate and water temperature at the condenser inlet. This further justified our

assumption of excluding condenser water loop from the optimization analysis.

4.5 Fuzzy-Set Based Control Variable Sensitivity Analysis

Similarly, by replacing control variables with fuzzy variables in model equations, the transformation method is used to investigate the sensitivities of the control inputs aiming at identifying the impacts of control variables on system responses. The following control inputs are considered:

- energy input to compressor motor U_{com};
- chilled water valve opening U_{val};
- energy input to fan motor U_{fan};
- zone1 and zone2 damper opening U_{z1} and U_{z2}.

The outputs of interest include:

- chilled water temperature, $T_{w,\text{sup}}$ and $T_{w,re}$;
- water temperature at the condenser outlet, $T_{w,con,re}$;
- cooling coil discharge air temperature, $T_{a,\text{sup}}$;
- air temperature in zone1 and zone2, T_{z1} and T_{z2};
- mass flow rates of the air entering zone1 and zone2, $\dot{m}_{z1}$ and $\dot{m}_{z2}$;
- mass flow rate of chilled water, $\dot{m}_{w,chi}$.

We assume that the variations of control inputs can be described with symmetric triangular membership functions as:

- U_{com}, U_{val} and U_{fan} are varied in the range of $[0.6\ \ 0.8]$ with nominal value

equal to 0.7,

- U_{z1}, U_{z2} are varied in the range of $[0.7 \;\; 0.9]$ with nominal value equal to 0.8.

All control inputs are treated as G-type variables and the general transformation method is used to calculate the sensitivities of control variables. Given refinement number $m = 3$, the control inputs are decomposed into intervals at membership levels $\mu = 0,\ 1/3,\ 2/3$ and 1. The model equations are solved with the same initial conditions, load profiles and all possible combinations of control inputs for different membership levels. The upper and lower bounds of model dynamic responses at different membership levels are illustrated in the left column of Figure 4-6 and the probability distributions of the outputs under steady state are plotted on the right column of Figure 4-6.

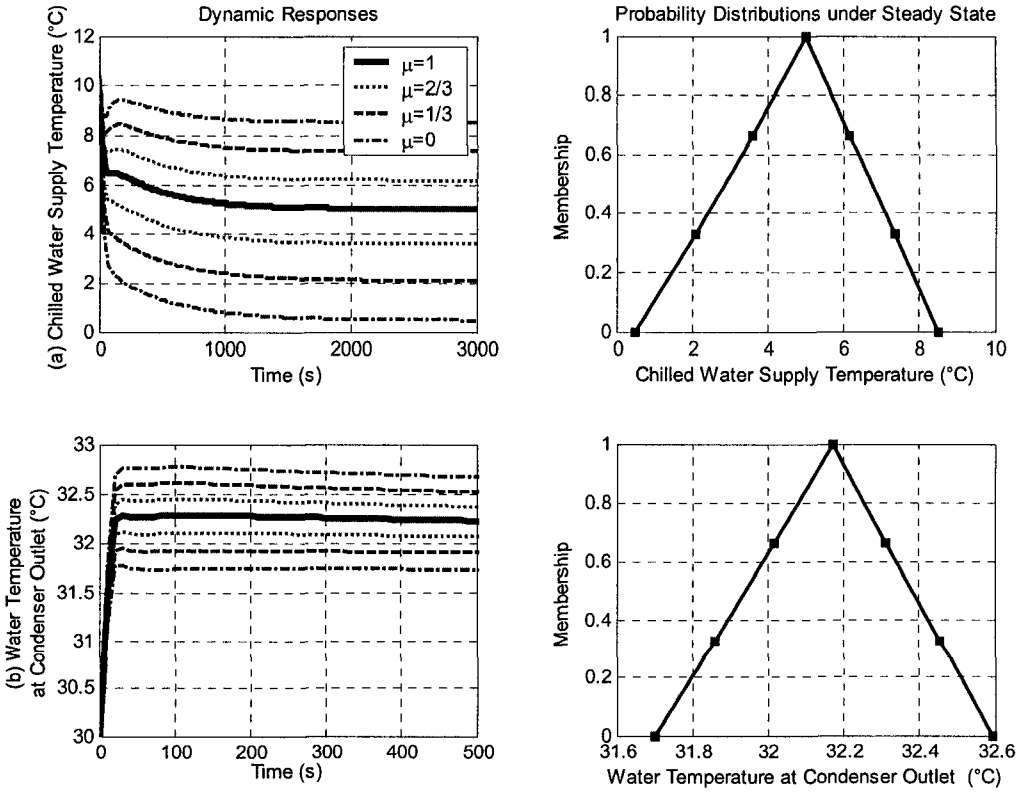

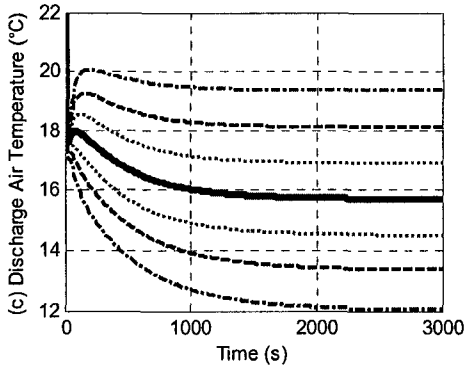
(c) Discharge Air Temperature (°C)
Time (s)

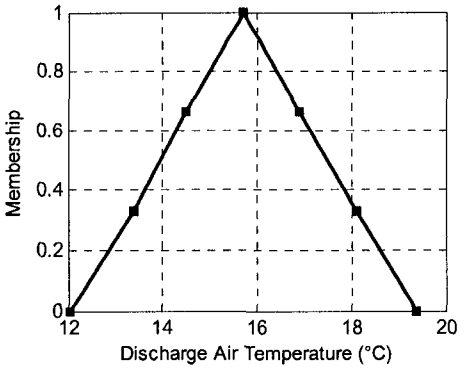
Membership
Discharge Air Temperature (°C)

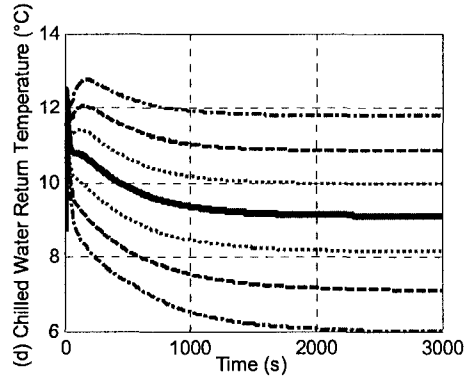
(d) Chilled Water Return Temperature (°C)
Time (s)

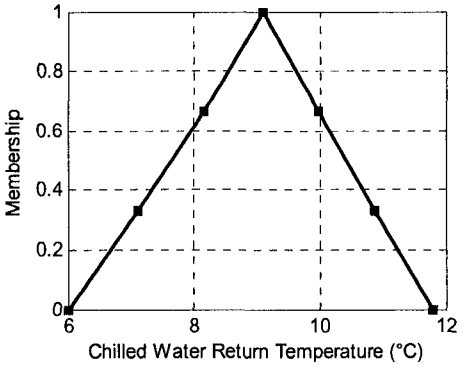
Membership
Chilled Water Return Temperature (°C)

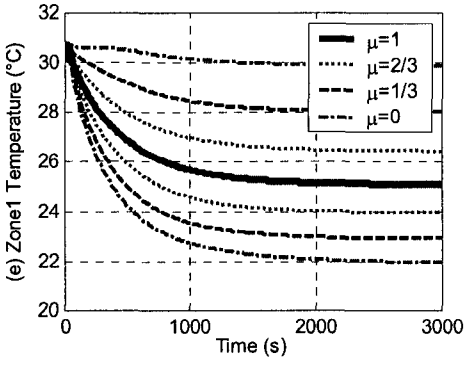
μ=1
μ=2/3
μ=1/3
μ=0
(e) Zone1 Temperature (°C)
Time (s)

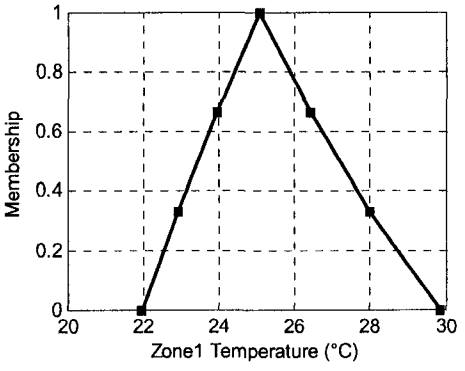
Membership
Zone1 Temperature (°C)

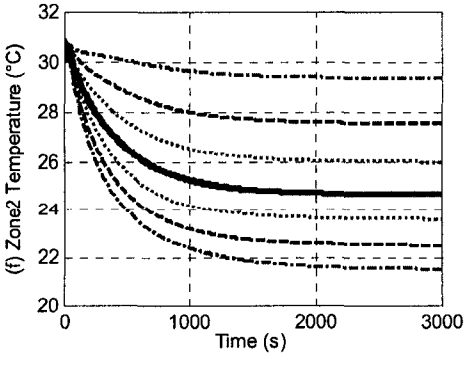
(f) Zone2 Temperature (°C)
Time (s)

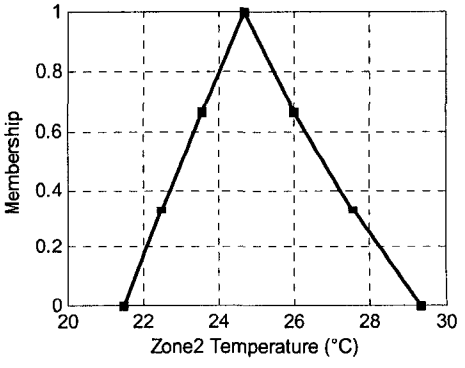
Membership
Zone2 Temperature (°C)

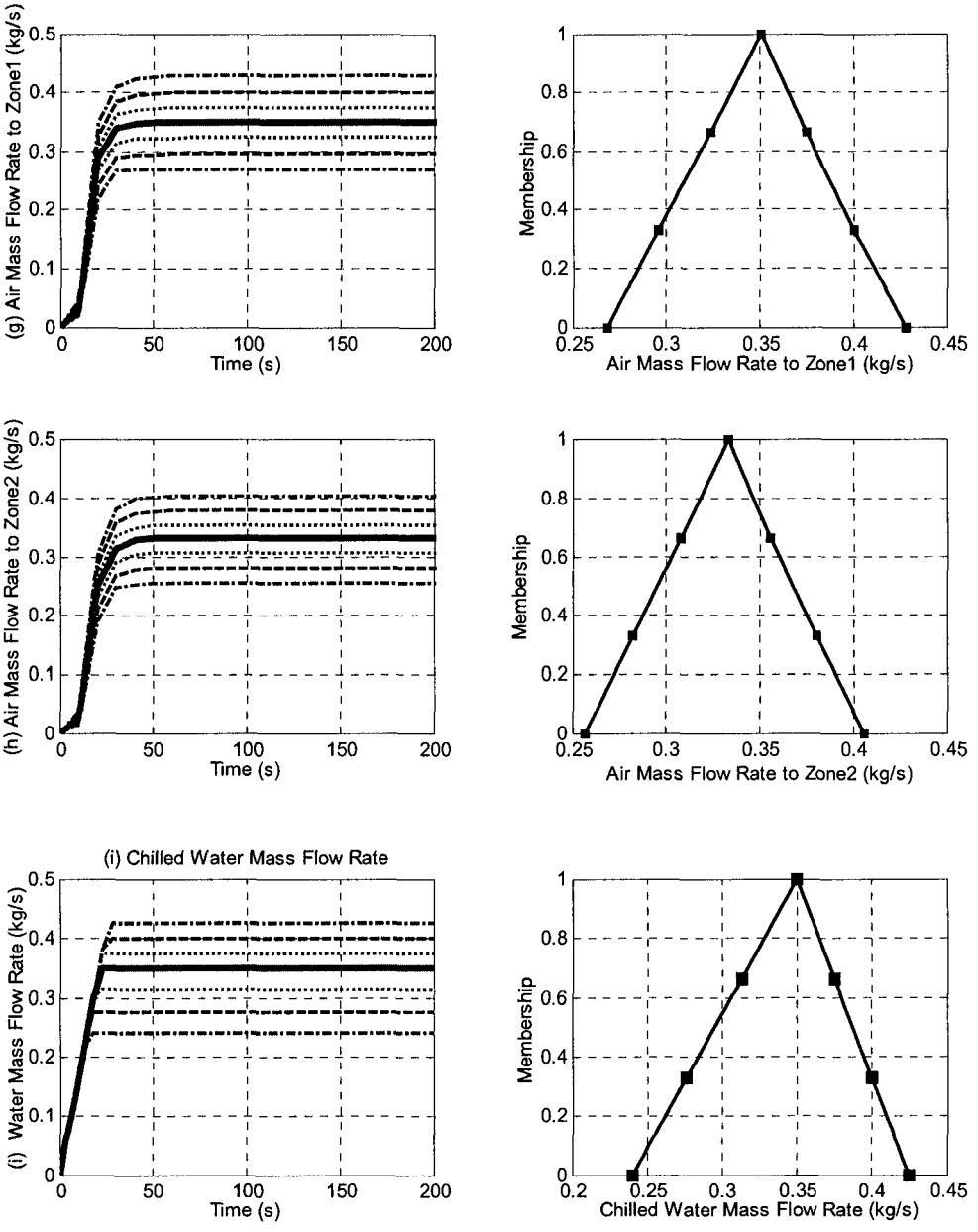

Figure 4-6 Model Dynamic Predictions and Approximate Distributions under Variations of Control inputs

The upper and lower bounds plotted in Figure 4-6 reflect the combined effects of variations in all control inputs at the same membership level. The contribution of individual control inputs with respect to a specific model output variations is computed using Eq.(4-21) and results are depicted in Table 4–3.

Table 4–3 Normalized Effects of Variation of Control Inputs on Model Predictions

	$T_{w,sup}$	$T_{w,con,re}$	T_{aisup}	$T_{w,re}$	T_{z1}	T_{z2}	$\dot{m}_{z1}$	$\dot{m}_{z2}$	$\dot{m}_w$
U_{com} (0.6-0.8)	52%	70%	45%	66%	42%	43%	0%	0%	0%
U_{val} (0.6-0.8)	28%	17%	21%	2%	18%	19%	0%	0%	100%
U_{fan} (0.6-0.8)	11%	7%	19%	18%	4%	2%	38%	38%	0%
U_{z1} (0.7-0.9)	5%	3%	8%	7%	22%	15%	48%	17%	0%
U_{z2} (0.7-0.9)	4%	3%	7%	7%	14%	21%	14%	45%	0%

By comparing the values in the same row listed in Table 4–3, we can see the impacts of individual control inputs on different model outputs:

(1) The compressor energy input U_{com} has dominant effects on the water temperature at the condenser outlet, chilled water supply and return temperature, discharge air temperature and zone air temperatures, while has no influence on the chilled water and air mass flow rates. Higher energy input to the compressor results in higher refrigeration capacity, therefore, more heat can be transferred from the building to the environment; and the higher refrigeration capacity also causes lower supply water temperature, which in turn causes lower discharge air temperature, lower zone air temperatures, and higher condenser water temperature because mass flow rates of the chilled water, condenser water and air are unchanged.

(2) The chilled water valve opening U_{val} fully controls the chilled water mass flow rate, and also influences the condenser water temperature, chilled water supply temperature, discharge air temperature and zone air temperature. With the opening of the chilled water valve, more chilled water circulates in the system and causes higher heat transfer rate in both cooling coil and evaporator; which results in higher condenser water

temperature, lower discharge air temperature and lower zone air temperature. U_{val} doesn't affect the air flow rates either.

(3) Fan energy input U_{fan} has strong impact on the air mass flow rates; 20% change in U_{fan} accounts for 38% changes in the air mass flow rates. U_{fan} also affects the chilled water temperature and discharge air temperature through modulation of the mass flow rate of the air entering the cooling coil and the condenser water temperature through the chilled water. The more energy input to the fan, the more air is circulated in the system, the more heat is transferred from air to water in the coil, which results in a higher chilled water temperature and a higher discharge air temperature. The influence of U_{fan} on zone air temperature is not significant because of the reverse effects of U_{fan} on the air mass flow rate and the discharge air temperature.

(4) The change in VAV damper opening U_{z1} or U_{z2} not only has significant influence on that zone air temperature and the flow rate of the air entering the corresponding zone but also affects the zone air temperature and flow rate of the air entering the other zone. The influence of U_{z1} and U_{z2} on chilled water temperature and discharge air temperature is insignificant. For condenser water temperature, the influence of U_{z1} and U_{z2} is negligible.

By comparing the values in the same column of Table 4–3, the significance of the control inputs with respect to the interested model predictions can be ranked as follows:

(1) Variations in chilled water mass flow rate are caused by the change of U_{val} only; the changes in other control inputs don't affect the chilled water mass flow rate.

(2) Mass flow rate of the air entering zone1/zone2 is not only determined by

damper opening of that zone U_{z1}/U_{z2} and fan energy input U_{fan} but also influenced by the opening of the neighboring damper U_{z2}/U_{z1}. U_{com} and U_{val} don't affect the air mass flow rates. To change the mass flow rate of the air entering zone1/zone2, the control variables with the greatest impact are ordered as U_{z1}/U_{z2}, U_{fan}, and then U_{z2}/U_{z1}.

(3) Supply water temperature variation is mainly caused by the energy input to the compressor U_{com} since supply water temperature is directly related to the refrigeration capacity of the chiller which in turn is determined by U_{com}. U_{val} has great effects on supply water temperature also because the change in U_{val} causes the change in chilled water mass flow rate. In addition, U_{fan} affect the supply water temperature as well because U_{fan} causes changes in air flow rate flowing through the coil and the air mass flow rate affects the coil efficiency and therefore affects the chilled water temperature. The influence of U_{z1} and U_{z2} on supply water temperature are small. To change the supply water temperature, the control variables with the greatest impact are ordered as U_{com}, U_{val}, and then U_{fan}.

(4) Although there is no control on condenser water temperature, the changes in control inputs reflect on the condenser water temperature variations through the flow of refrigerant. Variations in water temperature at the condenser outlet is mainly caused by the change of U_{com}, U_{val} and U_{fan}, in which U_{com} has the greatest impact. Compared to other control inputs, the impacts of U_{z1} and U_{z2} are small.

(5) Discharge air temperature variation is mainly caused by U_{com}, U_{val} and U_{fan} also. U_{com} affects the temperature of the chilled water entering the coil. U_{val} affects the

chilled water flow rate passing through the coil. With the change in chilled water temperature and flow rate, the coil capacity changes and thus causes change in the discharge air temperature. U_{fan} affects the air flow rate passing through the coil and therefore affects the discharge air temperature. The impacts of U_{z1} and U_{z2} on discharge air temperature are not significant. To change the discharge air temperature, the control variables with the greatest impact are ordered as U_{com} , U_{val}, U_{fan} and then U_{z1} and U_{z2}.

(6) The water temperature at the coil outlet (return water temperature) is not a controlled variable, changes in control inputs reflect on chilled water return temperature through air loop and chilled water loop. Variations in return water temperature is mainly caused by the change of U_{com} and U_{fan}. U_{z1} and U_{z2} affect the return water temperature also but not significantly. Compared to other control inputs, the impacts of U_{val} is very small.

(7) U_{com}, U_{val}, U_{z1} and U_{z2} all affect zone air temperature and the impact of U_{com} is the greatest. U_{com} and U_{val} affect the zone air temperature because they affect the discharge air temperature. U_{z1} and U_{z2} affect the zone air temperature through modulating the air mass flow rate entering the zone. To change zone1 temperature, the control variables with the greatest impact is ordered as U_{com}, U_{z1}, U_{val} and then U_{z2}. To change zone2 temperature, the control variables with the greatest impact are ordered as U_{com}, U_{z2}, U_{val}, and then U_{z1}.

From above analysis, we can further note that: first, since chilled water mass flow rate is regulated by U_{val}, and air flow rates in the system are determined by U_{z1}, U_{z2} and U_{fan}, air flow loop and chilled water flow loop can be treated as independent loops,

regulating one loop won't affect the responses of another loop. Second, supply water temperature, discharge air temperature and zone air temperature are integrated results of all control inputs to the system rather than results of individual control inputs. That means adjusting one of them by regulating the corresponding control input will affect the responses of other loops. The discharge air temperature control is not only influenced by airflow and water flow modulations but also influence by chilled water temperature modulation. The zone air temperature control is not only influenced by the airflow modulation but also influenced by the discharge air temperature modulation and the supply water temperature modulation. The chilled water supply temperature control is not only influenced by the refrigerant flow modulation but also influenced by the discharge air temperature modulation.

From the uncertainty analysis, it is apparent that model output predictions vary depending on the uncertainties in the input parameters. To deal with these modeling uncertainties, it is necessary to design adaptive controllers to regulate the system outputs in the presence of uncertainties. The design of proposed adaptive controller will be presented in Chapter 6.

Chapter 5 Neural Network Based Optimal Control of HVAC&R Systems

For HVAC&R systems, there are many variables that can be controlled to provide desired indoor environment in buildings. The controlled variables affect the energy use of the system. With the increase concern on energy cost, there has been a trend to use computational methods to design improved control strategies for more efficient operation of the HVAC&R systems in recent years. Optimal control of HVAC&R systems, aiming at operating HVAC&R system with the least energy while maintaining the desired indoor environment, is one of the areas of significant research interest. Such control strategies can be integrated into building energy management control systems (EMCS) as supervisory control. The optimal set points from the optimal operation scheme are downloaded to corresponding local controllers, which execute the control action and track the set point. The optimal set points are dependent on the uncontrolled variables such as outdoor air temperature, desired indoor temperature and building loads.

In this chapter, an optimal supervisory control algorithm for the two-zone VAV-HVAC & refrigeration system is developed, aiming at reducing the total energy consumption of the fan and the compressor while maintaining a desired zone air temperature. The set points for supply air temperature, supply water temperature and air handler fan static pressure are determined. The developed optimal control strategy integrates model-based prediction and neural network based optimization techniques. This approach allows the coupling of a detailed simulation model instead of empirical models with an efficient NN based optimization method.

The assumptions made in the development of optimal strategy are listed below:

(1) In addition to the independent optimization control, there exist local controls that could maintain the controlled variables at desired set points.

- The compressor speed is controlled such that the a specific supply water temperature is maintained.
- The cooling coil water flow rate is controlled to maintain a given discharge air temperature.
- The mass flow rate of air entering air-conditioned zone is controlled to maintain a desired zone air temperature.
- And fan speed is controlled to maintain the static pressure set point.

Theoretically, the dynamics of the local loop controls must be considered in order to maintain the prescribed set points in an efficient manner during the optimization process. However, for systems without significant thermal storage, these dynamics can be neglected in optimization analysis. (Braun et al. 1989)

(2) Quasi steady-state load is assumed during each optimization step. This assumption justifies because time constants for chilled water temperature, discharge air temperature, zone air temperature control loops are of the order of 20 minutes or less and HVAC plants can usually hold load at approximate steady state conditions for 15-20 minutes at a time. (Cascia, 2000)

(3) The condenser water loop and cooling tower fan speed control are excluded from the optimization analysis. Braun et al. (1989b, 1990) have shown that the coupling between optimal values of the chilled water loop and the condenser water loop is not strong and a near-optimal tower airflow calculation depends solely on the load of the

chilled water loop. These results justify treating the chilled water loop and condenser water including cooling tower as separate loops and including only the chiller and air handling units in the optimal operation analysis. Similar decoupling was adopted by Cascia (2000) in finding the near optimal chilled water temperature and discharge air temperature setpoints for HVAC plant.

(4) Outdoor air damper is held at 40% open during occupied hours.

5.1 Background of Neural Networks

The robustness and the ability of mapping arbitrary nonlinear functions make neural network (NN) an attractive candidate for nonlinear system control.

There are different types of neural networks but basically they all consist of simple elements (neurons) working in parallel. The architecture of NN, which includes the number of layers, the number of neurons in each layer, the connection of neurons, and the transform functions used to evaluate the layer outputs, is one of the key factors ensuring the success of its application. Figure 5-1 illustrates the structure of a three-layer feed forward neural network with biases. The three layers are an input layer, a middle/hidden layer and an output layer. Each layer has a weight matrix *W*, a bias vector *b* and an output vector *A*. A more complicated network may contain more than one middle layer and feedback between neurons.

For a given input vector *IN*, the output of a three-layer feed forward neural network, *OUT*, is computed as follows:

$$OUT = f_2(LW * f_1(IW * IN + b_1) + b_2) \qquad (5\text{-}1)$$

where, IW and LW are weights of the input layer and hidden layer respectively; b_1 and

b_2 are biases to be added to the weighed network inputs and weighted hidden layer outputs; f_1 and f_2 are transfer function for input layer and hidden layer respectively.

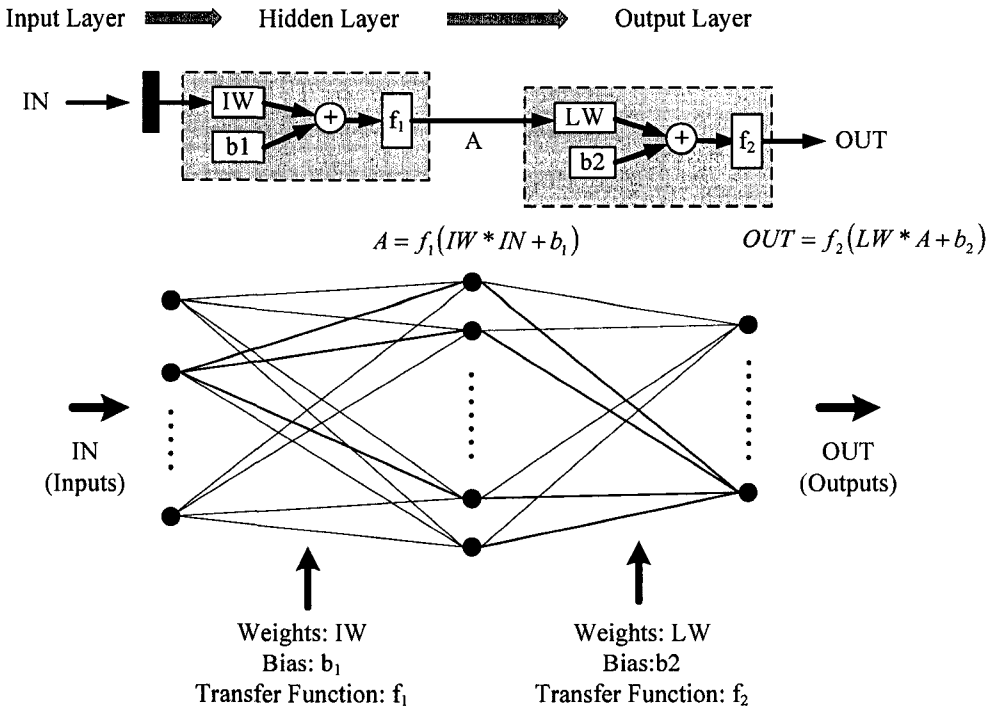

Figure 5-1 Architecture of a Three-Layer Feed forward Neural Network

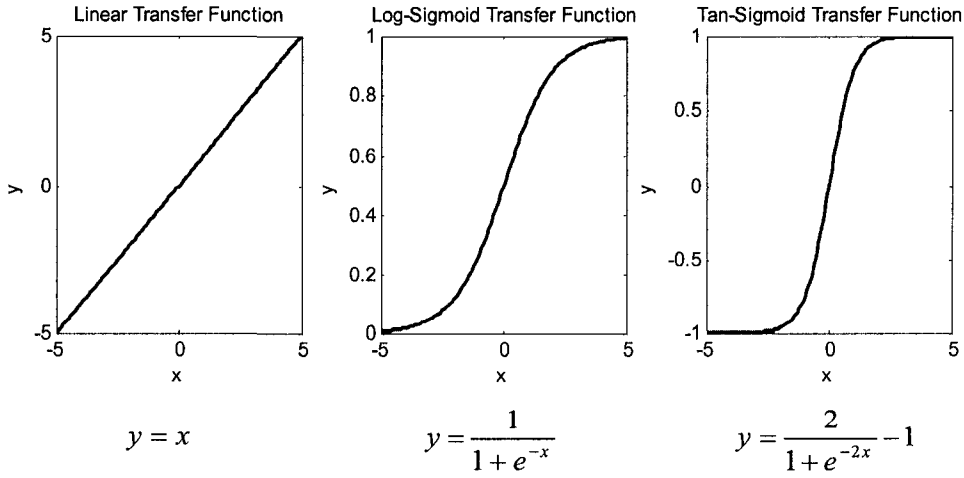

Figure 5-2 Transfer Functions

Figure 5-2 illustrates graphs of three typical transfer functions; they are linear

transfer function in (a), log-sigmoid transfer function in (b) and hyperbolic tangent transfer function in (c). The hyperbolic tangent function and log sigmoid function are monotonic S-shaped functions, the hyperbolic tangent function maps numbers in the interval $(-\infty, +\infty)$ to a finite interval (-1, 1) and the log sigmoid function maps numbers in the interval $(-\infty, +\infty)$ to a finite interval (0, +1) (Matlab, 2006).

A neural network can be trained to perform a particular function by adjusting the values of the weights and/or biases, such that a particular input leads to a specific target output. There are two types of training; one is supervised training and the other is unsupervised training. Supervised training has been the mainstream of neural networks development and applications, for which the training data consist of many pairs of input and output training pattern. The weights and/or biases are adjusted based on a comparison of the network output and the target, until the network output matches the target. For unsupervised training, the training data consist of input information but not with desired output information. The network adapts itself (adjusts its weights and/or biases) to minimize a cost function/performance index which could be any function of the input(s).

Back propagation (BP) is one of the most popular and simplest training methods. BP is a gradient descent algorithm based on chain rule of derivative estimation, in which the network weights and/or biases are adjusted along the direction of the negative of the gradient of the cost function with respect to the weights and/or biases. There are many variations in application of the BP algorithm, such as the steepest descent algorithm, gradient descent with momentum, conjugate gradient algorithm and Broyden-Fletcher-Goldfarb-Shanna (BFGS) quasi-Newton algorithm and Levenberg-Marquardt algorithm.

5.2 Formulation of Optimization Problem for HVAC&R System Operation

The difference between normal operation and optimal operation is that in optimal operation, the system is controlled not only to satisfy certain physical constraints but also a predefined performance index (PI) or cost function, which is a function of controlled and uncontrolled variables, is minimized or maximized at the same time.

For an HVAC&R system to maintain a comfortable indoor environment, the most important concern is the energy used to achieve the desired indoor environment, the smaller the energy use the better. Therefore, the total energy use during operation period is selected as the performance index for the optimal operation of HVAC&R system. To simplify the model and optimization analysis, energy use by chilled water pump is neglected. Other energy components in the HVAC&R system are fan and compressor. The performance index is defined as the total of energy use of compressor E_{com} and VAV fan E_{fan} over the prediction period $0-T$, and is represented mathematically as:

$$Min \ E_{total} = E_{com} + E_{fan} \qquad (5\text{-}2)$$

with,

$$E_{com} = \int_0^T eU_{com}I_{com}dt \qquad (5\text{-}3)$$

$$E_{fan} = \int_o^T eU_{fan}I_{fan}dt \qquad (5\text{-}4)$$

where U_{com} and U_{fan} are normalized voltage input to the compressor and fan motor; I_{com} and I_{fan} are current of the compressor motor and fan motor; e is armature voltage.

The energy consumption of the compressor and the fan is obtained by time

integration of the product of voltage and current. We introduced two states to represent the energy consumption rate of the compressor and the fan such that the energy consumption can be computed directly when the augmented model equations are solved. The state space equations are given as:

$$\frac{dE_{com}}{dt} = eU_{com}I_{com} \qquad (5\text{-}5)$$

$$\frac{dE_{fan}}{dt} = eU_{fan}I_{fan} \qquad (5\text{-}6)$$

with initial values are set to zero, since at $t = 0$, the energy use of the fan or compressor is zero.

In addition to the energy use, the operation of the HVAC&R system is subjected to constraints for proper operation of the mechanical system and constraints for maintaining indoor thermal comfort.

Thermal Comfort Constraints

From the view point of thermal comfort, zone air temperature floating in a certain range around the desired temperature won't sacrifice much comfort while the operation will be much more stable. A small range, for example, ±1°C from the desired temperature for occupied hours and a wider range for unoccupied hours is applied.

Mechanical System Constraints

(1) From the view point of proper operation of the mechanical system, the discharge air temperature $T_{a,\text{sup}}$ should be held in a certain range with the upper limit $T_{a,high}$ coming from thermal comfort requirements, and the lower limit $T_{a,low}$ based on avoiding insufficient ventilation and overcooling in the night. A range of 12-18°C is

normally recommended (Engdahl, 2004).

(2) The chilled water supply temperature $T_{w,\sup}$ should be high enough to avoid freezing in the evaporator and low enough to provide dehumidification of the air in the cooling coil. A generally acknowledged range of the lower limit is 3-7°C and the upper limit is 3-16°C (Lu, 2004).

Control Inputs Constraints

For proper operation of diffusers and achieving good air mixing in the zone, damper opening is confined in the range of [0.4, 1], while other control inputs are normalized in the range of [0, 1].

Mathematically the optimal operation problem is now defined as:

$$
\begin{aligned}
Min \quad & J = E_{com} + E_{fan} \\
subject\ to: \quad & 0.4 \le U_{z1},\ U_{z2} \le 1 \\
& 0 \le U_{com},\ U_{fan},\ U_{val} \le 1 \\
& T_{a,low} \le T_{a.\sup} \le T_{a,high} \\
& T_{w,low} \le T_{w.\sup} \le T_{w,high} \\
& T_{z,low} \le T_z \le T_{z,high} \\
& \dot{X} = f(X,U,Q)
\end{aligned}
\qquad (5\text{-}7)
$$

where the last differential equation represents HVAC&R system model.

Generally, local controls may not ensure stable control performance if the control set points are reset too frequently and by too great magnitudes even the controller is well-tuned or an adaptive one (House et al., 2003). Therefore, if time span of each stage is short enough, it will be justified converting the continuous optimization problem into a multi-stage optimization problem and the constraints on continuous variables are replaced by constraints on discrete variables, the final values of the variables at each stage.

Meanwhile, according to the penalty function theorem (Lillo et al., 1993), by adding a penalty term to the original performance equation whenever one or more constraints are violated, the constrained optimization problem can be approximated by an unconstrained optimization problem if the positive penalty parameter is large enough. Thus, above continuous constrained optimization problem defined in Eq. (5-7) is converted into an N-stage discrete unconstrained optimization problem as:

$$\begin{aligned} Min \quad & J = E_{com} + E_{fan} + \frac{S}{2}\sum_{N}\sum_{j} G_j^{\,2} \\ & subject\ to: \dot{X} = f(X,U,Q) \end{aligned} \tag{5-8}$$

where $S > 0$ is penalty parameter, the choice of S is a trade off between convergence speed and algorithm stability. The larger the S, the closer the unconstrained solution is to the constrained solution. However, a too large penalty parameter causes instability of the algorithm. G_j is the magnitude of the j^{th} constrained variable from the corresponding constraint:

$$G = \begin{cases} T - T_{low} & if \ T < T_{low} \\ 0 & if \ T_{low} \le T \le T_{high} \\ T - T_{high} & if \ T_{high} < T \end{cases} \tag{5-9}$$

Note that the penalty term doesn't account for the control inputs violating their ranges. Control inputs are automatically confined in the range of [0, 1] by the optimization algorithm described in later sections. If damper opening is less than 0.4, the optimization algorithm will simply set it back to 0.4.

Both energy consumption of the HVAC&R system and the penalty term in Eq. (5-8) are functions of the controlled and uncontrolled variables, in other words, the performance function J is a function of the controlled and uncontrolled variables. The

significant uncontrolled variables include cooling loads, ambient temperature and desired zone air temperature. The controlled variables include chilled water supply temperature, discharge air temperature, zone air temperature and fan static pressure. Therefore, the optimization problem in this study is stated as: find the optimal set points for chilled water supply temperature, discharge air temperature and fan static pressure such that for a given desired zone air temperature, zone loads and outdoor temperature profiles, the HVAC&R system maintains zone air temperature around the desired temperature with the least compressor and fan energy consumption.

5.3 NN Based Optimization Algorithm

The accuracy and reliability of the optimal supervisory control strategies depend strongly on the method used for finding the optimal control variables. Unlike linear systems, finding optimal control solutions for nonlinear systems is a difficult task, since analytic solution usually is not available for nonlinear system, numerical techniques, such as dynamic programming, gradient methods, have to be employed for most cases. Projected and augmented Lagrange multiplier methods do not perform well because of the equality constraints used in the problem formulation and the generalized reduced gradient method appears to provide consistent results if it starts with a feasible solution (Cumali, 1988). To this end, in this study, a neural network based approach is used to minimize the above cost function. Figure 5-3 illustrates the NN based optimization process and Figure 5-4 is the flow chart of the optimization algorithm.

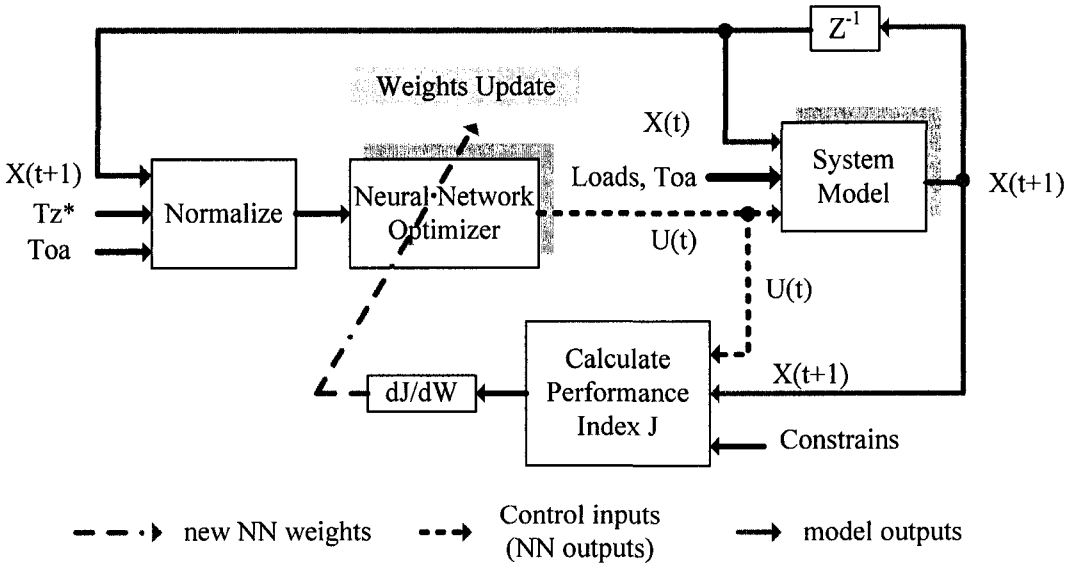

Figure 5-3 Neural Network Based Optimization Process

The optimization horizon is divided into N stages. At the beginning of each stage $t(t)$, a set of control inputs $U = [U_{com}; U_{val}; U_{fan}; U_{z1}; U_{z2}]$ is calculated using current NN weights and input vector, which includes fedback states, desired zone air temperature and outdoor air temperature; the system responses for the next time span (from $N(t)$ to $N(t+1)$) is simulated with this set of control inputs. Model predictions at $N(t+1)$ are initial conditions for the next stage. The supply water temperature, discharge air temperature and zone air temperature at $N(t+1)$ are fedback to the network as part of NN inputs for the next stage. At the same time, the penalty term is evaluated with model outputs at $N(t+1)$. At the end of optimization horizon, the performance index is evaluated and the derivatives of the performance index with respect to NN weights are computed and used to adjust the NN weights such that the weights move along the direction in which J decreases. Obviously, the network is adjusted in unsupervised mode. The adjusting is stopped when constraints on temperature are fulfilled and the

difference in J of two successive adjustments satisfies the following criteria:

$$\|J(k+1) - J(k)\| \leq \varepsilon \qquad (5\text{-}10)$$

where ε is a small positive number.

Obviously, the accuracy of the models used to predict system responses also plays an important role in the accuracy of the optimization solutions. Although simplified models, i.e. neural models and models derived from identification techniques, can usually guarantee the convergence of the solution, the solution derived based on predictions from such models may not be the optimal one. Therefore, in order to improve the accuracy of the optimization solutions, in this study, the dynamic model developed in Chapter 3 is employed to simulate the system behavior and the sensitivity derivatives of the system outputs with respect to the control inputs are evaluated with simulation results also though this may result in more calculations.

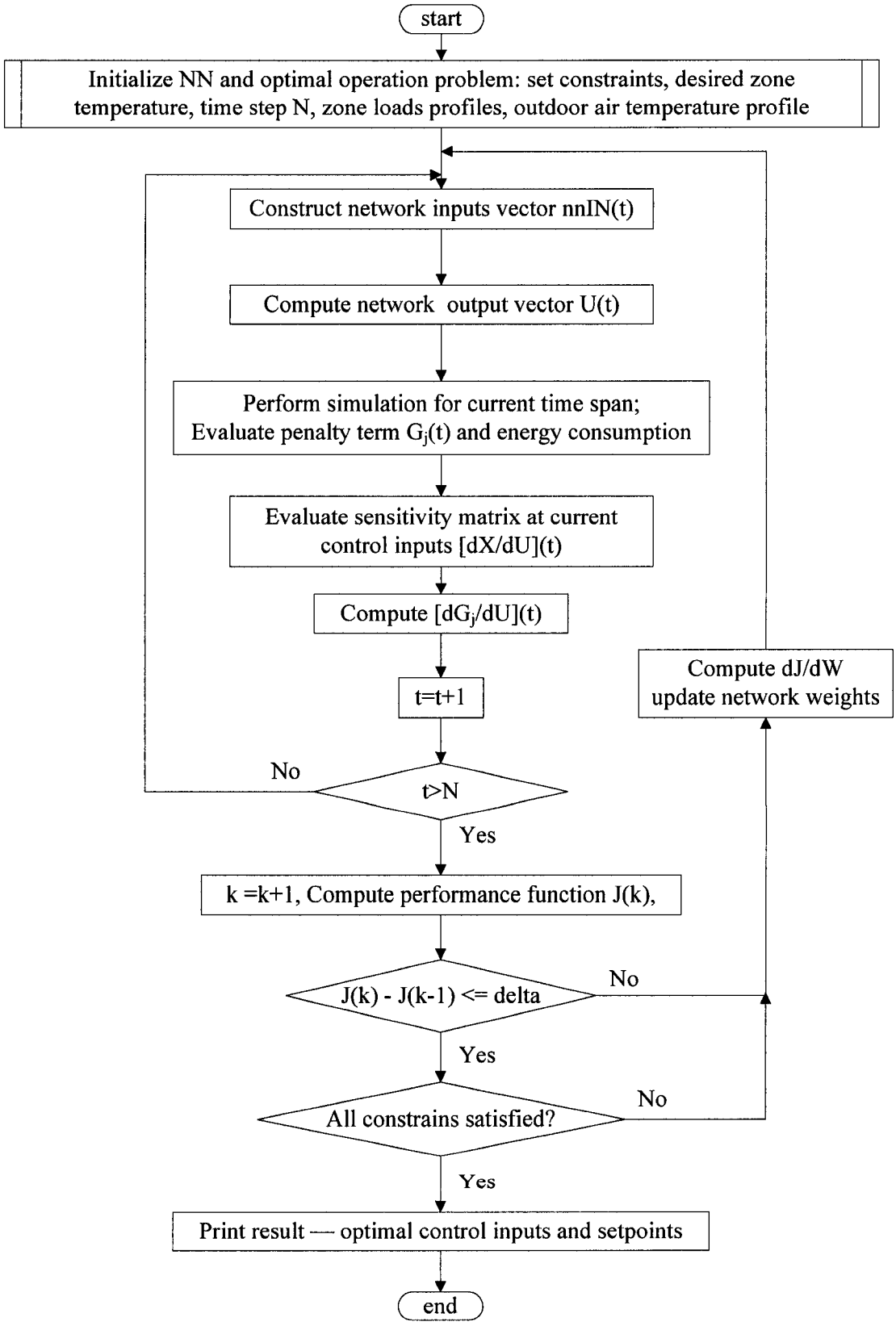

Figure 5-4 NN based Optimization Algorithm Flow Chart

5.3.1 Network Construction

A three layer feed forward neural network without biases is constructed and used to search the solutions for the optimization problem defined in Eq.(5-8). Together with dynamic model prediction, this network can be used as a supervisory optimization controller. The outputs of the neural network are control inputs to the system: U_{com}, U_{val}, U_{fan}, U_{z1} and U_{z2}. And the inputs of the neural network include energy consumption related controlled and uncontrolled variables:

- Outdoor air temperature, T_{oa}
- Desired zone1 temperature, T_{z1}^{*}
- Desired zone2 temperature, T_{z2}^{*}
- Supply water temperature, $T_{w,\mathrm{sup}}$
- Discharge air temperature, $T_{a,\mathrm{sup}}$
- Zone1 air temperature, T_{z1}
- Zone2 air temperature, T_{z1}

Among these inputs, outdoor air temperature and desired zone air temperature are uncontrolled variables. They affect system energy use and system operation mode, and in turn determine the optimal set points of the controlled variables to be set by the supervisory control. The rest of the inputs, supply water temperature, discharge air temperature and zone air temperature are feedback states. The state feedback makes this optimization approach more robust than the open loop techniques.

In order to improve the training efficiency and avoid dominating of the outputs by some inputs, the network inputs are normalized in the range of 0 to 1 as:

$$X_{norm} = \frac{X - X_{\min}}{X_{\max} - X_{\min}} \qquad (5\text{-}11)$$

The network has seven inputs and five outputs. The transfer function of the input layer is hyperbolic tangent function and the transfer function of the hidden layer is log sigmoid function. The outputs of the network automatically fall in the range of (0, +1), which means the control inputs are confined in the range of (0, +1) automatically.

After trying different numbers of neurons in the hidden layer, 40 hidden neurons were used, thus a three-layer (7-40-5) feed forward neural network was constructed and trained unsupervised to solve the optimization problem.

5.3.2 Adjusting the Network Weights

The weights of the network are initiated with a set of random numbers. The error back propagation (BP) algorithm is used to adjust the weights along the direction in which the performance index decreases. The basic BP algorithm adjusts the weights along the steepest descent direction (negative of the gradient). However, the steepest descent direction does not necessarily produce the fastest convergence. In order to achieve both fast decrease and fast convergence, two adjusting methods are used in this study, one is the gradient descent with momentum and variable learning rate algorithm, and the other is BFGS quasi-Newton algorithm. At the beginning of training, the weights of the neural network are adjusted using the gradient descent algorithm for fast decrease in the performance index and then the weights of the neural network are adjusted using the BFGS quasi-Newton algorithm for fast convergence.

The gradient descent algorithm adjusts the weights as follows:

$$W_{k+1} = W_k - mc\, dW_{k-1} - lr(1-mc)\frac{dJ}{dW_k} \qquad (5\text{-}12)$$

where mc is training momentum coefficient and lr is learning rate.

The BFGS algorithm adjusts the weights as followings:

$$W_{k+1} = W_k - lrH_k^{-1}\left(\frac{\partial J}{\partial W_k}\right)^T \qquad (5\text{-}13)$$

where, H_k is approximate Hessian matrix of the performance function J. H_k is updated as follows:

$$H_{k+1} = H_k + \frac{dW_k dW_k^T}{dW_k^T \Delta g_k} - \frac{H_k \Delta g_k (H_k \Delta g_k)^T}{\Delta g_k^T H_k \Delta g_k}$$

$$\text{with } dW_k = W_k - W_{k-1} = lrH_k^{-1}\left(\frac{\partial J}{\partial W_k}\right)^T, \quad \Delta g_k = \frac{\partial J}{\partial W_k} - \frac{\partial J}{\partial W_{k-1}} \qquad (5\text{-}14)$$

$$H_0 = I$$

where Δg_k is differential change in the derivative of performance function J with respect to weights, and dW_k is change in the weights.

For the gradient descent algorithm, proper selection of the learning rate dominates the performance of the algorithm and the selection of learning rate is a trade off between stability and fast convergence. A high learning rate could result in unstable results, and a low learning rate could reduce convergence speed. However, it is impossible to determine the optimal learning rate before training because the optimal learning rate changes during the training process as the algorithm moves across the performance surface. To improve the performance of gradient descent algorithm, instead of using fixed learning rate, the gradient descent algorithm is modified to include an adaptation of the learning rate during the training process. At each weight adjustment, new weights are calculated using current

learning rate and momentum, if the new value of the performance function is higher than the previous value, the new weights are discarded and the learning rate is decreased. Otherwise, the new weights are kept and the learning rate is increased. Thus the learning rate increases during the training process, but only to the extent that won't cause unstable process.

5.3.3 Derivative Calculation

For BP training algorithm, the computation of derivative of the performance index with respect to NN weights $\frac{\partial J}{\partial W}$ is indispensable. The computation is given as follows:

From the performance function Eq.(5-8), we have,

$$\frac{\partial J}{\partial W_k} = dJ_E + dJ_P \tag{5-15}$$

with,

$$dJ_E = \frac{\partial J}{\partial E_{com}} \frac{\partial E_{com}}{\partial W_k} + \frac{\partial J}{\partial E_{fan}} \frac{\partial E_{fan}}{\partial W_k} \tag{5-16}$$

$$dJ_P = \sum_{t=1}^{N} \left(\sum_j \left(\frac{\partial J}{\partial G_j(t)} \frac{\partial G_j(t)}{\partial T_j(t+1)} \frac{\partial T_j(t+1)}{\partial U(t)} \frac{\partial U(t)}{\partial W_k} \right) \right) \tag{5-17}$$

The total energy consumption of the compressor and fan during optimization horizon can be approximated as the sum of energy consumption of the compressor and fan during each stage, therefore,

$$dJ_E = \sum_{t=1}^{N} \begin{pmatrix} \frac{\partial J}{\partial E_{com}(t)} \frac{\partial E_{com}(t)}{\partial U(t)} \frac{\partial U(t)}{\partial W_k} + \frac{\partial J}{\partial E_{com}(t)} \frac{\partial E_{com}(t)}{\partial I_{com}(t+1)} \frac{\partial I_{com}(t+1)}{\partial U(t)} \frac{\partial U(t)}{\partial W_k} \\ \frac{\partial J}{\partial E_{fan}(t)} \frac{\partial E_{fan}(t)}{\partial U(t)} \frac{\partial U(t)}{\partial W_k} + \frac{\partial J}{\partial E_{fan}(t)} \frac{\partial E_{fan}(t)}{\partial I_{fan}(t+1)} \frac{\partial I_{fan}(t+1)}{\partial U(t)} \frac{\partial U(t)}{\partial W_k} \end{pmatrix} \tag{5-18}$$

From Eq. (5-3), (5-4) and (5-8), we have,

$$\frac{\partial J}{\partial E_{com}(t)}\frac{\partial E_{com}(t)}{\partial U(t)} = eI_{com}(t+1) \qquad (5\text{-}19)$$

$$\frac{\partial J}{\partial E_{fan}(t)}\frac{\partial E_{fan}(t)}{\partial U(t)} = eI_{fan}(t+1) \qquad (5\text{-}20)$$

$$\frac{\partial J}{\partial E_{com}(t)}\frac{\partial E_{com}(t)}{\partial I_{com}(t+1)} = eU_{com}(t) \qquad (5\text{-}21)$$

$$\frac{\partial J}{\partial E_{fan}(t)}\frac{\partial E_{fan}(t)}{\partial I_{fan}(t+1)} = eU_{fan}(t) \qquad (5\text{-}22)$$

$$\frac{\partial J}{\partial G_j(t)}\frac{\partial G_j(t)}{\partial X_j(t+1)} = 2S * G_j(t) \qquad (5\text{-}23)$$

The partial derivatives $\frac{\partial U(t)}{\partial W_k}$ are computed using the conventional BP algorithm

The sensitivity derivatives $\frac{\partial I(t+1)}{\partial U(t)}$ and $\frac{\partial T(t+1)}{\partial U(t)}$ are computed from model equations using perturbation method as follows: for current initial condition and control inputs, record the simulation results and denote the final values of the interested outputs as XF^o; then giving a small disturbance to one control input U_i at a time, such as a decrease by ΔU_i, using the same initial conditions and the new set of control inputs, run the model and record the final values of the interested outputs as XF_i, then the sensitivity derivative is computed from:

$$\frac{\partial X(t+1)}{\partial U_i(t)} = \frac{XF^o - XF_i}{\Delta U_i} \qquad (5\text{-}24)$$

5.4 Simulation Results

To evaluate the performance of the proposed neural network based optimal supervisory strategy, two cooling days operations were simulated. One represents full load operation and the other represents partial load operation. Simulation results were compared with night reset operation strategy.

Figure 5-5 and Figure 5-6 illustrate the load profiles and outdoor air temperature profile of two simulation days under the full load (simulation case1) and partial load (simulation case2) respectively. Zone1 represents the exterior zone and its load profile follows the outdoor air temperature shape, which is approximated as a sine function. Zone2 represents the interior zone, for which load is determined by the building operation schedule. The building and system operating conditions are depicted in Table 5–1.

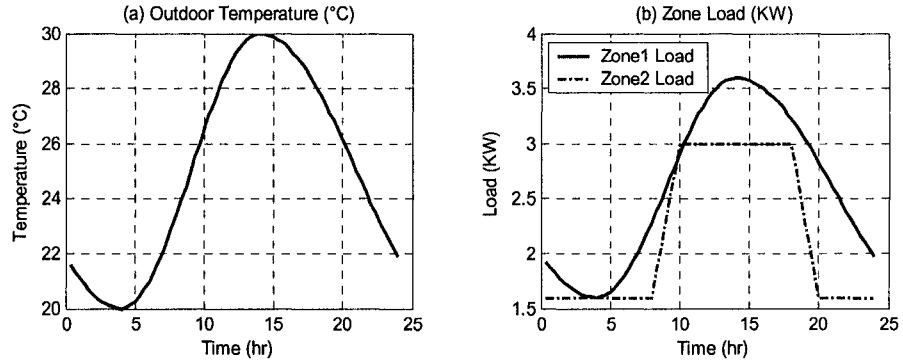

Figure 5-5 Outdoor Air Temperature and Zone Cooling Load Profiles – Full Load

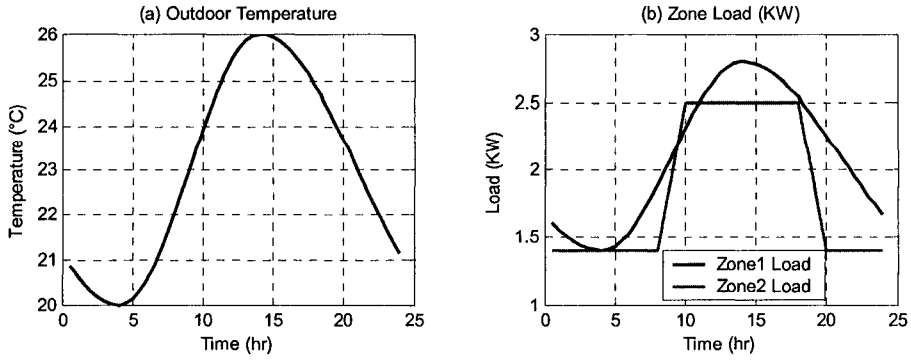

Figure 5-6 Outdoor Air Temperature and Zone Cooling Load Profiles – Partial Load

Table 5–1 System Operation Conditions

	Schedule	$T_{v,sup}$ (°C)	$T_{a,sup}$ (°C)	T_z (°C)
Occupied Hours	9am-18pm	4-10	10-17	23±1
Unoccupied Hours	19pm-8am	⩾8	10-23	24-27
Transition Hours	8-9am, 18-19pm	4-20	10-23	23-25

The simulation day is divided into 72 time stages. The optimal set points are updated every 20 minutes. Simulation results from proposed optimization method are depicted in Figure 5-7 (for full load case) and Figure 5-8 (for partial load case), which include the energy consumption of compressor and fan in figure (a), fan static pressure in figure (b), discharge air temperature in figure (c), supply water temperature in figure (d), zone air temperature in figure (e) and figure (f), mass flow rate of air to each zone in figure (g), chilled water flow rate in figure (h) and control inputs in figure (i)- (j). From Figure 5-7 and Figure 5-8, we note that:

(1) From figure (b)-(d), we can see that the optimal supply water temperature, discharge air temperature and static pressure change with the variations of total load. The influence of the total load on the optimal set points is relatively high. The higher the load, the lower are the supply water and discharge air temperatures. The temperature difference between the optimal discharge air and chilled water set points increases with load.

(2) From figure (b)-(d) and (i), we can see that the chiller and the fan operation follow the load variations. The chiller and fan operates at lower capacity when the load is low, as such high chilled water temperature and discharge air temperature are maintained. With the increase in cooling load, the chiller operates at higher capacity to maintain a lower chilled water temperature and discharge air temperature. However, the fan is

operated at a higher rate than the chiller, especially during the unoccupied hours. That is because compared to the chiller energy consumption; the fan energy consumption is much smaller, higher air flow rate results in higher coil heat transfer efficiency and thus improves the overall efficiency of system, especially under the partial load conditions. In addition, during the unoccupied hours, ambient temperature is lower than the indoor temperature, with fixed outdoor air damper opening, the higher fan pressure gain in the system, the more outdoor air is introduced into the building and therefore reduces the load on the chiller and in turn reduces the chiller energy consumption.

(3) From figure (i), we see that once the chiller is in operation, the chilled water valve tends to open fully. This is because we neglect the energy consumption of the chilled water pump. Therefore, whenever the chiller is start-up, the chilled water valve tends to be fully open to enable the chilled water transfer as much heat from VAV system to chiller as possible. At the same time, the higher water flow rate brings higher cooling coil efficiency. The cooling generated by the chiller can be used to the greatest extent.

(4) Figure (e) and (f) show that the optimization strategy minimizes the energy consumption by keeping the zone air temperatures near the high limit. From figure (j), we see that the zone1 damper is almost fully open throughout the day, while the zone2 damper opening experiences large variations. With the same supply air temperature, the zone with higher load requires more conditioned air and therefore opens the damper fully. The zone with lower load adjusts its damper opening according to the load difference of two zones. When the load difference is low, the damper opens more towards full open position.

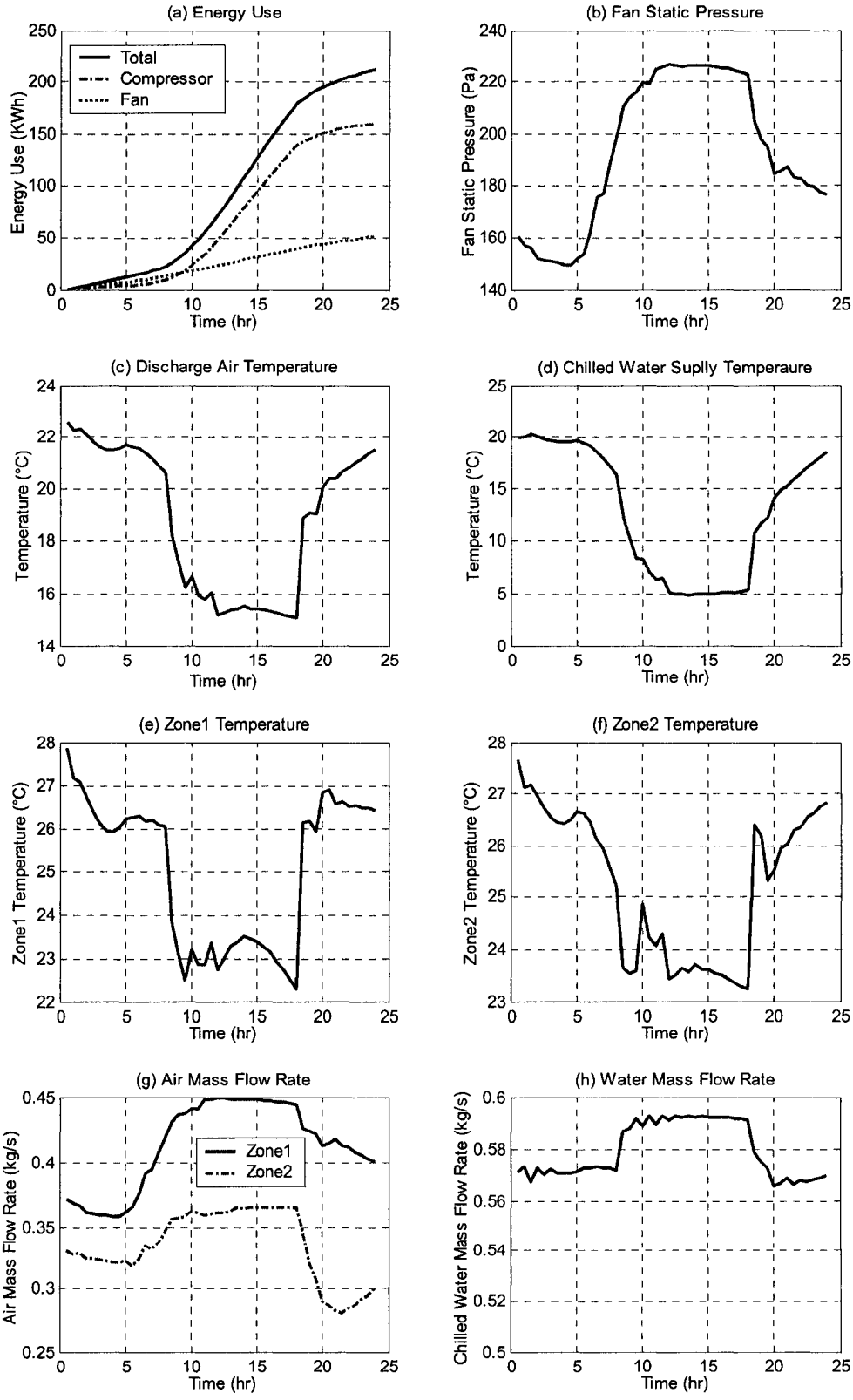
(a) Energy Use
Total
Compressor
Fan
Energy Use (KWh)
Time (hr)
(b) Fan Static Pressure
Fan Static Pressure (Pa)
Time (hr)
(c) Discharge Air Temperature
Temperature (°C)
Time (hr)
(d) Chilled Water Suplly Temperaure
Temperature (°C)
Time (hr)
(e) Zone1 Temperature
Zone1 Temperature (°C)
Time (hr)
(f) Zone2 Temperature
Zone2 Temperature (°C)
Time (hr)
(g) Air Mass Flow Rate
Zone1
Zone2
Air Mass Flow Rate (kg/s)
Time (hr)
(h) Water Mass Flow Rate
Chilled Water Mass Flow Rate (kg/s)
Time (hr)

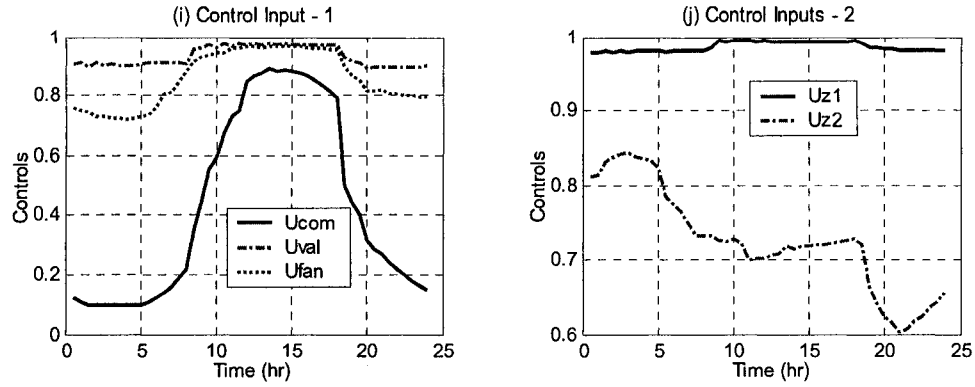

Figure 5-7 Simulation Results from Optimal Operation – Full Load Case

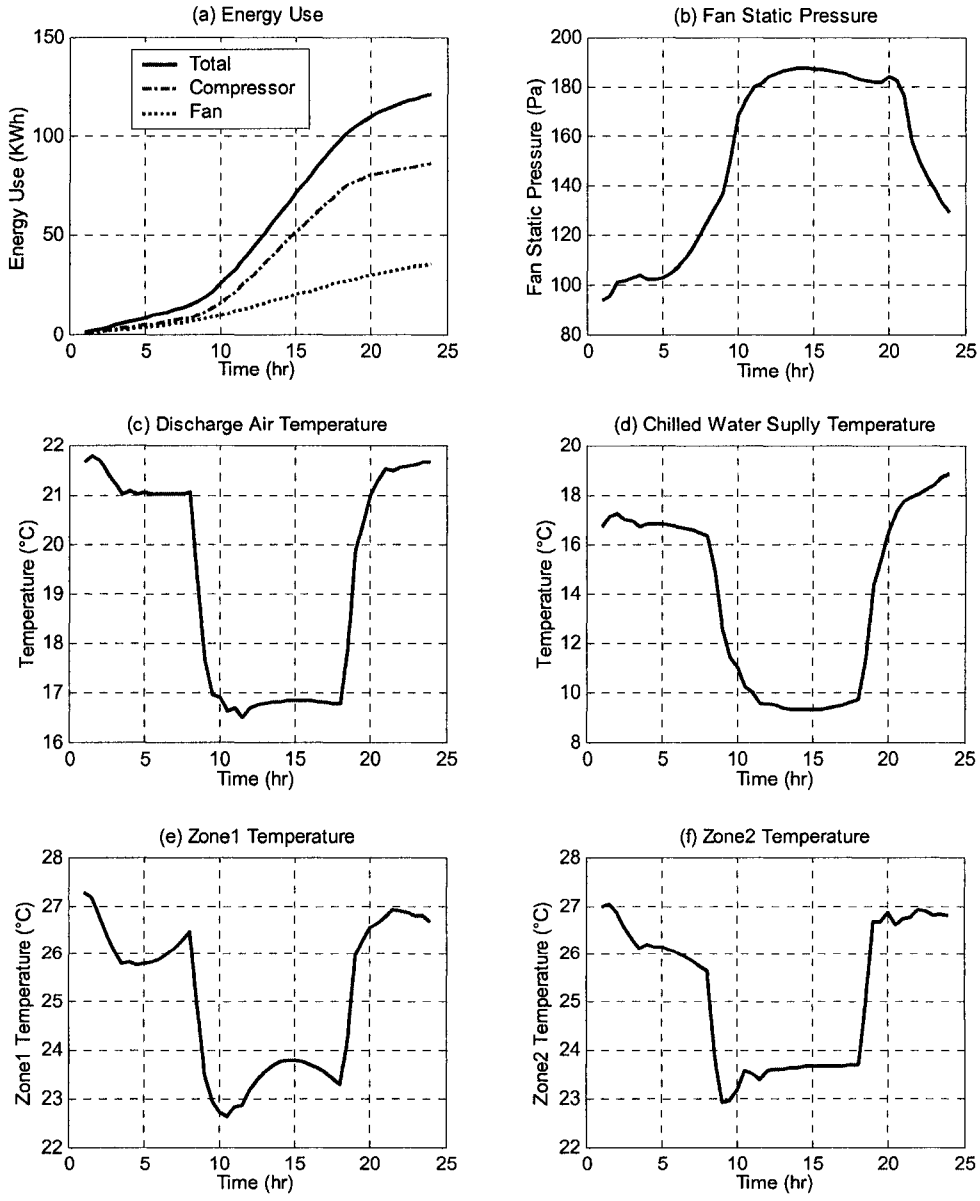

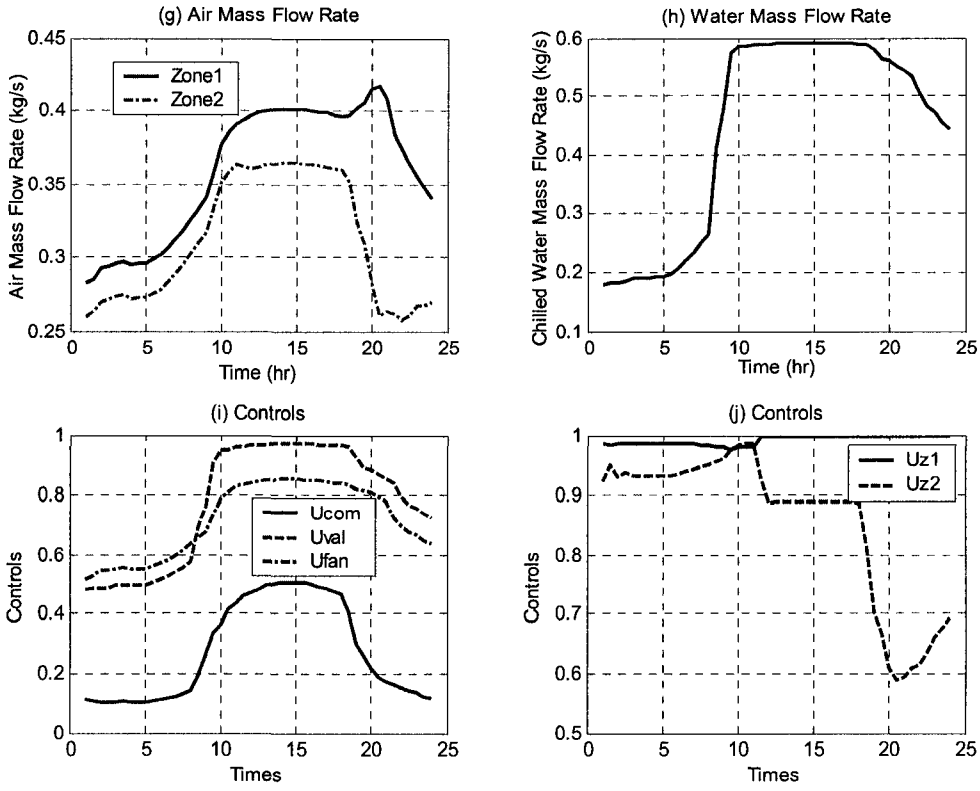

Figure 5-8 Simulation Results from Optimal Operation – Partial Load Case

To evaluate the performance of the optimal operation strategy, system responses under conventional night reset operation scheme are simulated with the same operating conditions as illustrated in Figure 5-5, Figure 5-6 and Table 5–1. During the unoccupied hours, the zone air temperature, supply water temperature and discharge air temperature are set to higher values as depicted in Table 5–2 to save energy. U_{com}, U_{val}, U_{z1} and U_{z2} are adjusted every 20 minutes to maintain the water and air temperature set points. U_{fan} is fixed as indicated in Table 5–2.

Table 5–2 Night Reset Operation Scheme

	Schedule	$T_{w,sup}$(°C)	$T_{da,sup}$(°C)	T_z(°C)	U_{fan}
Full Load Case	Occupied Hours (9am-18pm)	5	14.5	23±1	1
	Unoccupied Hours (19pm-8am)	10	19	24-27	0.6
	Transition Hours (8-9am, 18-19pm)	6	14.5-19	23-25	1
Partial Load Case	Occupied Hours (9am-18pm)	8	18	23±1	0.9
	Unoccupied Hours (0-8am, 19-23pm)	16.5	20.5	24-27	0.75
	Transition Hours (8-9am, 18-19pm)	13	17-19	23-25	0.75

Simulation results from night reset operation are shown in Figure 5-9 and Figure 5-10, which also include time history of energy consumption of fan and compressor, fan static pressure, supply water temperature, discharge air temperature, zone air temperature, mass flow rate of the air entering each zone, chilled water flow rate and control inputs.

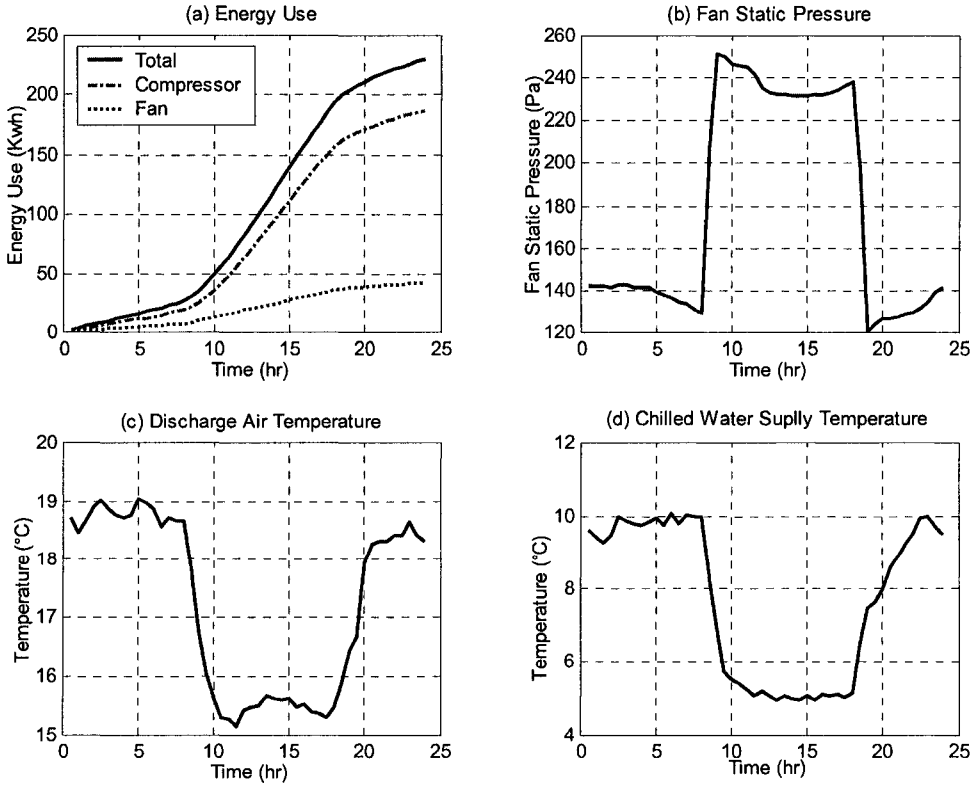

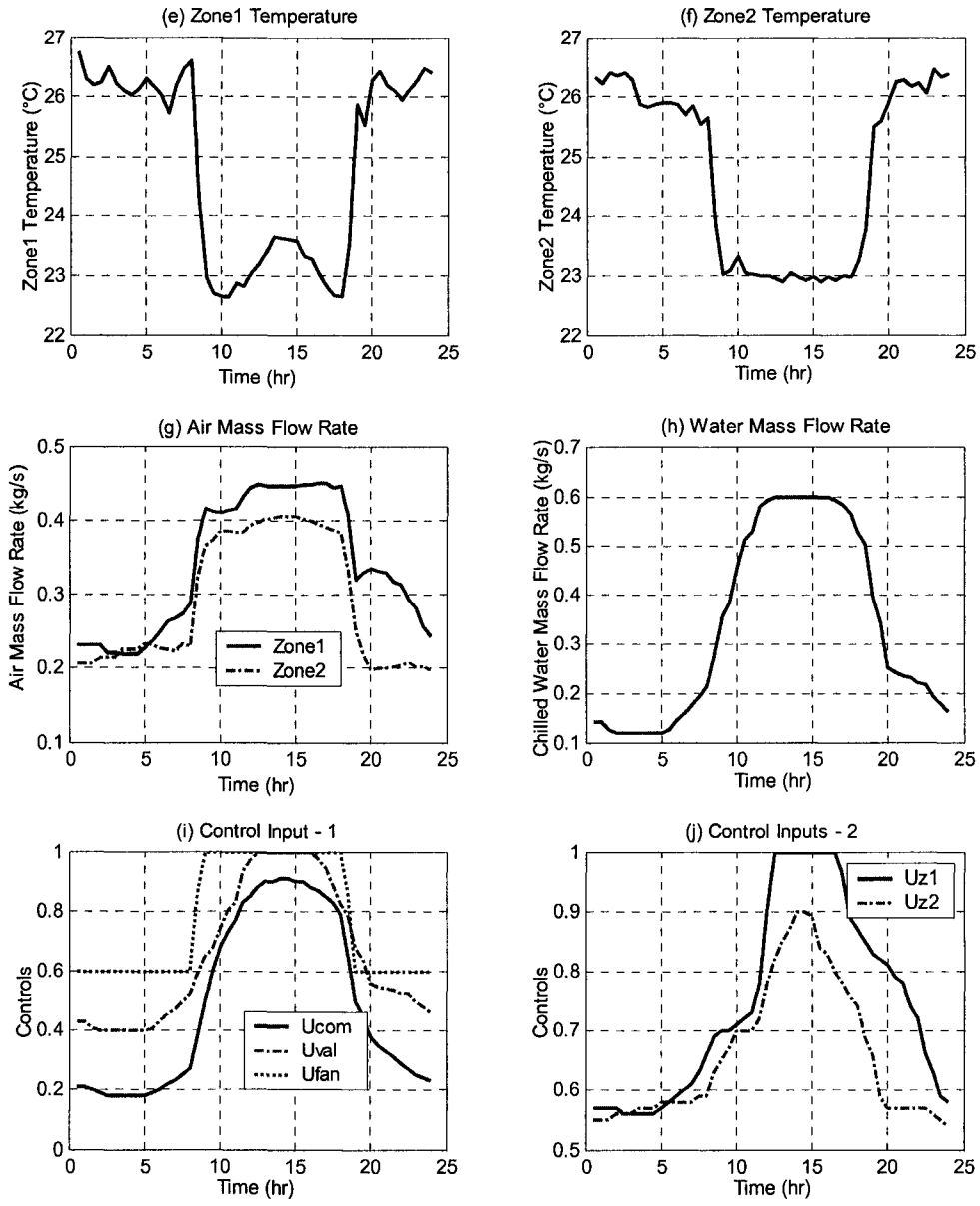

Figure 5-9 Simulation Results from Night Reset Operation Scheme – Full Load

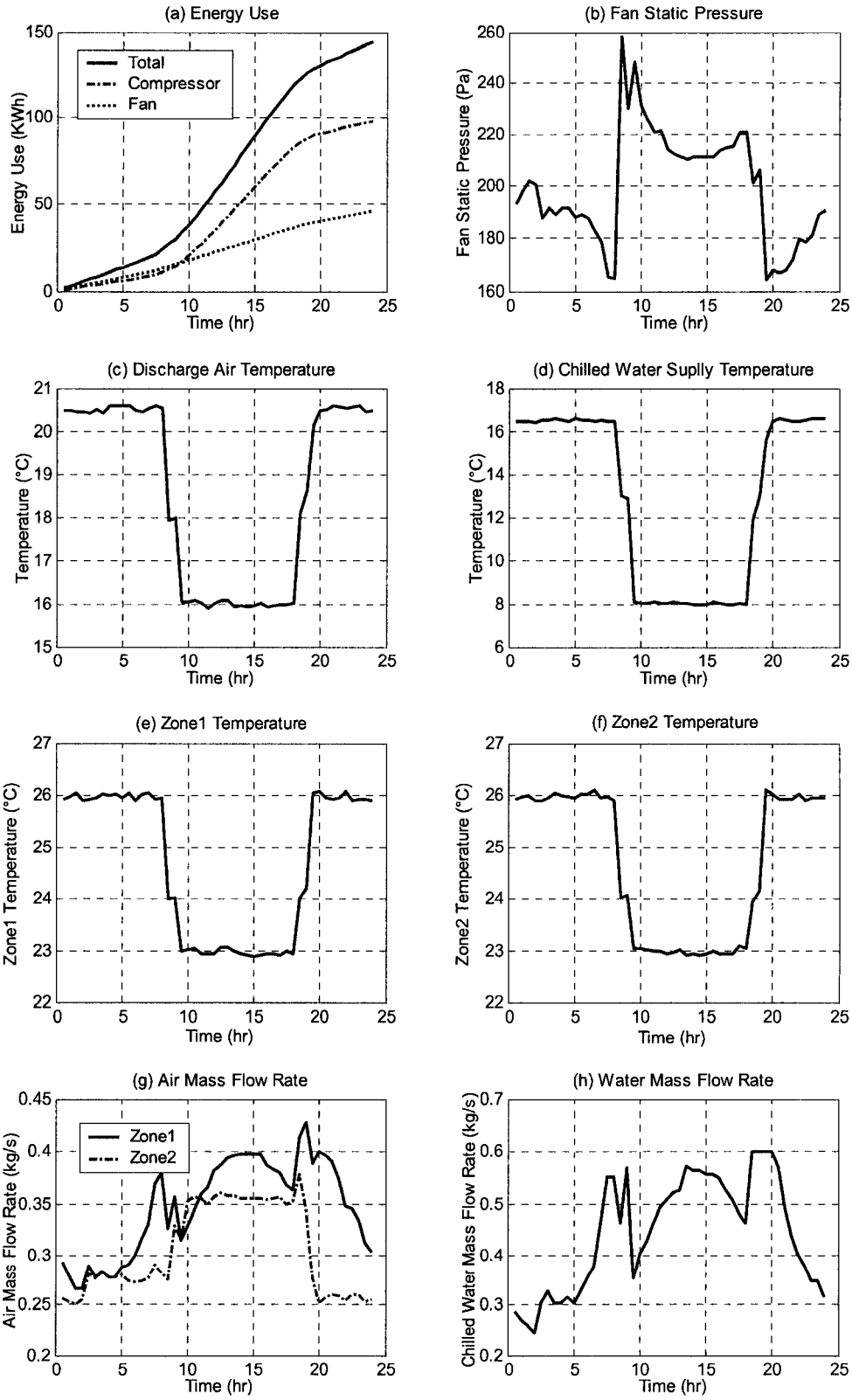
(a) Energy Use
Total
Compressor
Fan
Energy Use (KWh)
Time (hr)
(b) Fan Static Pressure
Fan Static Pressure (Pa)
Time (hr)
(c) Discharge Air Temperature
Temperature (°C)
Time (hr)
(d) Chilled Water Suplly Temperature
Temperature (°C)
Time (hr)
(e) Zone1 Temperature
Zone1 Temperature (°C)
Time (hr)
(f) Zone2 Temperature
Zone2 Temperature (°C)
Time (hr)
(g) Air Mass Flow Rate
Zone1
Zone2
Air Mass Flow Rate (kg/s)
Time (hr)
(h) Water Mass Flow Rate
Chilled Water Mass Flow Rate (kg/s)
Time (hr)

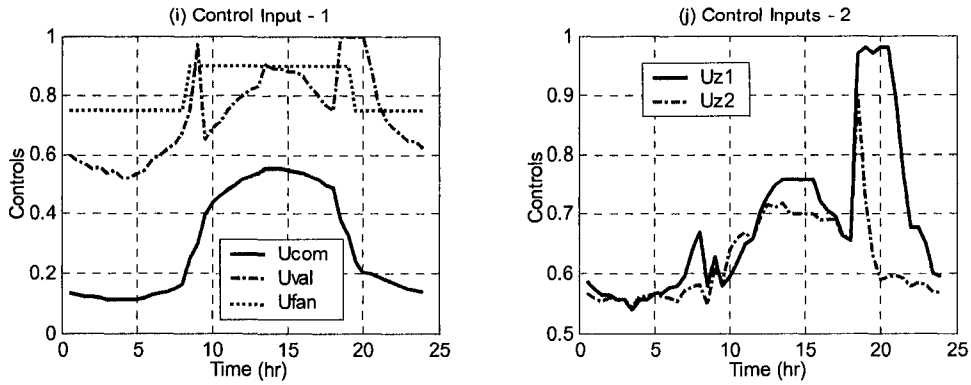

Figure 5-10 Simulation Results from Night Reset Operation Scheme – Partial Load

By comparing the responses in Figure 5-7 with Figure 5-9, Figure 5-8 with Figure 5-10, we note that both control strategies maintain zone air temperatures around the desired value and fulfill other operating constraints, however, the energy consumption is different. Table 5–3 summarizes the energy consumptions of two cases.

Table 5–3 Energy consumption Comparison of Two Operation Schemes

	Energy Component	Optimal Operation (kwh)			Night Reset Operation (kwh)		
		Unoccupied Hours	Occupied Hours	Total	Unoccupied Hours	Occupied Hours	Total
Full Load Case	Fan	24.7	26.8	51.5	13.7	19.2	42.9
	Compressor	30.1	130.2	160.3	49.3	137.1	186.4
	Total			211.8			229.3
Partial Load Case	Fan	11.9	23.5	35.4	19.6	26.9	46.5
	Compressor	14.4	71.2	85.6	17.7	79.3	97.0
	Total			121.0			143.5

The daily total energy consumption under the optimal operation strategy is 8% and 19% less than the energy consumption under the night reset operation for full load condition and partial load condition respectively. In the full load operation, the energy

consumption of the chiller in optimal operation is less than that in the conventional operation of the order of 47% and 5% saving during the unoccupied hours and occupied hours respectively. However, the energy consumption of the fan in the optimal operation is higher than that in the conventional operation, especially during the unoccupied hours. This is because the optimal operation scheme tends to take full advantage of the cold outdoor air in the early morning and late night to reduce the chiller load. In partial load operation, the energy consumption of the chiller in optimal operation is 23% and 10% less than the night reset operation during unoccupied hours and occupied hours respectively; the energy consumption of the fan in the optimal operation is 65% and 14% less than the night reset operation during unoccupied hours and occupied hours respectively.

For the conventional night reset operation strategy, the selection of chilled water temperature is directly related to the energy consumption of the compressor. The higher the supply water temperature, the less will be the energy consumption of the chiller. However, there are no general rules available for operators selecting proper water and air temperature set points. In practice, the selection of temperature set points is based on engineering experience and cannot ensure greatest energy saving. The optimization operation algorithm presented above provides a method to find control set points that could ensure the energy saving. Comparing the two simulation cases, we can see that for the full load operation, the temperature set points in the night reset operation scheme is closer to the optimal values, and therefore, the energy saving potential of the optimal operation scheme is not very high. However, for the partial load operation, the temperature set points in night reset operation scheme are away from the optimal values

and therefore the saving potential of the optimal operation scheme is much higher.

Chapter 6 Adaptive Control Design for HVAC&R Systems

So far, the optimal operation scheme of the two-zone HVAC&R system has been determined at the supervisory level with the assumption that existing local controls can maintain the controlled variables at desired optimal set points. In this chapter, we will discuss the design of local controllers to implement the optimal operation at the local loop level. PI and PID controllers have been the most popular controllers in HVAC&R applications for decades because of their simple structure and reliable control performance. However, HVAC&R systems are complicated multi-input-multi-output (MIMO), time-varying, highly non-linear systems with different scale of time constants. The conventional PI/PID controllers are therefore not able to provide consistent good performances even when they are well tuned because:

(1) The conventional PI/PID controllers are designed for single-input-single-output individual control loops without counting in the influence of other control loops. However, neglecting the strong coupling effects between control loops in the HVAC&R systems is detrimental to the performance of the PI/PID controller.

(2) The PI/PID controllers designed for different local control loops with different scale of time constants (from tens of seconds to thousands of seconds) have to work together. Therefore, the longer time lags need to be compensated to improve regulation properties of controllers.

(3) The conventional PI/PID controllers are tuned under certain conditions and can provide good performance for certain range of operation conditions. However, the dynamics of the HVAC&R system are changing with time and the operation conditions

which vary within a wide range. The conventional PI/PID controller with predefined control parameters is unlikely to provide consistent satisfactory control performance for all possible operating conditions. To address these problems, adaptive control that adjusts the control parameters on-line is designed in this chapter.

To this end, in this chapter, five neural network model based auto-tuned PI controllers are designed to effectively stabilize the HVAC&R system and track the desired reference set-points at local control level. The five controllers are used to control:

- zone air temperature by modulating corresponding VAV damper opening;
- discharge air temperature by modulating the chilled water valve opening;
- supply water temperature by modulating the energy input to the compressor;
- and static pressure at the fan outlet by modulating the energy input to the fan.

This auto-tuning method integrates a PI control, an auto-tuning algorithm and an adaptive neural network model prediction. Control parameters (proportional gain and integral gain) of the PI controller are adjusted to reduce the predicted tracking error. From the viewpoint of on-line application, the less calculations, the better. In this sense, neural network model is more appropriate than the complicated dynamic model developed in Chapter 3 for on-line updating of controller's parameters. Furthermore, the universal mapping property of neural network makes it preferable as well because of the inability of the theoretical model to describe or identify the system dynamics and uncertainties accurately. The weights of the NN model are updated on-line to learn the local loop dynamics once operating data is available such that the accuracy of the NN model prediction is ensured. The auto-tuning algorithm computes new control parameters to minimize the predicted tracking errors. Lyapunov stability analysis is performed to

derive the auto-tuning algorithm so that the convergence of the predicted tracking error is guaranteed.

6.1 NN-Based auto-tuning PI Control

6.1.1 The Structure of NN Model Prediction Based Adaptive Control

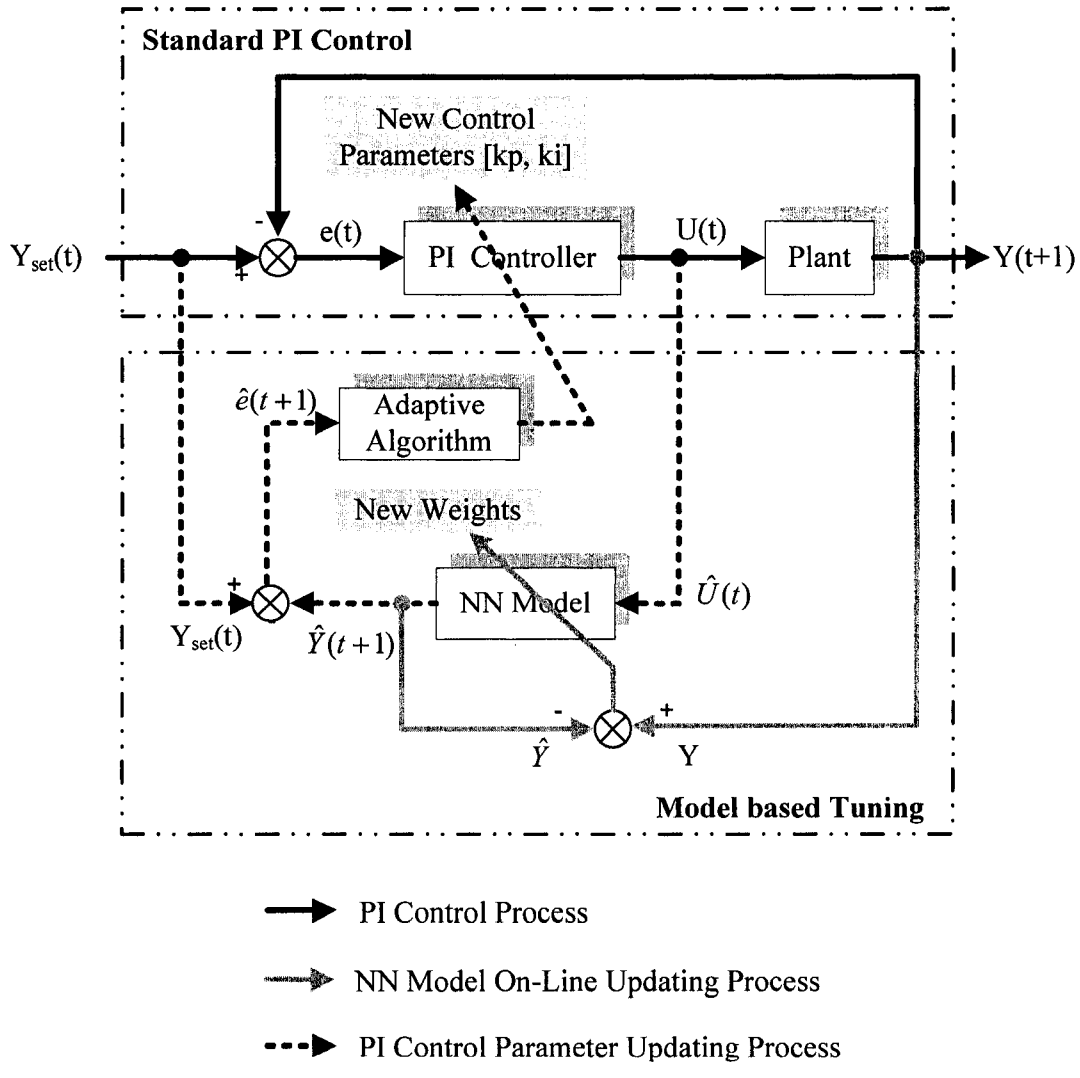

Figure 6-1 Block Diagram of Neural Network Based Adaptive Control

As shown in Figure 6-1, the NN model based predictive auto-tuning control contains two levels, a lower level and a higher tuning level. The lower level contains a

conventional PI control. This process is represented with dark solid line in the figure. The higher level, represented by dash line in the figure, computes a set of new control parameters for the PI controller through minimizing the predicted tracking error $\hat{e}(t+1)$ from the neural network model prediction once the operating condition changes or the PI control with current control parameters cannot maintain satisfactory control performance.

6.1.2 Adaptive Neural Network Model

The basis of this adaptive control is the on-line prediction of the responses of the control loop. Multilayer feed forward neural network as shown in Figure 5-1 is used to model the dynamics of the control loop. The accuracy of the model predictions is directly related to the performance of the controller. To reduce the discrepancies between the actual process and the model predictions and better capture the time-varying dynamics of the process, the neural network is online updated with available data using BFGS BP algorithm to reduce the network prediction error $Y(t)-\hat{Y}(t)$. The network model updating process is represented by light solid line in Figure 6-1.

6.1.3 Adaptation Rules

The PI control algorithm is described by:

$$u(t) = k_p e(t) + k_i \sum_{n=1}^{t} e(t) \qquad (6\text{-}1)$$

where k_p represents proportional gain and k_i represents integral gain, $e(t)$ is the process tracking error defined as:

$$e(t) = Y_{set}(t) - Y(t) \qquad (6\text{-}2)$$

with $Y_{set}(t)$ being the control set point. For conventional control, control parameters k_p and k_i are determined in advance and applied to the system; for auto-tuning control, new k_p and k_i are calculated on-line through minimizing the predicted performance index. In this study, k_p and k_i, are derived from minimizing the predicted tracking error:

$$\hat{e}(t+1) = Y_{set}(t+1) - \hat{Y}(t+1) \qquad (6\text{-}3)$$

with $Y_{set}(t+1)$ being the set point for next time step, and $\hat{Y}(t+1)$ being the network prediction with control input $\hat{U}(t+1)$ calculated with current control parameters, $k_p^{(m)}$ and $k_i^{(m)}$, and past process error $e(t)$ using Eq. (6-1) as:

$$\hat{U}(t+1) = k_p^{(m)} e(t) + k_i^{(m)} \sum_{n=1}^{t} e(i) \qquad (6\text{-}4)$$

The optimal k_p and k_i are derived iteratively. To do this, a new argument 'm' is introduced to denote the iterative step of updating k_p and k_i between control intervals.

$$\begin{bmatrix} k_p^{(m+1)} \\ k_i^{(m+1)} \end{bmatrix} = \begin{bmatrix} k_p^{(m)} \\ k_i^{(m)} \end{bmatrix} + \begin{bmatrix} \Delta k_p^{(m)} \\ \Delta k_i^{(m)} \end{bmatrix} \hat{e}(t+1)^{(m)} \qquad (6\text{-}5)$$

Denote $K = \begin{bmatrix} k_p \\ k_i \end{bmatrix}$, above equation is rewritten as:

$$K^{(m+1)} = K^{(m)} + \Delta K^{(m)} \hat{e}(t+1)^{(m)} \qquad (6\text{-}6)$$

where $\hat{e}(t+1)^{(m)}$ is the predicted NN model tracking error for $t+1$ at iterative step m:

$$\hat{e}(t+1)^{(m)} = Y_{set}(t+1) - \hat{Y}(t+1)^{(m)} \qquad (6\text{-}7)$$

with $\hat{Y}(t+1)^{(m)}$ being the NN model output at iterative step m for $t+1$.

Select a discrete Lyapunov function as:

$$V(m)=\frac{1}{2}\left(\hat{e}(t+1)^{(m)}\right)^2 \tag{6-8}$$

Obviously, $V(m)$ is positive defined. Then the increment of the Lyapunov function is:

$$\Delta V(m)=V(m+1)-V(m)=\frac{1}{2}\left(\left(\hat{e}(t+1)^{(m+1)}\right)^2-\left(\hat{e}(t+1)^{(m)}\right)^2\right) \tag{6-9}$$

Define

$$\begin{aligned}\Delta\hat{e}(t+1)^{(m)}&=\hat{e}(t+1)^{(m+1)}-\hat{e}(t+1)^{(m)}=-\hat{Y}(t+1)^{(m+1)}+\hat{Y}(t+1)^{(m)}\\&=-\frac{\partial\hat{Y}(t+1)^{(m)}}{\partial K^{(m)}}\Delta K^{(m)}\hat{e}(t+1)^{(m)}\end{aligned} \tag{6-10}$$

Then we have,

$$\begin{aligned}\Delta V(m)&=\frac{1}{2}\left(\left(\hat{e}(t+1)^{(m+1)}\right)^2-\left(\hat{e}(t+1)^{(m)}\right)^2\right)=\Delta\hat{e}(t+1)^{(m)}\left(2\hat{e}(t+1)^{(m)}+\Delta\hat{e}(t+1)^{(m)}\right)\\&=\left(-\frac{\partial\hat{Y}(t+1)^{(m)}}{\partial K^{(m)}}\Delta K^{(m)}\hat{e}(t+1)^{(m)}\right)\left(2\hat{e}(t+1)^{(m)}-\frac{\partial\hat{Y}(t+1)^{(m)}}{\partial K^{(m)}}\Delta K^{(m)}\hat{e}(t+1)^{(m)}\right)\\&=-\left(\hat{e}(t+1)^{(m)}\right)^2\left(-\frac{\partial\hat{Y}(t+1)^{(m)}}{\partial K^{(m)}}\Delta K^{(m)}\right)\left(2-\frac{\partial\hat{Y}(t+1)^{(m)}}{\partial K^{(m)}}\Delta K^{(m)}\right)\end{aligned} \tag{6-11}$$

Set adaptation law as:

$$\begin{aligned}&K^{(m+1)}=K^{(m)}+\Delta K^{(m)}\hat{e}(t+1)^{(m)}\\&\quad with\quad \Delta K^{(m)}=\delta\left(\frac{\partial\hat{Y}(t+1)^{(m)}}{\partial K^{(m)}}\right)^{-1},\quad 0<\delta<2\end{aligned} \tag{6-12}$$

the Jacobian vector is computed as follows:

$$\frac{\partial\hat{Y}(t+1)^{(m)}}{\partial K^{(m)}}=\frac{\partial\hat{Y}(t+1)^{(m)}}{\partial u(t)}\frac{\partial u(t)}{\partial\left[k_p^{(m)},k_p^{(m)}\right]}=\frac{\partial\hat{Y}(t+1)^{(m)}}{\partial u(t)}\begin{bmatrix}e(t)\\\sum_{n=1}^{t}e(i)\end{bmatrix} \tag{6-13}$$

where $\frac{\partial\hat{Y}(t+1)^{(m)}}{\partial u(t)}$ can be computed from the multi-layer NN model using BP algorithm.

then we have:

$$\Delta V(m) = -\delta(2-\delta)\left(\hat{e}(t+1)^{(m)}\right)^2 < 0 \qquad (6\text{-}14)$$

According to Lyapunov stability analysis, the predictive tracking error is guaranteed to converge to zero.

For a given control set point, the auto-tuning procedure is described as follows:

STEP 1:

At sample time $t+1$ and iteration step m, obtain set point $Y_{set}(t+1)$, the past tracking error $e(t)$ and newest control parameters $k_p{}^{(m)}$ and $k_i{}^{(m)}$.

STEP 2:

- calculate control variable $\hat{U}(t+1)$ according to Eq. (6-4);
- construct the neural network model input vector;
- calculate the network model output, which is the prediction of the process output for the next sample time $\hat{Y}(t+1)$ at current updating step;
- calculate the predicted tracking error $\hat{e}(t+1)^{(m)}$ according to Eq. (6-7);

STEP 3:

Calculate new control parameters according to Eq. (6-12) and Eq. (6-14), set $m = m+1$.

STEP 4:

Repeat STEP 1 – STEP 3 until the predicted tracking error $\hat{e}(t+1)^{(m)}$ is less than a pre-specified threshold or the maximum iteration step m is reached.

Figure 6-2 is the flow chart of the adaptive control process.

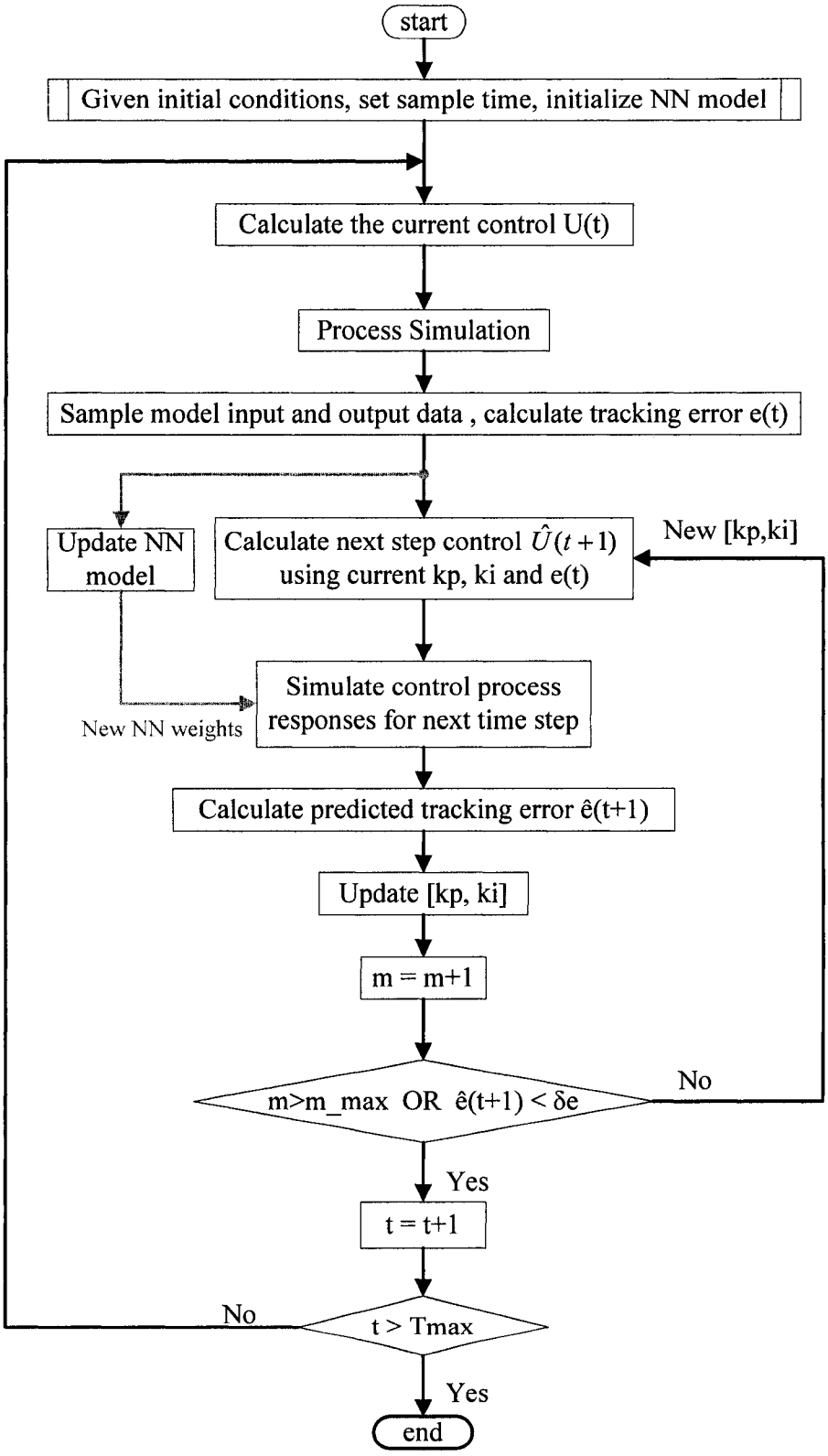

Figure 6-2 Flow Chart of Neural Network Based Adaptive Control

6.1.4 Simulation Results

To verify the effectiveness of above adaptive algorithm, an adaptive PI controller and a well-tuned PI controller are applied to control the discharge air temperature of the two-zone VAV system to track set point step changes. Simulations are performed under following conditions:

- The control interval is 120s for both controllers.
- Constant chilled water temperature at the cooling coil inlet, $T_{w,\text{sup}} = 5^{\circ}C$
- Constant zone loads: $Q_{s1} = 3\,kW$, $Q_{l1} = 0.75\,kW$, $Q_{s2} = 2.6\,kW$ and $Q_{ls2} = 0.6\,kW$
- Constant outdoor air temperature, $T_{oa} = 27^{\circ}C$
- Discharge air temperature set points decrease from 16°C to 14°C after 40 minutes and increases from 14°C to 15°C after another 40 minutes.

Simulation results are shown in Figure 6-3 and Figure 6-4 respectively, in which figure (a) is the responses of the discharge air temperature and figure (b) is the normalized chilled water valve opening.

From Figure 6-3 and Figure 6-4, we can observe that both controllers provide good performance under fixed operating conditions. The offset bands between the set point and responses after the transient phase for both controllers are negligible. However, the response of the adaptive control is superior to that of the PI control. The response of adaptive control to the set point change is faster than the PI control and the overshoot is smaller. The rise time for PI control is 15-20 minutes, while the rise time for adaptive PI control is 2-8 minutes. The cost for this advantage is the requirement of model prediction

and on-line updating of control parameters.

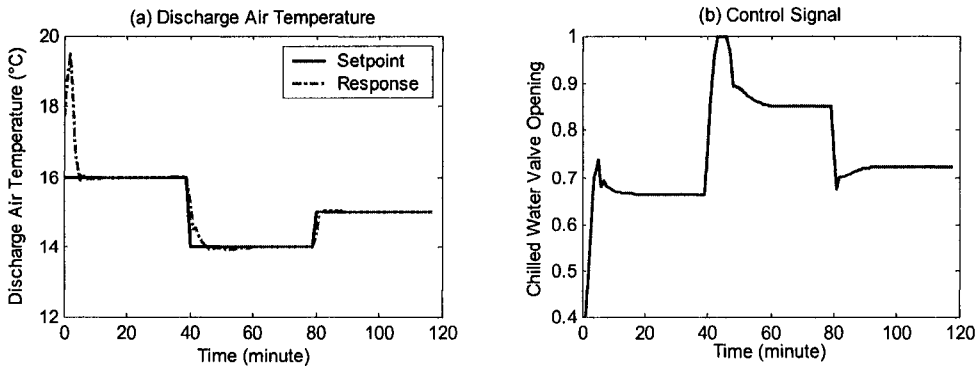

Figure 6-3 Response of Discharge Air Temperature with Adaptive PI Control

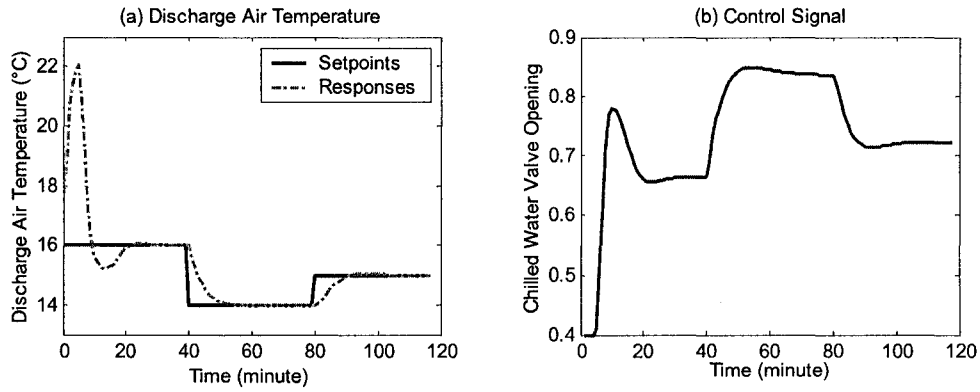

Figure 6-4 Response of Discharge Air Temperature with PI Control

Comparisons between PI controller and adaptive PI controller applied to the discharge air temperature control are summarized in Table 6–1. The responses of PI control could be different with different control parameters.

Table 6–1 Comparisons of adaptive PI and PI controllers

Controller	PI	Adaptive PI
Pre-Tuning	Yes	No
Response Speed	Slow	Fast
Offset	Small	Small
Response Predicteion	No	Yes

6.2 Implementation of the Optimal Set Points – Local Control Design

In Chapter 5, we have calculated the optimal set points for the supply water temperature, discharge air temperature and fan pressure at the supervisory level with the assumption that existing local controls that can maintain the controlled variables at desired set points. In this section, five adaptive PI controllers are designed to control the local loops and realize the optimal operation scheme. The five controllers are used to:

- modulate air flows into the air-conditioned zones by adjusting corresponding VAV damper opening to maintain the desired zone air temperature;
- modulate chilled water flow rate by adjusting the chilled water valve opening to maintain the discharge air temperature set point;
- modulate the compressor speed by adjusting the energy input to the compressor motor to maintain the supply water temperature set point;
- and modulate the fan speed by adjusting the energy input to the fan motor to maintain the static pressure at the fan outlet.

6.2.1 Construction of Local Neural Network Models

The basis of this adaptive control is the availability of robust neural network model which could predict the responses of the control process with certain accuracy. The implementation of the adaptive control design starts with constructing NN models. To simplify the structure of the neural network and reduce the calculations of on-line updating and predictions, instead of using one neural network with complicated structure to model the overall responses of the two-zone VAV-HVAC&R system, four NN models are constructed to simulate local control loops separately. All neural networks are three-

layer feed forward networks.

Network Model 1: NN-P_{fan}

Neural network model, NN-P_{fan}, is constructed to model the fan pressure gain in the two-zone VAV system. The output of NN-P_{fan} is the pressure at fan outlet, $P_{fan}(t+1)$. As mentioned in Chapter 3, the air flow loop is independent of other loops, the total air flow rate and fan pressure gain are determined by the normalized energy input to the fan motor, the opening of both dampers. NN-P_{fan} has three inputs:

- the normalized energy input to the fan motor, $U_{fan}(t)$
- the opening of two zone dampers, $U_{z1}(t)$ and $U_{z2}(t)$

Network Model 2: NN-T_z

Neural network model, NN-T_z, is constructed to model the zone air temperature. For a given load, the zone air temperature is determined by the flow rate and temperature of the air entering the zone. From the analysis in Chapter 4 (refer to Table 4–3), we can see that for two zone system, the air flow rate of one zone is not only the result of corresponding damper opening, but also influenced by the damper opening of the other zone. Variation in one zone damper position affects the mass flow rates of both zones and in turn affects the temperature of the other zone. Therefore, instead of using two models to simulate zone air temperature separately, one network model is constructed to simulate the air temperatures in both zones. The outputs of NN-T_z are temperature of two zones, $T_{z1}(t+1)$ and $T_{z2}(t+1)$. The responses of the zone air temperature is very slow, the time constant of zone is much larger than the control intervals. For an on-line model used for one-step ahead prediction, the present zone air temperature has great impact on the zone

air temperature for the next time-step. Therefore, the inputs for NN-T_z include:

- the opening of both dampers, $U_{z1}(t)$ and $U_{z2}(t)$
- discharge air temperature, $T_{a,\text{sup}}(t)$
- current zone air temperature $T_{z1}(t)$ and $T_{z2}(t)$

Network Model 3: NN-T_{asup}

Neural network model, NN-T_{asup}, is constructed to model the discharge air temperature at the cooling coil outlet. The outputs of NN-T_{asup} is the discharge air temperature, $T_{a,\text{sup}}(t+1)$. The discharge air temperature is affected by the flow rate and temperature of the chilled water and air at the coil inlet. The chilled water flow rate is determined by the chilled water valve opening, and the air flow rate is determined by fan pressure and damper opening. Since the time constant of the coil is much larger than the control interval, current discharge air temperature is useful for better prediction of the discharge air temperature for the next time step. Therefore, the inputs for NN-T_{asup} include:

- the normalized chilled water valve opening, $U_{val}(t)$
- the normalized energy input to the fan motor, $U_{fan}(t)$
- the opening of both dampers, $U_{z1}(t)$ and $U_{z2}(t)$
- current supply water temperature, $T_{w,\text{sup}}(t)$
- current discharge air temperature, $T_{a,\text{sup}}(t)$
- current air temperature at coil inlet, $T_{a,cc,in}(t)$

Network Model 4: NN-T_{wsup}

Neural network model, NN-T_{wsup}, is constructed to model the supply water temperature. The outputs of NN-T_{wsup} is the supply water temperature, $T_{w,sup}(t+1)$. The supply water temperature is determined by the compressor work, the chilled water flow rate and the water temperature at the evaporator inlet. The inputs for NN-T_{wsup} include:

- the normalized energy input to the compressor, $U_{com}(t)$
- the normalized chilled water valve opening, $U_{val}(t)$
- current return water temperature, $T_{w,re}(t)$
- current supply water temperature, $T_{w,sup}(t)$

It is noted that all the input data and outputs of above four NN models are either measurable system states or control inputs which make the on-line NN model updating possible. The structural details of above NN models are summarized in Table 6–2.

Table 6–2 Structural Details of Neural Network Models

NN Model	NN-Pfan	NN-Tz	NN-Tasup	NN-Twsup
No. of Inputs	3	5	7	4
No. of Neurons in Hidden Layer	5	9	10	7
No. of Output(s)	1	2	1	1

6.2.2 Simulation Results

After determining the structure of the on-line NN models, the adaptive PI control algorithm is implemented on the full order two-zone HVAC&R system to track the temperature and pressure set points. Simulation is performed with the same operation conditions used to derive the optimal set points for full load operation given in Chapter 5, including the loads profiles, outdoor air temperature profile and initial conditions used to

solve the model equations as well.

The simulation results are shown in Figure 6-5. Figure (a) shows the supply water temperature responses, figure (b) is normalized energy input to the compressor; figure (c) shows the discharge air temperature responses, and figure (d) is normalized chilled water valve opening; figure (e) and figure (g) show the zone1 and zone2 temperature responses, figure (f) and figure (h) are normalized VAV damper opening of zone1 and zone2; figure (i) shows the fan pressure responses and figure (j) is normalized energy input of the fan.

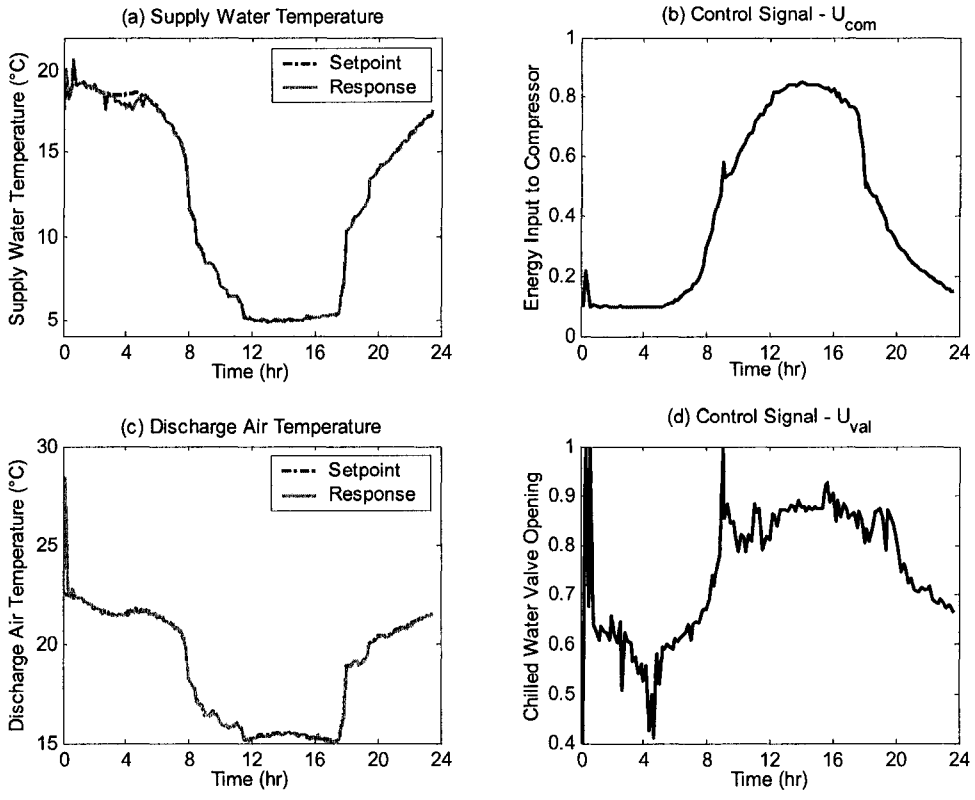

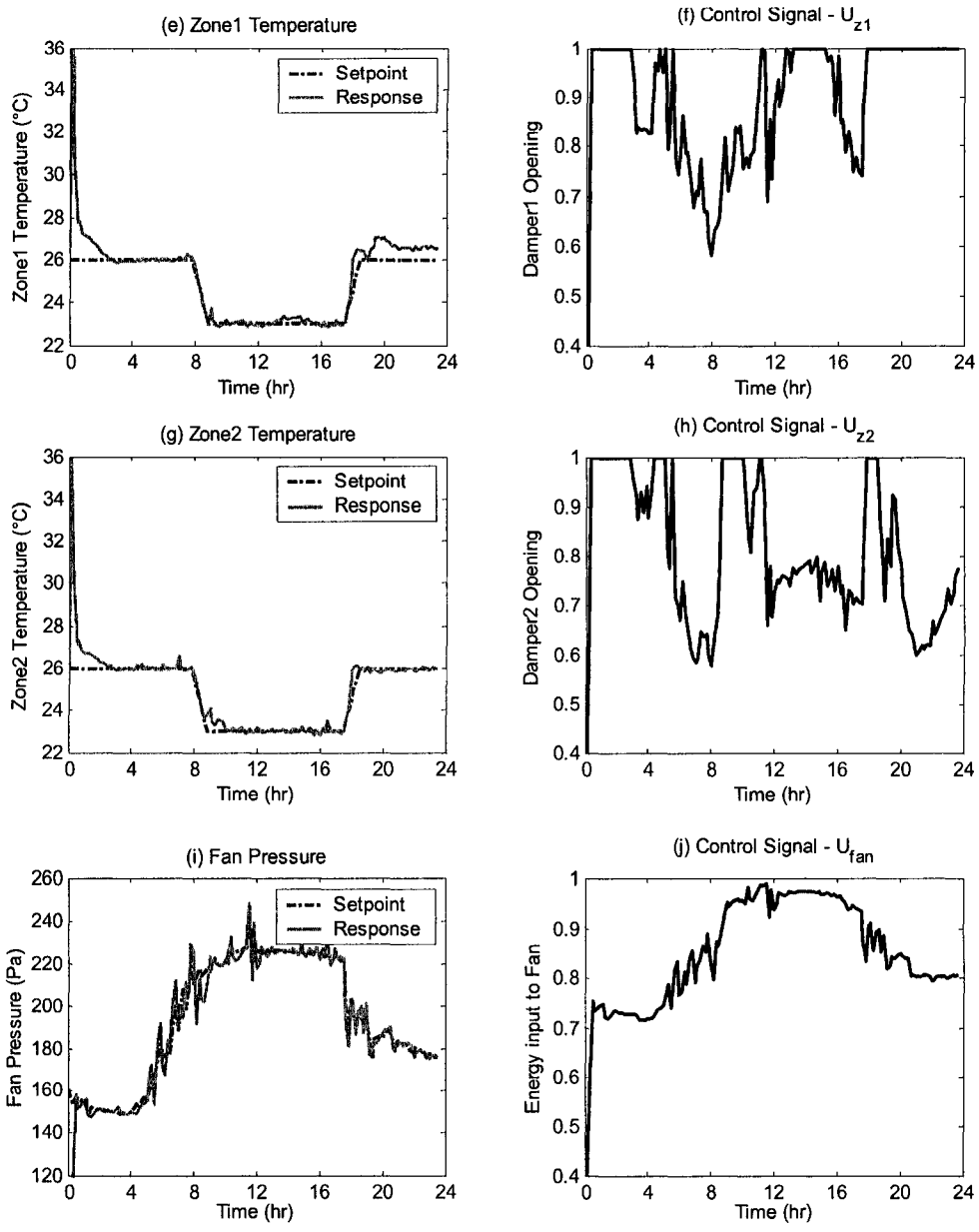

Figure 6-5 Response of Integrated Two-Zone VAV-HVAC&R System with Adaptive PI Control (Full Load)

From Figure 6-5, we can see that the adaptive control works pretty well. After oscillations during the first hour, the system responses are very stable and the setpoints are well traced. From these figures, we note that:

(1) The offsets of the responses are almost negligible except for the Zone1 temperature responses after 19pm. From Figure 6-5 (e) and (f), we can see that after

19pm, zone1 temperature is around 26.8°C and the zone1 damper is fully opened while the set point is 26°C. This means that discharge air temperature is higher than it should for maintaining the zone1 temperature at 26°C with the same fan speed and zone2 damper opening. Recall the analysis in Chapter 5 (refer to Table 5–1), during the unoccupied hours, the optimal set points are derived with the assumption of zone air temperature allowed to float in the range of 24-27°C. Zone1 temperature is still in the acceptable range. And at the same time, the higher zone air temperature is explainable because in order to decrease the energy consumption, the chiller and the fan operate at lower capacity and as such high chilled water temperature and high discharge air temperature are maintained.

(2) From Figure 6-5 (i), we can see that compared to temperature responses, the pressure responses have higher offsets and oscillation. This is because the time constant of the air flow is much less than the time constant of the thermal loop and the control intervals. Reducing the control intervals will improve the pressure responses, but further reducing the control interval is impractical because it may cause unstable temperature responses.

(3) From Figure 6-5 (a), (c), (e) and (g), we can see that the settling time of zone air temperature responses is much longer than the settling times of discharge air temperature and supply water temperature; this is the result of larger capacity of the zone air.

Chapter 7 Conclusions and Suggested Future Work

7.1 Summary and Conclusions

With the growing concerns on energy consumption, computational based control schemes are widely applied for more efficient operation of HVAC&R systems, which include the model simulation and simulation based applications, e.g. controller design, FDD and optimization.

The objective of this thesis is to design and realize a robust and efficient simulation-based optimal operation of a two-zone VAV-HVAC and refrigeration system under variable operating conditions from the viewpoint of improving overall system performance, in the sense of providing desired indoor environment with the least energy consumption. The proposed methodology integrates dynamic model simulation, neural network based optimization and neural model based adaptive control. The major steps that lead to realize the stated objective are summarized in the following subsections.

Development of a Dynamic Model for the Two-Zone VAV-HVAC&R System

Model prediction is the basis of this study. Chapter 3 described the development of a dynamic two-zone VAV-HVAC and refrigeration system model. The overall system model was achieved by integrating a two-zone VAV system model and a water cooled chiller model. Both VAV system model and chiller model are component based and derived from the energy, momentum and mass conservation principles. Dynamic models for main components were developed first and then connected to each other according to the physical layout and corresponding input and output information to form the integrated

system model. The two zone VAV system model includes a zone model, a variable speed fan with DC motor model, a cooling and dehumidifying coil model and an air flow model. The chiller model includes an evaporator model, a condenser model, a compressor model and a thermal expansion valve model. Considering model accuracy and computational efforts, moving boundary approach was used to model the evaporator and condenser.

From the open-loop simulation results presented in Figure 3-5 - Figure 3-9, we can conclude that:

- There are two distinct time scales involved in the system, the dynamics of the airflow loop and water flow (tens of seconds) are much faster than the thermal loop, including cooling and dehumidifying coil, zone, evaporator and condenser (hundreds to thousands of seconds).
- The integration of VAV system and refrigeration system results in slower overall system responses. The dynamic responses of thermal loop are slower after the integration due to the coupling effects between the coil and the evaporator. Since the refrigerant flow is directly related to the evaporator pressure, the dynamics of the refrigerant flows are much slower after the integration also.
- In the integrated system, the discharge air temperature is not only influenced by the air flow and chilled water flow, but also influenced by the chilled water temperature. Therefore it is more susceptible to load changes in the integrated system.
- Condenser water loop is pretty stable before and after the integration and

therefore it is justified to decouple it in the optimization analysis.

- There are more than one operation scheme that could maintain the same indoor environment; however, the energy consumption is different. Therefore, it is possible to reduce the total energy consumption by proper operation while maintaining desired indoor air conditions.

Extended Transformation Approach to Identify Uncertainties in Model Predictions Caused by Pre-Selected Uncertain Parameters (Model Uncertainty Analysis)

Mathematical model exhibits more or less uncertainties caused by neglecting and inaccurately description of some dynamics and using inaccurate parameters. Fuzzy-set based extended transformation approach was used to evaluate the probability distributions of model outputs caused by the following selected uncertain parameters: mass flow rate of condenser water $\dot{m}_{w,con}$, mass flow rate of chilled water $\dot{m}_{w,chi}$, water temperature at the condenser inlet $T_{w,con,in}$, cooling coil air side heat transfer coefficient $h_{a,cc}$, and sensible cooling loads Q_{s1} and Q_{s2}. The uncertain parameters were treated as fuzzy variables and assumed to have symmetric triangular membership functions. The integrated effects of all uncertain parameters on model outputs were calculated, and sensitivity coefficients of the interested model outputs with respect to certain uncertain parameter were computed to evaluate the impacts of individual uncertain parameters on corresponding outputs. The approximate distributions of water, air and zone air temperatures at different α-cut levels and different time were derived and illustrated in Figure 4-4. In addition, from simulation results we can note that:

- The ranges of the distributions of the model outputs also illustrate dynamics

and the dynamics are directly related to the dynamics of corresponding output responses. The distribution range tends to increase with time and reaches the maximum range when the corresponding output reaches steady state.

- The uncertainties of system outputs caused by the uncertain model parameters are different and the effects of individual uncertain parameters on the interested temperature are different as well. The variations in condenser water temperature are mainly caused by the variations in the condenser water mass flow rate and condenser water inlet temperature. This justified our assumption of excluding condenser water loop from the optimization analysis.

Transformation Approach to Identify the Impact of Control Variables on System Responses (Sensitivity Analysis of Control Variables)

HVAC&R system is a highly coupled system; the coupling effects in local control loops affect the control performance. The sensitivities of control inputs were computed using the same extended transformation approach to identify the impact of individual control variables on system responses. The control inputs were treated as fuzzy variables with symmetric triangular membership function. The significance of control inputs with respect to the interested model outputs were ranked in Chapter 4. From the simulation results illustrated in Figure 4-6 and Table 4–3, we can conclude that:

- Airflow loop is independent of the rest of the system. U_{com} and U_{val} do not influence the air mass flow rates. The air flow is the result of U_{z1}, U_{z2} and U_{fan}. Zone VAV damper opening and U_{fan} have great influence on the air

flow rate for that zone, but the air flow rate is affected by the opening of the neighbouring VAV box damper as well.

- Water flow loop is independent of other loops in the system also. The chilled water flow rate is determined by U_{val} only.
- The thermal loops, including the discharge air loop, zone air temperate, chilled water loop and condenser water loop are interconnected. Thermal responses of the system are determined by the integrated effects of U_{com}, U_{val}, U_{fan}, U_{z1} and U_{z2}, but U_{com} has the dominant effect. Adjusting one of these temperatures by modulating the corresponding control input affects the responses of other temperatures as well.

Neural Network Based Optimal Operation

Chapter 5 demonstrated the implementation of a three-layer feed forward neural network as supervisory controller to achieve optimal operation of the HVAC&R system at the supervisory control level aiming at maintaining the desired zone air temperature with the least energy consumption and satisfying the mechanical system constraints at the same time. A neural network was trained unsupervised to minimize the cost function. The cost function was composed of weighted energy consumption of current operation scheme and a penalty term which accounted for the violation of constraints and/or when the zone air temperature was away from the desired values. In order to improve the training efficiency and avoid domination of the outputs by some inputs, the network inputs were normalized in the range of 0 to 1. In order to achieve both fast decrease in cost function and fast convergence, two training methods were used to adjust the network weights, the gradient descent with momentum and variable learning rate algorithm was

used at early stage to achieve fast decrease of the cost function, the BFGS quasi-Newton algorithm was used after to achieve fast convergence. The outputs of the neural network were control inputs, with these control inputs, the optimal set points for the static pressure at fan outlet, discharge air temperature and supply water temperature were derived from simulations. This optimal operation scheme was compared with the night reset operation strategy. From simulation results presented in Figure 5-7 and Figure 5-9, we note that:

- Compared to the night reset operation strategy, the optimal operation scheme consumes less energy while maintaining the indoor temperature in an acceptable range. Unoccupied hours have high energy saving potential than occupied hours because of 'free cooling' during the night. In addition, by keeping the zone air temperatures near high limit also saves energy.
- The cooling loads directly affected the optimization set points. The lower the load, the lower are the capacity of the fan and the compressor and the smaller is the difference between the supply water and the discharge air temperature.

Design of Adaptive Control System to Realize the Optimal Operation

Besides finding the optimal operation set points, local controllers are needed to implement the optimal operation, track the desired optimal set points. To overcome the deficiencies of PI control with fixed control parameters, five on-line adaptive PI controllers were designed in Chapter 6 based on neural network model predictions. This adaptive control integrated PI control, auto-tuning algorithm and adaptive neural network model prediction. The adaptive control had two control levels; the lower level accomplished a conventional PI control process, the higher level computed control parameters to reduce the model prediction tracking errors. In order to simplify the

network updating and predicting process, instead of using one network with complex structure to model the dynamics of overall system, four three-layer feed forward neural networks were used to perform on-line one-step forward predictions of the fan pressure gain, zone air temperatures, discharge air temperature and supply water temperature respectively. The weights of neural models were updated on-line for better capturing the time-varying dynamics of the control loops. The updating rule for control parameters was derived from Lyapunov stability analysis and therefore the convergence of the predicted tracking error was guaranteed. Simulation results indicated that adaptive PI control worked pretty well in term of good tracking and stable control.

7.2 Contributions of This Study

Compared to other studies in modeling and operation of HVAC&R systems, the main contributions of this study are summarized as:

(1) In most studies, the HVAC system and refrigeration system were investigated separately without considering the interactions between them. However, the interactions between HVAC systems and refrigeration systems have great impacts on the overall system performance and control design. In order to achieve the optimal operation of the HVAC&R system, a dynamic model for two-zone VAV-HVAC&R systems, which integrates a VAV model with a water cooled vapor compression refrigeration system model, is developed in this study. The optimal operation schemes derived from model simulations better represent the dynamic behavior of the overall system.

(2) The interactions between the VAV system and refrigeration system are investigated with the help of integrated system model. The open-loop simulation results

from separate systems and integrated system are compared.

(3) Fuzzy-set based extended transformation method is used to evaluate the uncertainties in model predictions caused by pre-selected uncertain parameters. The probability distribution ranges of model outputs are determined. These bounds can help us to achieve better predictions of the responses of the HVAC&R system by quantifying the range within which the responses fall. At the same time, the contributions of individual uncertain parameters to the uncertainties of model outputs are computed as well. This information could help us to identify important parameters in term of improving model accuracy.

(4) The sensitivities of the control inputs with respect to the interested model predictions are computed using fuzzy-set based general transformation method and the impacts of control parameters on controlled variables are identified as well. This knowledge provides guidelines to design control system.

(5) A neural network based optimization algorithm is developed to search the optimal operation solutions for the two-zone VAV-HVAC&R system at the supervisory level. With the feedback of states and control errors, this supervisory control strategy is more robust than the solutions derived from open-loop simulations. Compared with the night reset operation scheme, the optimal operation strategy consumes less energy for maintaining the desired indoor temperature without violating operation constraints.

(6) Five neural model based adaptive PI controllers are designed to implement the optimal set points. Control parameters are updated on line to reduce the predicted tracking errors. The updating rule for control parameters is derived from Lyapunov stability analysis and therefore guarantees the convergence of the tracking errors.

Simulation results showe good control performance.

7.3 Recommendations for Future Work

This work presentes a simulation-based optimal operation and adaptive control of the HVAC&R system as an integrated system. This study also indicates some areas worth further investigation. Meanwhile there is still lot of work needs to be done before we can advance the method presented in this thesis into practical applications.

(1) The cooling load plays an important role in HVAC&R system operation and the optimal set points are directly influenced by the loads. It is worth to integrate a load prediction model into the system model. Accurate load prediction helps improving model prediction results and the optimization results will be closer to the optimal values.

(2) As we concluded in Chapter 4, uncertain parameters cause uncertainties in simulation results and the influence of uncertain parameters on simulation results is different. In this study, only six uncertain parameters are selected and their impacts are investigated. It would be interesting to include more uncertain parameters in model uncertainty analysis and identify their impacts on the model outputs.

(3) A three-layer feed forward neural network is 'trained' unsupervised to find the optimization solutions. The calculation of the gradient of the cost with respect to the network weights involves the calculation of the sensitivity derivatives of the system outputs with respect to control inputs. The perturbation method used in this work needs large number of calculations. Therefore, more efficient algorithms to compute the derivatives of the performance index are of interested and will help improving the algorithm efficiency.

(4) As discussed before, HVAC&R systems are multi-input multi-output (MIMO) systems consisting of interconnected subsystems with nonlinear uncertain coupling matrix. Design of MIMO controllers for HVAC&R would be an interesting topic for future work.

(5) HVAC&R system model are subjected to uncertainties; develop an improved robust adaptive control algorithm to include model uncertainties would be beneficial.

(6) Experimental work is needed in the future to evaluate the proposed optimization method and adaptive control algorithm.

References

[1] http://www.eere.energy.gov/buildings/tools_directory/alpha_list.cfm

[2] Abdel-Tawab, K. and A.K. Noor. 1999. '*A Fuzzy-Set Analysis for A Dynamic Thermo-Elasto-Viscoplastic Damage Response*'. Computers and Structure, Vol. 70: pp.91-107.

[3] Ahmed, M.S. and M.A. Al-Dajani. 2000. '*Neural Net Control of Nonlinear Plants through State Feedback*'. Optimal Control Applications and Methods, Vol.21: pp.63-90

[4] Ahmed, O. 1991. '*DDC applications in Variable-Water-Volume systems*'. ASHRAE Transactions 97 (1): pp.751–758

[5] Ahn, B.C. and J.W. Mitchell. 2001. '*Optimal Control Development for Chilled Water Plants Using a Quadratic Representation*'. Energy and Buildings 33: pp.371-378

[6] Anderson, M., P. Young, D. Hittle, C. Anderson, J.L. Tu and D. Hodgson. 2002. '*MIMO Robust Control for Heating, Ventilating and Air Conditioning (HVAC) Systems*'. Proceedings of the IEEE Conference on Decision and Control, Vol.1: pp. 167-172

[7] ASHRAE Fundamentals Handbook. 1993. American Society of Heating, Refrigerating and Air-Conditioning Engineers, Inc. Atlanta.

[8] ASHRAE Fundamentals Handbook. 2005. American Society of Heating, Refrigerating and Air-Conditioning Engineers, Inc. Atlanta.

[9] Astrom, K.J. and B. Wittenmark. 1989. Adaptive Control. Addison-Wesley Publication Company

[10] Austin, S.B. 1993. '*Chilled Water System Optimization*'. ASHRAE Journal 35(7): pp. 50-56

[11] Bechtler, H., M.W. Browne, P.K. Bansal and V. Kecman. 2001. '*New Approach to Dynamic Modeling of Vapor-Compression Liquid Chillers: Artificial Neural Networks*'. Applied Thermal Engineering 21: pp.941-953

[12] Beck, B.T. and G.L. Wedekind. 1981. '*A Generalization of the System Mean Void Fraction Model for Transient Two-Phase Evaporating Flows*'. ASME Journal of Heat Transfer 103(1): pp. 81-85

[13] Bendapudi, S., J.E. Braun and E.A. Groll. 2005. '*Dynamic Model of a Centrifugal Chiller System-Model Development, Numerical Study and Validation*'. ASHRAE Transactions, Vol.111 (1): pp. 132-148

[14] Bensafi A., S. Borg and D. Parent. 1997. '*CYRANO: A Computational Model for the Detailed Design of Plate-Fin-and-Tube Heat Exchangers Using Pure and Mixed Refrigerants*'. International Journal of Refrigeration, Vol.20 (3): pp.218–228

[15] Betzaida, A. and V. Miguel. 1995. '*Design of a Nonlinear HVAC Control System with Thermal Load Estimation*'. IEEE Conference on Control Applications – Proceedings: pp.33-39

[16] Biondini F., F. Nontempi and P.G. Malerba. 2004. '*Fuzzy Reliability Analysis of Concrete Structures*'. Computer and Structure, Vol.82: pp.1033-1052.

[17] Borresen, B.A. 1981. '*Thermal Room Models for Control Analysis*'. ASHRAE Transactions 87(2): pp.251-261

[18] Bonarini, A. and G. Nontempi. 1994. '*A Qualitative Simulation Approach for Fuzzy Dynamical Model'*. ACM Transactions Modeling and Computer Simulation, Vol. 4 (4): pp.285-313

[19] Bondia, J. and J. Pico. 2004. '*Application of Functional Intervals to the Response Evaluation of Linear Time-Invariant Systems with Fuzzy Input*'. Reliable Computing, Vol.10: pp.369–387.

[20] Braun, J.E., S.A. Klein, J.W. Mitchell and W.A. Beckman. 1989. '*Methodologies for Optimal Control of Chilled Water Systems without Storage*'. ASHRAE Transactions 95(1A) : pp.652-662

[21] Braun, J.E., S.A. Klein, J.W. Mitchell. 1989. '*Effective Models for Cooling Towers and Cooling Coils*'. ASHRAE Transactions 95(2): pp.164-174

[22] Braun, J.E. and G.T. Doderrich 1990. '*Near Optimal Control of Cooling Towers for Chilled Water Systems*'. ASHRAE Transactions 96(2): pp.806-813

[23] Browne, M.W. and P.K. Bansal. 2002. '*Transient Simulation of Vapor-*

Compression Packaged Liquid Chillers'. International Journal of Refrigeration 25: pp.597–610

[24] Cascia, M.A. 2000. '*Implementation of a Near-Optimal Global Set Point Control Method in a DDC Controller*'. ASHRAE Transactions 106(1): pp.249-263

[25] Casciaro, S. and J.R. Thome. 2001. '*Thermal Performance of Flooded Evaporators, Part 2: Review of Void Fraction, Two-Phase Pressure Drop, and Flow Pattern Studies*'. ASHRAE Transactions 107(1): pp.919-930

[26] Chang, Y.C., J.K. Lin and M.H. Chuang. 2005. *'Optimal Chiller Loading by Genetic Algorithm for Reducing Energy Consumption*'. Energy and Buildings 37: pp.147–155

[27] Chen, Steve and S. Demster. 1995. Variable Air Volume Systems for Environmental Quality. McGraw-Hill.

[28] Chen, H.J., David W.P. Wang and S.L. Chen. 2005. '*Optimization of an ice-storage air conditioning system using dynamic programming method*'. Applied Thermal Engineering (25): pp.461–472

[29] Chen, T.Y. 2002. '*Application of Adaptive Predictive Control to a Floor Heating System with a Large Thermal Lag*'. Energy and Buildings 34: pp.45-51

[30] Cheng, Tao, X. He, H.A. Asada and S. Kasahara. 2005. '*Heat Exchanger Dynamic Observer Design*'. ASHRAE Transactions 111(1): pp.328-335

[31] Chow, T.T, G.Q. Zhang, Z. Lin and C.L Song. 2002. '*Global Optimization of Absorption Chiller System by Generic Algorithm and Neural Network*'. Energy and Buildings 34: pp.103–109.

[32] Clark, D.R, C.W. Hurley and C.R. Hill. 1985. '*Dynamic Models for HVAC System Components*'. ASHRAE Transactions 91(1B): pp.737-751

[33] Cui, Y.J., M. Liu and K. Conger. 2004. '*Optimal Airflow Control of Laboratory Air Handling Unit (LAHU) Systems*'. Transactions of the ASME 126: pp.750-758

[34] Cumali, Z. 1988. '*Global Optimization of HVAC System Operations in Real Time*'. ASHRAE Transactions: pp.DA-88-23-1

[35] Curtiss, P.S, J.F. Kreider and M.J. Brandemuehl. 1993. '*Energy Management in Central HVAC Plant Using Neural Networks*'. ASHRAE Transactions 99 (1):

pp.486-504.

[36] Curtiss, P.S, J.F. Kreider and M.J. Brandemuehl. 1994. '*Adaptive Control of HVAC Processes Using Predictive Neural*'. ASHRAE Transactions 100 (1): pp.476-493.

[37] Curtiss, P.S, G. Shavit and J.F. Kreider. 1996. '*Neural Networks Applied to Buildings - A Tutorial and Case Studies in Prediction and Adaptive Control*'. ASHRAE Transactions 102 (1B): pp.1141-1146.

[38] Dexter, A.L. and P. Haves. 1989. '*A Robust Self-Tuning Predictive Controller for HVAC Applications*'. ASHRAE Transactions 95(2): pp.431-438

[39] DOE-2. 1981. DOE-2: Building Energy User Analysis Program, Engineering Manual Version 2.1A. Laurence Berkerly Laboratory

[40] Dong, W. and H.C. Shah. 1987. '*Vertex Method for Computing Functions of Fuzzy Variables*'. Fuzzy Sets and Systems, Vol.24: pp.65–78.

[41] Dowlati, R., M. Kawaji and A.M.C. Chan. 1996. '*Two-Phase Cross Flow and Boiling Heat Transfer in Horizontal Tube Bundles*'. Journal of Heat Transfer Vol.1181: pp. 24-31

[42] Engdahl, F. and J. Dennis. 2004. '*Optimal Supply Air Temperature with Respect to Energy Use in a Variable Air Volume System*'. Energy and Buildings 36: pp.205-218

[43] Fu, L., G.L. Ding, Z.J. Su, and G.Q. Zhao. 2002. '*Steady-State Simulation of Screw Liquid Chillers*'. Applied Thermal Engineering 22 (15): pp. 1731–1748

[44] Garde, F., F. Lucas, H. Boyer and J. Braun. 2001. '*Multiple Model Approach of a Residential Heat Pump for Integrated in a Building Thermal Simulation Code and Comparison with Experimental Results*'. ASHRAE Transactions 107(1): pp.14-25.

[45] Gartner, J.R. and H.L. Harrison 1963. '*Frequency Response Transfer Functions for a Tube*'. ASHRAE Transactions 69: pp. 320-330

[46] Gartner, J.R. and H.L. Harrison 1965. '*Dynamic Characteristics of Water-to-Air Cross Flow Heat Exchangers*'. ASHRAE Transactions 71: pp. 212-223

[47] Gartner, J.R. and L.E. Daane. 1969. '*Dynamic Response Relations for a Serpentine Cross-Flow Heat Exchanger with Water Velocity Disturbance*'. ASHRAE Transactions 75 (1): pp.53–68.

[48] Gartner, J.R. 1972. '*Simplified Dynamic Response Relations for Finned-Coil Heat Exchangers*'. ASHRAE Transactions 78(2): pp.163-169

[49] Ge, S.S. and C. Wang. 2004. '*Adaptive Neural Control of Uncertain MIMO Nonlinear Systems*'. IEEE Transactions on Neural Networks, Vol.15(3): pp.674-692

[50] Hanss, M. 2002. '*The Transformation Method for the Simulation and Analysis of Systems with Uncertain Parameters*'. Fuzzy Sets and Systems, Vol.130: pp.277–289.

[51] Hanss, M. 2003. '*The Extended Transformation Method for the Simulation and Analysis of Fuzzy-Parameterized Models*'. International Journal of Uncertainty, Fuzziness, and Knowledge-Based Systems, Vol.11(6): pp.711-727.

[52] Harms, T.M, J.E. Braun, and E.A Groll. 2004. '*The Impact of Modeling Complexity and Two-Phase Flow Parameters on the Accuracy of System Modeling for Unitary Air Conditioners*'. HVAC&R Research, Vol.10 (1): pp. 5-20

[53] Hartman, T.B. 1988. '*Dynamic Control: Fundamentals and Considerations*', ASHRAE Transactions 94(1): pp.599-609

[54] He, X.D. and S. Liu. 1998. '*Multivariable Control of Vapor Compression Systems*'. HVAC&R Research 4(3): pp.205-230

[55] Hill, C.R. 1985. '*Simulation of a Multizone Air Handler*'. ASHRAE Transactions. 91(1B): pp.752-764

[56] Hill, J.M. and S.M. Jeter. 1991. '*A Linear Subgrid Cooling and Dehumidification Coil Model with Emphasis on Mass Transfer*'. ASHRAE Transactions 97(2): pp.118-128

[57] Holman, J.P. 2002. Heat Transfer. Ninth Edition. McGraw-Hill Companies, Inc.

[58] House J.M. and T.F.Smith 1995. '*A System Approach to Optimal Control for HVAC and Building Systems*'. ASHRAE Transactions 101 (2): pp.647–660

[59] House J.M., K.D. Lee and L.K. Norford. 2003. '*Controls and Diagnostics for Air Distribution Systems*'. Journal of Solar Energy Engineering, Vol. 125: pp.310-318

[60] Huang, H. and F. Haghighat. 2005. '*An Integrated Zonal Model for Predicting Indoor Airflow Temperature and VOC Distributions*'. ASHRAE Transactions 111

(1): pp.601-611

[61] Huang, W. and H.N. Lam. 1997. '*Using Genetic Algorithms to Optimize Controller Parameters for HVAC Systems*'. Energy and Buildings 26: pp.277-282

[62] Huang, S.H. and R.M. Nelson. 1999. '*Development of a Self-Tuning Fuzzy Logic Controller*'. ASHRAE Transactions 105 (1): pp.206-213

[63] Hugh, F. and J. Crowther. 2004. '*Optimizing Chillers and Towers*'. ASHRAE Journal 46(7): pp34-44

[64] Jette, I., M. Zaheeruddin and P. Fazio. 1998. '*PI-Control of Dual Duct System: Manual Tuning and Control Loop Interaction*'. Energy Conservation Management, Vol.39(14): pp.1741-1482

[65] Jia. X, C.P. Tso, P.K. Chia and P. Jolly. 1995. '*A Distributed Model for Prediction of the Transient Response of an Evaporator*'. International Journal of Refrigeration 18: pp. 336-342

[66] Jia. X, C.P. Tso, P. Jolly and Y.W. Wong. 1999. '*Distributed Steady and Dynamic Modeling of Dry-Expansion Evaporators*'. International Journal of Refrigeration 22: pp.126-136

[67] Jian W.L. 1996. '*Dynamic Modeling and On-Off Switching Control of a Chilled Water Cooling System with Storage*'. Mater's Thesis, Concordia University

[68] Jiang, H.B. and R. Radermacher. 2003. '*A Distributed Model of a Space Heat Pump under Transient Conditions*'. International Journal of Energy Research 27: pp.145-160

[69] Kamimura, K. et al. 1994. '*CAT (Computer-Aided-Tuning) Software for PID Controllers*'. ASHRAE Transactions 100(1): pp.180-189

[70] Kamimura, K., Y. Hashimoto, T. Yamazaki, Y. Noda and S. Kurosu. 2002. '*A Comparison of Controller Tuning Methods of the Potential for Energy Saving*'. ASHRAE Transactions 108(2): pp.155-165

[71] Kasahara, M., T. Matsuba, Y. Kuzuu, T. Yamazaki, Y. Hashimoto, K. Kamimura and S. Kurosu. 1999. '*Design and Tuning of Robust PID Controller for HVAC Systems*'. ASHRAE Transactions 105(2): pp.154-166

[72] Kasahara, M., Y. Kuzuu, T. Matsuba, Y. Hashimoto, K. Kamimura and S. Kurosu.

2000. '*Physical Model of an Air-Conditioned Space for Control Analysis*'. ASHRAE Transactions 106(2): pp.304-317

[73] Kasahara, M., T. Yamazaki, Y. Kuzuu, Y. Hashimoto, K. Kamimura, T. Matsuba, and S. Kurosu. 2001. '*Stability Analysis and Tuning of PID Controller in VAV Systems*'. ASHRAE Transactions 107(1): pp.285-296

[74] Khan, A.Y. 1994. '*Heat and Mass Transfer Performance Analysis of Cooling Coils at Part-Load Operating Conditions*'. ASHRAE Transactions, Vol. 100(2): pp.54–62.

[75] Kim, M.H. and C.W. Bullard. 2001. '*A Simple Approach to Thermal Performance Analysis of Small Hermetic Reciprocating Compressors*'. ASHRAE Transactions 107 (1): pp.109-119

[76] Ke, Y.P., S.A. Mumma and D. Stanke. 1997. '*Simulation Result and Analysis of Eight Ventilation Control Strategies in VAV Systems*'. ASHRAE Transactions 103(2): pp.381-392

[77] Kimbara, A., M. Kasahara, S.Kurosu, K. Kamimura, T. Matsuba and A. Yamada. 1995. '*A Modeling of an Environmental Chamber*'. ASHRAE Transactions 101(1): pp.262-274

[78] Kirsner, W. 1996. '*3 GPM/Ton Condenser Water Flow Rate: Dose it waste Energy?*' ASHRAE Journal 38(2): pp.63-69

[79] Klaczek, W., M.A. Ackerman, P. Fleming and B. Fleck. 2005. '*Field Performance Assessment of VAV Control Systems to Determine the Longevity of Recommissioning*'. ASHRAE Transactions 111(1): pp.37-52

[80] Klein, S.A. et al. 1983. TRNSYS, A Transient Simulation Program, Report 38-12, Version 12.1. Engineering Experimentation Station, University of Wisconsin-Madison.

[81] Klimke, A., K. Willner and B. Wohlmuth. 2004. '*Uncertainty Modeling Using Fuzzy Arithmetic Based on Sparse Grids: Applications to Dynamic Systems*'. International Journal of Uncertainty, Fuzziness, and Knowledge-Based Systems, Vol. 12(6): pp.745-759.

[82] Kokototic, P. and M. Arcak. 2001. '*Constructive Nonlinear Control: A Historical Perspective*'. Automatica 37: pp. 637-662.

[83] Koury, R.N.N., L. Machado and K.A.R. Ismail. 2001. '*Numerical Simulation of a Variable Speed Refrigeration System*'. International Journal of Refrigeration 24: pp.192–200

[84] Krakow, K.I., S. Lin and Z.S. Zeng. 1995. '*Temperature and Humidity Control during Cooling and Dehumidifying by Compressor and Evaporator Fan Speed Variation*'. ASHRAE Transactions 101(1): pp.292-304

[85] Krakow, K.I., S. Lin and Z.S. Zeng. 1995. '*Analytical Determination of PID Coefficients for Temperature and Humidity Control during Cooling and Dehumidifying by Compressor and Evaporator Fan Speed Variation*'. ASHRAE Transactions 101(1): pp.343-353.

[86] Isidori, A. 1995. Nonlinear Control Systems. Third Edition, Springer

[87] Lillo, W.E., M.H. Loh, S. Hui and S.H. Zak. 1993. '*On Solving Constrained Optimization Problems with Neural Networks: A Penalty Method Approach*'. IEEE Transactions on Neural Networks, Vol.4(6): pp.931-939

[88] Liu, M.S. 2003. '*Variable Speed Drive Volumetric Tracking for Airflow Control in Variable Air Volume Systems*'. Journal of Solar Energy Engineering, Transactions of the ASME, Vol.125(3): pp.318-323

[89] Lu, L., W.J. Cai, Y.C. Soh, L.H. Xie and A.J. Li. 2004. '*HVAC System Optimization - Condenser Water Loop*'. Energy Conversion and Management (45): pp.613-630

[90] Lu, L., W.J. Cai, L.H. Xie, S.J. Li and Y.C. Soh. 2005. '*HVAC System Optimization - In-Building Section*'. Energy and Buildings, Vol. 37: pp 11-22

[91] Lu, L., W.J. Cai, Y.C. Soh, L.H. Xie. 2005. '*Global Optimization for Overall HVAC systems—Part II Problem Solution and Simulations*'. Energy Conversion and Management 46: pp.1015–1028

[92] MacArthur, J.W. 1984. '*Theoretical Analysis of the Dynamic Interactions of Vapour Compression Heat Pumps*'. Energy Conservation and Management 24(1): pp. 49-66

[93] MacArthur, J.W. and E.W. Grald. 1987. '*Prediction of Cyclic Heat Pump Performance with a Fully Distributed Model and a Comparison with Experimental Data*'. ASHRAE Transactions 93 (2): pp. 1158-1178.

[94] Massie, D.D., P.S. Curtiss and J.F. Kreider. 1998. '*Predicting Central Plant HVAC Equipment Performance Using Neural Networks –Laboratory System Test Results*'. ASHRAE Transactions 104 (1A): pp. 221-228.

[95] Massie, D.D., J.F. Kreider and P.S. Curtiss. 2004. '*Neural Network Optimal Controller for Commercial Ice Thermal Storage Systems*'. ASHRAE Transactions 114 (2): pp. 361-369

[96] Matlab 2006. Documentation. Version 7.1. MathWorks Inc.

[97] McQuiston, F.C., J.D. Parker and J.D. Spitler. 2000. Heating, Ventilating and Air-Conditioning: Analysis and Design. Fifth edition. John Wiley & Sons. Inc.

[98] Mei, L. and G.J. Levermore. 2002. '*Simulation and Validation of a VAV System with an ANN Fan Model and a Non-Linear VAV Box Model*'. Building and Environment 37: pp.277-284

[99] Miller, D.E. 1982. *'A Simulation to Study HVAC Processes*'. ASHRAE Transactions 88(2): pp.809-825

[100] Mithraratne, P., N.E. Wijeysundera and T.Y. Bong. 2000. '*Dynamic Simulation of a Thermostatically Controlled Counter Flow Evaporator*'. International Journal of Refrigeration 23: pp.174-189

[101] Nanayakkara, V.K., Y. Ikegami and H. Uehara. 2002. '*Evolutionary Design of Dynamic Neural Networks for Evaporator Control*'. International Journal of Refrigeration 25: pp.813 –826

[102] Nassif, N., S. Kajl and R. Sabourin. 2005. '*Optimization of HVAC Control System Strategy Using Two-Objective Genetic Algorithm*'. HVAC&R Research, Vol.11 (3): pp.459-486

[103] Nesler. C.G. and W.F. Stoecker. 1984. '*Selecting the Proportional and Integral Constants in the Direct Digital Control of Discharge Air Temperature*'. ASHRAE Transactions 90(2B): pp.834-845

[104] Oskarsson, S.P., K.I. Krakow and S. Lin. 1990. '*Evaporator Models for Operation with Dry, Wet and Frosted Surfaces. Part II: Evaporator Models and Verification*'. ASHRAE Transactions Vol. 96(1): 381-392

[105] Otto, K.N., A.D. Lewis and E.K. Antonsson. 1993. '*Approximating α-cuts with the*

Vertex Method'. Fuzzy Sets and Systems, Vol. 55: pp.43–50

[106] Park, C., D.R. Clark and G.E. Kelly. 1985. '*An Overview of HVACSIM+: a Dynamic Building/HVAC/Control System Simulation Program*'. Building Energy Simulation Conference, Seattle, August, pp.175-185

[107] Parlos, A.G., K.T. Chong and A.F. Atiya. 1994. '*Application of the Recurrent Multilayer Perceptron in Modeling Complex Process Dynamics*'. IEEE Transactions on Neural Network: pp.255-266

[108] Rahmati, A., F. Rashidi and M. Rashidi. 2003. '*Hybrid Fuzzy Logic and PID Controller for Control of Nonlinear HVAC System*'. Proceedings of the IEEE International Conference on Systems, Man and Cybernetics, Vol.3: pp 2249-2254

[109] Rasmussen, B.P. and A.G. Alleyne. 2004. '*Control-Oriented Modeling of Transcritical Vapor Compression Systems*'. ASME Journal of Dynamic Systems, Measurement and Control 126: pp. 54-64

[110] Ratnam, E., T. Campbell and R. Bradely. 1998. '*Advanced Feedback Control of Indoor Air Quality Using Real-Time Computational Fluid Dynamics.*' ASHRAE Transactions 104(1A): pp.612-627

[111] Rice, J.K. 1987. '*The Effect of Void Fraction Correlation and Heat Flux Assumption on Refrigerant Charge Inventory Predictions*'. ASRAE Transactions 93(1): pp. 341-367

[112] Roberts, A.S. and M.P. Oak. 1991. '*Nonlinear Dynamics and Control for Thermal Room Model*'. ASHRAE Transactions 97(1): pp.722-726

[113] Sakamoto, Y., A. Nagaiwa, S. Kobayasi and T. Shinozaki. 1999. '*An Optimization Method of District Heating and Cooling Plant Operation Based on Genetic Algorithm*'. ASHRAE Transactions 105(2): pp.104-115

[114] Seem, J.E. 1998. '*A New Pattern Recognition Adaptive Controller with Application to HVAC System*'. Automatica, Vol.34, No.8: pp.969-982

[115] Semsar, E., M.J. Yazdanpanah and C. Lucas. 2003. '*Nonlinear Control and Disturbance Decoupling of and HVAC System via Feedback Linearization and Back-Stepping*'. Proceedings of IEEE Conference on Control Applications –Vol. 1: pp.646-650

[116] Serbric, J., Q. Chen and L.R. Glicksman. 2000. '*A Coupled Airflow and Energy Simulation Program for Indoor Thermal Environmental Studies*'. ASHRAE Transactions 106(1):pp. 465-476

[117] Shavit G. and S.G. Brandt. 1982. '*The Dynamic Performance of a Discharge Air Temperature System with a PI Controller*'. ASHRAE Transactions 88(2):pp. 826-838

[118] Shelton, S.V. and C.T. Joyce. 1991. '*Cooling Tower Optimization for Centrifugal Chillers*'. ASHRAE Journal 33(6): pp.28-36

[119] Shin, S. 1995. '*Adaptive Control and Neural Network*'. Journal of the Society of Instrument and Control Engineers 35(6): pp. 437-441

[120] So, A.T.P, W.L. Chan, T.T. Chow and W.L. Tse. 1995. '*A Neural Networks based Identifier/Controller for Modern HVAC Control*'. ASHRAE Transactions 101(2):pp.14-31

[121] Stoecker, W.F. and J.W. Jones. 1989. Refrigeration and Air Conditioning. 2nd edition. McGraw-Hill Book Company.

[122] Sun, J. and A. Reddy. 2005. '*Optimal Control of Building HVAC&R Systems Using Complete Simulation-Based Sequential Quadratic Programming (CSB-SQP)*'. Building and Environment 40(5): pp.657-669

[123] Tandon, T.N., H.K. Varma, and C.P. Gupta. 1985. '*A Void Fraction Model for Annular Two-Phase Flow*'. International Journal of Heat Mass Transfer, Vol.28: pp. 191-198

[124] Tanyolu, T. 1999. *'A Neural Network Approach with Self-Organized Principal Component Analysis for Identifications of Dehumidifying Coils*'. ASHRAE Transactions 105(1):pp.96-109

[125] Tong, S.C., C. Bin, and Y.F. Wang. 2005. *'Fuzzy Adaptive Output Feedback Control for MIMO nonlinear Systems*'. Fuzzy Sets and Systems, Vol.156: pp. 285-299

[126] Veelenturf, L.P.J. 1995. Analysis and Application of Artificial Neural Network. United Kindom: Prentice Hall

[127] Virk, G.S. and D.L. Loveday. 1991. '*A Comparison of Predictive, PID and On/Off*

Techniques for Energy Management and Control'. ASHRAE Transactions 97 (2): pp. 3-10

[128] Wang, H. and Touber S. 1991. '*Distributed and Non-Steady State Modeling of an Air Cooler*'. International Journal of Refrigeration 14: pp. 98-111

[129] Wang, S.W. 1999. '*Dynamic Simulation of Building VAV Air-Conditioning System and Evaluation of EMCS On-Line Control Strategies*'. Building and Environment (34): pp. 681-705

[130] Wang, S.W. and X.Q. Jin. 2000. '*Model-based Optimal Control of VAV Air-conditioning System Using Genetic Algorithm*'. Building and Environment (35): pp. 471-487

[131] Wang, Y.G., Shi Z.G, Cai W.J. 2001. '*PID Autotuner and Its Application in HVAC Systems*'. Proceedings of the American Control Conference, Arlington, VA, June 25-27. pp.2192-2196

[132] Wang, Y.W., W.J. Cai, Y.C. Soh, S. Li, L. Lu and L.H. Xie. 2004. '*A Simplified Modeling of Cooling Coils for Control and Optimization of HVAC Systems*'. Energy Conversion and Management (45): pp.2915–2930

[133] Willatzen, M, N.B.O.L. Pettit and L. Ploug-Sorensen. 1998. '*A General Dynamic Simulation Model for Evaporators and Condensers in Refrigeration. Part 1: Moving-Boundary Formulation of Two-Phase Flows with Heat Exchange*'. International Journal of Refrigeration 21(5): pp. 398-403

[134] Xu, M., S. Li and W. Cai. 2005. '*Practical Receding-Horizon Optimization Control of the Air Handling Unit in HVAC Systems*'. Industrial and Engineering Chemistry Research 44(8): pp.2848-2855

[135] Yang, H.Q., H. Yao and J.D. Jones. 1993. '*Calculating Functions of Fuzzy Numbers*'. Fuzzy Sets and Systems, Vol.55: pp.273–283

[136] Yao, Y. 2004. '*Thermal Analysis of Cooling Coils Based on a Dynamic Model*'. Applied Thermal Engineering, Vol.24: pp.1037–50.

[137] Zadeh, L.A. 1965. '*Fuzzy Sets*'. Information and Control, Vol.8: pp.338-353.

[138] Zadeh, L.A. 1978. '*Fuzzy Sets as a Basis for a Possibility Theory*'. Fuzzy Sets and Systems, Vol.1(1): pp.3-28.

[139] Zaheeruddin, M. and Goh P.A. 1991. '*Transient Responses of a Closed-Loop VAV System*'. ASHRAE Transactions 97(2): pp.

[140] Zaheeruddin, M. and M. Ning. 2003. '*Dynamic Model of a VAV System with Compression Refrigeration Water Chiller'*. International Conference on Computational Mechanics, Kanpur, India, December

[141] Zaheeruddin, M. and N. Tudoroiu. 2004. '*Neuro-Models for Discharge Air Temperature System*'. Energy Conversion and Management (45): pp.901 –910

[142] Zhang, H.G. and L.L. Cai. 2002. '*Decentralized Nonlinear Adaptive Control of An HVAC System. IEEE Transactions on Systems*'. Man and Cybernetics—Part C: Applications and Reviews, Vol. 32(4): pp.493-498

[143] Zhang, T.P. 2004. 'Stable Direct Adaptive Fuzzy Control for a Class of MIMO Non-Linear Systems'. International Journal of Systems Science, Vol. 34 (6): pp.375-388

[144] Zhang, Q, Y.W. Wong, S.C. Fok and T.Y. Bong. 2005. '*Neural Based Air-Handling Unit for Indoor Relative Humidity and Temperature Control*'. ASHRAE Transactions 111(1): pp.63-70

[145] Zheng, G.R. 1997. Dynamic Modeling and Global Optimal Operation of Multizone Variable Air Volume HVAC System. Ph.D Dissertation, Concordia University, Montreal, Canada